



Submitted to: JHEP

CERN-EP-2024-198
24th July 2024

Differential cross-section measurements of Higgs boson production in the $H \rightarrow \tau^+\tau^-$ decay channel in pp collisions at $\sqrt{s} = 13$ TeV with the ATLAS detector

The ATLAS Collaboration

Differential measurements of Higgs boson production in the τ -lepton-pair decay channel are presented in the gluon fusion, vector-boson fusion (VBF), VH and $t\bar{t}H$ associated production modes, with particular focus on the VBF production mode. The data used to perform the measurements correspond to 140 fb^{-1} of proton–proton collisions collected by the ATLAS experiment at the LHC. Two methods are used to perform the measurements: the *Simplified Template Cross-Section* (STXS) approach and an *Unfolded Fiducial Differential* measurement considering only the VBF phase space. For the STXS measurement, events are categorized by their production mode and kinematic properties such as the Higgs boson’s transverse momentum (p_{T}^{H}), the number of jets produced in association with the Higgs boson, or the invariant mass of the two leading jets (m_{jj}). For the VBF production mode, the ratio of the measured cross-section to the Standard Model prediction for $m_{jj} > 1.5$ TeV and $p_{\text{T}}^{\text{H}} > 200$ GeV ($p_{\text{T}}^{\text{H}} < 200$ GeV) is $1.29^{+0.39}_{-0.34}$ ($0.12^{+0.34}_{-0.33}$). This is the first VBF measurement for the higher- p_{T}^{H} criteria, and the most precise for the lower- p_{T}^{H} criteria. The *fiducial* cross-section measurements, which only consider the kinematic properties of the event, are performed as functions of variables characterizing the VBF topology, such as the signed $\Delta\phi_{jj}$ between the two leading jets. The measurements have a precision of 30%–50% and agree well with the Standard Model predictions. These results are interpreted in the SMEFT framework, and place the strongest constraints to date on the CP-odd Wilson coefficient $c_{H\bar{W}}$.

Contents

1	Introduction	2
2	ATLAS detector	4
3	Data and simulated event samples	5
4	Object reconstruction and event selection	7
5	Event categorization	9
5.1	VBF categorization	9
5.2	$tt(0\ell)H \rightarrow \tau_{\text{had}}\tau_{\text{had}}$ categorization	13
5.3	V(had)H categorization	14
5.4	Boost categorization	14
6	Background estimation	14
7	Systematic uncertainties	16
8	Simplified template cross-section measurement results	17
8.1	Simplified template cross-section measurement fit model	18
8.2	Simplified template cross-section results	19
9	Unfolded fiducial differential cross-section measurement results	26
9.1	Fiducial phase space	26
9.2	Differential variables	27
9.3	Differential cross-section measurement fit model	28
9.4	Differential cross-section measurement results	28
9.5	Interpretation of the differential cross-section measurement in an Effective Field Theory	31
10	Conclusion	35

1 Introduction

Since the discovery of the Higgs boson by the ATLAS [1] and CMS [2] Collaborations in 2012, studying the properties of this boson has been a priority of the LHC experiments. The main Higgs boson production mode at the LHC is gluon–gluon fusion (ggF), followed by vector boson fusion (VBF) production, associated production with a vector boson (VH , $V = W$ or Z) and associated production with a top-antitop quark pair ($t\bar{t}H$). In the Standard Model (SM), the decay into a $\tau^+\tau^-$ pair¹ has the largest branching ratio of all leptonic Higgs boson decays.

Previously, the ATLAS Collaboration used the Run 2 dataset to study the $H \rightarrow \tau\tau$ final state [3] and three measurements were performed: the total Higgs boson production cross-section, the cross-sections for the four dominant production modes, and a measurement of the cross-section in nine phase-space regions

¹ For simplicity, a $\tau^+\tau^-$ pair is denoted by $\tau\tau$ throughout this paper.

(bins) in the Simplified Template Cross-Section (STXS) framework [4]. For the STXS measurement, cross-sections for Higgs boson production were measured as a function of the transverse momentum (p_T) of the Higgs boson (p_T^H), the number of jets produced in association with the Higgs boson, and the invariant mass of the two leading jets (m_{jj}) where applicable. Higgs boson production through VBF was confirmed in this decay channel with an observed (expected) significance of 5.3σ (6.2σ) over the SM background, and a cross-section of $0.90^{+0.20}_{-0.17}$ times the SM prediction. Of all the Higgs boson decay channels explored by ATLAS [3, 5–7], $H \rightarrow \tau\tau$ provided the most precise single measurement of VBF production and motivates further studies of the kinematics of Higgs boson production using this channel. The results in this paper constitute the final Run 2 measurements in the $H \rightarrow \tau\tau$ final state and supersede those in Ref. [3]. A similar measurement was also performed by the CMS Collaboration using the Run 2 dataset [8], where the cross-section for the Higgs boson production through VBF was measured as 0.81 ± 0.17 times the SM prediction.

Two approaches for investigating the properties of VBF events in the $H \rightarrow \tau\tau$ decay channel are reported in this paper. The first approach is to perform a cross-section measurement within the STXS framework, expanding on the measurement of Ref. [3] in which only a single bin in the VBF phase space was measured. In this context, the extracted cross-sections are based on the production mode and the kinematics of the events; in the particular case of VBF production, the events are separated into bins based on p_T^H and m_{jj} . Similar measurements were also pursued for other Higgs boson decay channels such as $H \rightarrow ZZ^*$ [5, 9], $H \rightarrow \gamma\gamma$ [6, 10] and $H \rightarrow WW^*$ [7, 11]. The second approach is to measure *fiducial* differential production cross-sections for $H \rightarrow \tau\tau$ events. The fiducial measurement approach does not distinguish between the different Higgs boson production modes, but a phase-space region enriched in VBF events is defined to ensure optimal measurement sensitivity. This results in a less model-dependent approach than the STXS framework, although still relying on simulated SM samples to derive response matrices. The cross-section is measured as a function of several variables, including p_T^H , the azimuthal angle $\Delta\phi_{jj}^{\text{signed}}$ between the jets, and the leading jet’s transverse momentum, $p_T(j_0)$. They are chosen to test the kinematics of the SM Higgs boson and the VBF production mode, as well as to provide sensitivity to contributions from physics beyond the SM. Differential measurements in the VBF phase space were performed previously in the $H \rightarrow \gamma\gamma$ [12] and $H \rightarrow WW^*$ [13] channels, while this is the first differential measurement performed in the $H \rightarrow \tau\tau$ channel.

Additionally, the results reported in this paper extend the study of $t\bar{t}H$ production in the STXS framework. In Ref. [3], an inclusive measurement of $t\bar{t}H$ production was performed in the fully hadronic final state, whereas this paper considers multiple bins in p_T^H because higher momentum bins are expected to be more sensitive to physics beyond the SM.

This paper is organized as follows. The ATLAS detector is described in Section 2, followed by the data and simulated samples in Section 3, and the object reconstruction and main event selection in Section 4. Section 5 discusses the event categorization, and then Section 6 delves into more details of the background estimation methods. The systematic uncertainties are discussed in Section 7, followed by the STXS cross-section measurement results in Section 8 and the differential cross-section measurement results in Section 9. Conclusions are reported in Section 10.

2 ATLAS detector

The ATLAS detector [14] at the LHC covers nearly the entire solid angle around the collision point.² It consists of an inner tracking detector surrounded by a thin superconducting solenoid, electromagnetic and hadronic calorimeters, and a muon spectrometer incorporating three large superconducting air-core toroidal magnets.

The inner-detector system (ID) is immersed in a 2 T axial magnetic field and provides charged-particle tracking in the range $|\eta| < 2.5$. The high-granularity silicon pixel detector covers the vertex region and typically provides four measurements per track, the first hit generally being in the insertable B-layer (IBL) installed before Run 2 [15, 16]. It is followed by the Semiconductor Tracker (SCT), which usually provides eight measurements per track. These silicon detectors are complemented by the transition radiation tracker (TRT), which enables radially extended track reconstruction up to $|\eta| = 2.0$. The TRT also provides electron identification information based on the fraction of hits (typically 30 in total) above a higher energy-deposit threshold corresponding to transition radiation.

The calorimeter system covers the pseudorapidity range $|\eta| < 4.9$. Within the region $|\eta| < 3.2$, electromagnetic calorimetry is provided by barrel and endcap high-granularity lead/liquid-argon (LAr) calorimeters, with an additional thin LAr presampler covering $|\eta| < 1.8$ to correct for energy loss in material upstream of the calorimeters. Hadronic calorimetry is provided by the steel/scintillator-tile calorimeter, segmented into three barrel structures within $|\eta| < 1.7$, and two copper/LAr hadronic endcap calorimeters. The solid angle coverage is completed with forward copper/LAr and tungsten/LAr calorimeter modules optimised for electromagnetic and hadronic energy measurements respectively.

The muon spectrometer (MS) comprises separate trigger and high-precision tracking chambers measuring the deflection of muons in a magnetic field generated by the superconducting air-core toroidal magnets. The field integral of the toroids ranges between 2.0 and 6.0 T m across most of the detector. Three layers of precision chambers, each consisting of layers of monitored drift tubes, cover the region $|\eta| < 2.7$, complemented by cathode-strip chambers in the forward region, where the background is highest. The muon trigger system covers the range $|\eta| < 2.4$ with resistive-plate chambers in the barrel, and thin-gap chambers in the endcap regions.

The luminosity is measured mainly by the LUCID-2 [17] detector that records Cherenkov light produced in the quartz windows of photomultipliers located close to the beampipe.

Events are selected by the first-level trigger system implemented in custom hardware, followed by selections made by algorithms implemented in software in the high-level trigger [18]. The first-level trigger accepts events from the 40 MHz bunch crossings at a rate below 100 kHz, which the high-level trigger further reduces in order to record complete events to disk at about 1 kHz.

A software suite [19] is used in data simulation, in the reconstruction and analysis of real and simulated data, in detector operations, and in the trigger and data acquisition systems of the experiment.

² ATLAS uses a right-handed coordinate system with its origin at the nominal interaction point (IP) in the centre of the detector and the z -axis along the beam pipe. The x -axis points from the IP to the centre of the LHC ring, and the y -axis points upwards. Polar coordinates (r, ϕ) are used in the transverse plane, ϕ being the azimuthal angle around the z -axis. The pseudorapidity is defined in terms of the polar angle θ as $\eta = -\ln \tan(\theta/2)$ and is equal to the rapidity $y = \frac{1}{2} \ln \left(\frac{E+p_z c}{E-p_z c} \right)$ in the relativistic limit. Angular distance is measured in units of $\Delta R \equiv \sqrt{(\Delta y)^2 + (\Delta \phi)^2}$.

3 Data and simulated event samples

The data used to perform this analysis correspond to proton–proton collisions at a centre-of-mass energy $\sqrt{s} = 13$ TeV collected by the ATLAS detector during Run 2 of the LHC (2015–2018). Events are selected for analysis only if they pass a good-quality requirement and all relevant detector components were in good operating condition [20]. This yields a total integrated luminosity of 140.1 fb^{-1} [21]. The uncertainty in the integrated luminosity is 0.83% [21], obtained using the LUCID-2 detector [17] for the primary luminosity measurements, complemented by measurements using the inner detector and calorimeters.

Monte Carlo (MC) simulated event samples are used to model the $H \rightarrow \tau\tau$ signal and most of the backgrounds from SM processes. A summary of the generators used for the simulation is shown in Table 1. The same MC samples were also used in Ref. [3], and only a brief description of the main samples is reported in this section. All MC samples were reconstructed in the same manner as the data.

Table 1: Summary of the MC generators used for the main signal and background samples. Information about the matrix element (ME) generator, parton shower (PS), parton distribution function (PDF) set used in the ME and the PS, and set of tuned parameter (Tune) is provided. The column labelled ‘Normalization’ specifies the order of the cross-section calculation used for the normalization of the simulated samples.

Process	Generator		PDF set		Tune	Normalization
	ME	PS	ME	PS		
Higgs boson						
ggF	POWHEG BOX v2	PYTHIA 8	PDF4LHC15NNLO	CTEQ6L1	AZNLO	N ³ LO QCD + NLO EW
VBF	POWHEG BOX v2	PYTHIA 8	PDF4LHC15NNLO	CTEQ6L1	AZNLO	NNLO QCD + NLO EW
VH	POWHEG BOX v2	PYTHIA 8	PDF4LHC15NNLO	CTEQ6L1	AZNLO	NNLO QCD + NLO EW
$t\bar{t}H$	POWHEG BOX v2	PYTHIA 8	NNPDF3.0NNLO	NNPDF2.3LO	A14	NLO QCD + NLO EW
Background						
V + jets (QCD/EW)	SHERPA 2.2.1		NNPDF3.0NNLO		SHERPA	NNLO for QCD, LO for EW
$t\bar{t}$	POWHEG BOX v2	PYTHIA 8	NNPDF3.0NNLO	NNPDF2.3LO	A14	NNLO + NNLL QCD

The dominant Higgs boson production mode at the LHC is ggF, with a cross-section of 48.6 pb ,³ followed by VBF production, with a cross-section of 3.78 pb , then VH production, with a cross-section of 2.25 pb , and $t\bar{t}H$ production, with a cross-section of 0.51 pb .

Higgs boson production via ggF was simulated using the POWHEG BOX v2 [22–26] generator at next-to-next-to-leading-order (NNLO) accuracy in QCD. The MC simulated samples are normalized to the next-to-next-to-next-to-leading-order (N³LO) cross-section in QCD plus electroweak (EW) corrections at next-to-leading order (NLO) [4, 27–36]. For this process the PDF4LHC15NNLO set of parton distribution functions (PDF) [37] was used, while the parton shower (PS) and non-perturbative effects were modelled with PYTHIA 8.230 [38] with parameter values set to those of the AZNLO [39] set of tuned parameters (tune).

Higgs boson production via VBF was simulated using POWHEG BOX v2 at NLO accuracy in QCD. It was tuned to match calculations with effects due to finite heavy-quark masses and soft-gluon resummation up to next-to-next-to-leading logarithms (NNLL). The MC simulated samples are normalized to an approximate-NNLO QCD cross-section with NLO electroweak corrections [40–42]. The PDF4LHC15NNLO PDF set was used, while PYTHIA 8.230 with the AZNLO tune was used for PS simulation.

³ The cross-sections are reported for a centre-of-mass energy of $\sqrt{s} = 13$ TeV.

Higgs boson production via VH was simulated with POWHEG Box v2 at NLO accuracy in QCD for VH plus one-jet production. The loop-induced $gg \rightarrow ZH$ process was generated separately at leading order (LO) in QCD. The MC simulated samples are normalized to cross-sections calculated at NNLO in QCD with NLO electroweak corrections for $pp \rightarrow VH$ and at NLO and next-to-leading-logarithm accuracy in QCD for $gg \rightarrow ZH$ [43–49]. Similarly to the VBF samples, the PDF4LHC15_{NLO} PDF set was used, while PYTHIA 8.230 with the AZNLO tune was used for PS simulation.

The production of $t\bar{t}H$ events was simulated at NLO accuracy in QCD using POWHEG Box v2, with the decays of bottom and charm hadrons performed by EVTGEN 1.6.0 [50]. The cross-section used to normalize the $t\bar{t}H$ process is calculated at NLO in QCD and electroweak couplings [4, 51–54]. For this sample, the NNPDF3.0_{NLO} PDF set [55] was used, with the PS modelled by PYTHIA 8.230 with the A14 tune [56].

The normalization of all Higgs boson samples accounts for the decay branching ratio calculated with HDECAY [57–59] and PROPHECY4F [60–62]. The decays and spin correlations for τ -leptons are handled by PYTHIA. The SM prediction of the $H \rightarrow \tau\tau$ branching ratio (0.0625 ± 0.0014) and a Higgs boson mass of 125.09 GeV are assumed in the calculation of the expected cross-sections throughout this measurement.

The QCD production of the V + jets background was simulated with the SHERPA 2.2.1 [63] generator using NLO matrix elements for up to two partons, and LO matrix elements for up to four partons, calculated with the COMIX [64] and OPENLOOPS [65–67] libraries. They were matched with the SHERPA parton shower [68] using the MEPS@NLO prescription [69–72] using the set of tuned parameters developed by the SHERPA authors. The NNPDF3.0_{NNLO} set of PDFs [55] was used and the samples are normalized to a NNLO prediction [73]. Electroweak production of the $lljj$ final state (with $l = e, \mu, \tau$, and j denoting a jet) was simulated with SHERPA 2.2.1 using LO matrix elements with up to two additional parton emissions. The LO cross-section is multiplied by a factor 1.7 to match the cross-section value measured in Ref. [74]; this scaling was also applied in Ref. [75]. For the matching with the parton shower, the same prescription as for the QCD V + jets processes was used. The samples were produced using the VBF approximation, which avoids overlap with semileptonic diboson topologies by requiring a t -channel colour-singlet exchange.

The production of $t\bar{t}$ events was modelled at NLO in QCD by POWHEG Box v2 with the NNPDF3.0_{NLO} PDF set and with the h_{damp} parameter⁴ set to $1.5 m_{\text{top}}$ [76]. The events were interfaced to PYTHIA 8.230 to model the parton shower, hadronization, and underlying event, with parameters set according to the A14 tune and using the NNPDF2.3_{LO} set of PDFs. The decays of bottom and charm hadrons were performed by EVTGEN, as they were for the $t\bar{t}H$ sample. The $t\bar{t}$ sample is normalized to the cross-section prediction at NNLO in QCD, including the resummation of NNLL soft-gluon terms, calculated using TOP++ 2.0 [77–83].

To simulate the effects of additional pp collisions in the same, next or previous bunch crossing (pile-up), additional interactions were generated using the soft QCD processes provided by PYTHIA 8.186 [84] with the A3 tune [85] and the MSTW2008LO PDF set [86], and overlaid onto each simulated hard-scatter event. The MC samples were reweighted so that the pile-up distribution matches the one observed in the data, and were processed through an ATLAS detector simulation [87] based on GEANT4 [88].

⁴ The h_{damp} parameter is a resummation damping factor and one of the parameters that controls the matching of POWHEG matrix elements to the parton shower and thus effectively regulates the high- p_T radiation against which the $t\bar{t}$ system recoils.

4 Object reconstruction and event selection

The selection of $H \rightarrow \tau\tau$ events requires the reconstruction of electrons, muons, the visible products of hadronically decaying τ -leptons ($\tau_{\text{had-vis}}$), jets (including their b -tagging properties) and missing transverse momentum. The numbers of reconstructed light leptons (electrons and muons, globally referred to as ‘leptons’ or ℓ) and $\tau_{\text{had-vis}}$ in each event are used for its assignment to one of the three channels used in the analysis. Requirements on the number of additional jets in the event are then used in the signal region categorization and for background suppression. Both the object selection criteria and the basic event selection are taken from Ref. [3].

Three channels from the $H \rightarrow \tau\tau$ decay are considered: two hadronically decaying τ -leptons (τ_{had} , where the τ -lepton decays into hadrons plus a neutrino), denoted by $\tau_{\text{had}}\tau_{\text{had}}$; one leptonically decaying τ -lepton (τ_{lep}) and one τ_{had} , denoted by $\tau_{\text{lep}}\tau_{\text{had}}$; and two τ_{lep} with different flavours, denoted by $\tau_e\tau_\mu$. Events were collected with single-lepton, dilepton or di-hadronic τ -lepton triggers [89–92]. The requirements imposed on the p_T of the reconstructed electrons, muons or $\tau_{\text{had-vis}}$ in the analysis are tighter than those applied in the trigger-object reconstruction and trigger decision, in order to be on the trigger efficiency plateau.

Electrons are reconstructed from topological clusters of energy deposits in the electromagnetic calorimeter which are matched to a track reconstructed in the ID [93]. They are required to satisfy the ‘Loose’ identification criteria described in Ref. [93], to have $p_T > 15$ GeV, and to be in the fiducial volume of the ID and the high-granularity electromagnetic calorimeters, $|\eta_{\text{cluster}}| < 2.47$, with the exclusion of the LAr barrel–endcap transition region $1.37 < |\eta_{\text{cluster}}| < 1.52$. In the $\tau_e\tau_\mu$ and $\tau_e\tau_{\text{had}}$ channels, the selected electron is also required to satisfy the ‘Medium’ identification and the ‘Loose’ isolation criterion [93] in the signal regions and in most of the control regions. The ‘Medium’ identification has an efficiency of 80% to 90%, while ‘Loose’ isolation has an efficiency of 90% for candidates with $p_T = 15$ GeV, and it increases to more than 98% for candidates with $p_T = 30$ GeV. The p_T requirement is tightened if the event is accepted by the single-electron trigger or the electron–muon trigger, as shown in Table 2.

Muons are reconstructed from signals in the MS matched with tracks in the ID. They are required to satisfy the ‘Loose’ identification criteria [94] and to have $p_T > 10$ GeV and $|\eta| < 2.5$. In the $\tau_e\tau_\mu$ and $\tau_\mu\tau_{\text{had}}$ channels, the selected muon in the signal regions is also required to satisfy the ‘Medium’ identification and the ‘Tight’ isolation criterion [94] based on track information. The ‘Medium’ identification has an efficiency above 97%, while the ‘Tight’ isolation has an efficiency increasing from 85% to 99% for muons with p_T increasing from 10 GeV to 50 GeV. The p_T requirement is tightened if the event is accepted by the single-muon trigger or the electron–muon trigger, as shown in Table 2.

Jets are reconstructed by applying the anti- k_t algorithm [99, 100] with a radius parameter of $R = 0.4$ to topological calorimeter-energy clusters and charged-particle tracks processed with a particle-flow algorithm [101]. The energy of the jets is corrected for the non-compensating calorimeter response, noise threshold effects, energy loss from inactive material, and pile-up contamination [102]. Only jets with $p_T > 20$ GeV and $|\eta| < 4.5$ are considered. A jet vertex tagger (JVT) [103] is used to remove jets with $p_T < 60$ GeV and $|\eta| < 2.5$ that are identified as not being associated with the event’s primary vertex. Similarly, pile-up jets in the forward region are suppressed with a ‘forward JVT’ [104] algorithm, which exploits jet shapes and topological jet correlations in pile-up interactions and is applied to all jets with $p_T < 60$ GeV and $|\eta| > 2.5$. Jets with $p_T > 20$ GeV and $|\eta| < 2.5$ containing b -hadrons are identified using the DL1r b -tagging algorithm [105]. Two different working points (WP) for b -tagging are used depending on the channel: one with 85% efficiency is used in the $\tau_e\tau_\mu$ and $\tau_{\text{lep}}\tau_{\text{had}}$ channels, while another with 70% efficiency is used in the $\tau_{\text{had}}\tau_{\text{had}}$ channel. The rejection factors for b -tagging of jets initiated by

Table 2: Transverse momentum thresholds applied to the selected electrons, muons and $\tau_{\text{had-vis}}$ depending on the trigger signature and the data-taking period. The p_{T} thresholds of the lowest- p_{T} unprescaled triggers during the Run 2 ATLAS data-taking are reported in Refs. [95–98].

Trigger signature	Data-taking period	p_{T} threshold [GeV] used in event selection
Single electron	2015	$p_{\text{T}}(e) > 25$
	2016–2018	$p_{\text{T}}(e) > 27$
Single muon	2015	$p_{\text{T}}(\mu) > 21$
	2016–2018	$p_{\text{T}}(\mu) > 27.3$
One electron, one muon	2015–2018	$p_{\text{T}}(e) > 18, p_{\text{T}}(\mu) > 14.7$
Two $\tau_{\text{had-vis}}$	2015–2018	$p_{\text{T}}(\text{leading } \tau_{\text{had-vis}}) > 40$ $p_{\text{T}}(\text{sub-leading } \tau_{\text{had-vis}}) > 30$

c -quarks and light partons are 9.4 (2.6) and 390 (29) respectively for the 70% (85%) efficiency working point.

Hadronic τ -lepton decays produce a neutrino and visible decay products, mostly one or three charged pions and mostly up to two neutral pions. The reconstruction of the $\tau_{\text{had-vis}}$ is seeded by jets reconstructed using the anti- k_t algorithm with a radius parameter of $R = 0.4$. Reconstructed tracks are then matched to $\tau_{\text{had-vis}}$ candidates. A multivariate discriminant is used to identify the tracks which are likely to have been produced by the charged τ_{had} decay products, while rejecting tracks originating from other interactions, nearby jets, photon conversions or misreconstructed tracks [106]. The $\tau_{\text{had-vis}}$ objects are required to have one or three associated tracks selected by using this discriminant. Their charge (q) is defined as the sum of the measured charges of these associated tracks and is required to be $|q| = 1$. The $\tau_{\text{had-vis}}$ objects must also satisfy the requirements $p_{\text{T}} > 20$ GeV and $|\eta| < 2.47$, excluding the region $1.37 < |\eta| < 1.52$. The p_{T} requirement is tightened if the event is accepted by a di-hadronic τ -trigger, as shown in Table 2. In order to separate the $\tau_{\text{had-vis}}$ candidates produced by hadronic τ decays from those produced by jets initiated by quarks or gluons, a recurrent neural-network identification algorithm [107] is used. This algorithm uses information from reconstructed charged-particle tracks and calorimeter energy clusters associated with $\tau_{\text{had-vis}}$ candidates, together with the values of high-level discriminating variables. In the signal regions of the $\tau_{\text{lep}}\tau_{\text{had}}$ and $\tau_{\text{had}}\tau_{\text{had}}$ channels, the $\tau_{\text{had-vis}}$ objects are required to fulfil the ‘Medium’ identification criterion, which has an efficiency of 75% (60%) for candidates with one (three) associated track(s). A separate discriminant (‘eBDT’) is constructed to reject backgrounds originating from electrons misidentified as $\tau_{\text{had-vis}}$, arising mostly from $Z \rightarrow ee$ events in this analysis. In the $\tau_e\tau_{\text{had}}$ channel, for events where only one charged track is matched to the $\tau_{\text{had-vis}}$ object, the $\tau_{\text{had-vis}}$ is required to pass the ‘Medium’ working point of the eBDT algorithm, which has an 85% efficiency for candidates satisfying the identification requirement.

Since the objects used in the analysis are reconstructed from the same set of tracks and calorimetric energy clusters, some constituents can be associated with multiple objects. These overlaps between different objects are resolved with the procedure described in Ref. [3].

Simulated events are corrected for differences between data and MC simulation seen in jet vertex tagger and b -tagging efficiencies as well as b -tagging mis-tag rates [103, 108–110]. Corrections are also applied to account for minor differences between data and MC simulation seen in the lepton and τ -lepton trigger, reconstruction, identification and isolation efficiencies [93, 94, 111].

The missing transverse momentum vector, \vec{p}_T^{miss} , is reconstructed as the negative vector sum of the transverse momenta of leptons, $\tau_{\text{had-vis}}$ and jets, and a soft term, which is calculated as the vectorial sum of the p_T of tracks matched to the primary vertex but not associated with a reconstructed lepton, $\tau_{\text{had-vis}}$ or jet [112]. The magnitude of \vec{p}_T^{miss} is referred to as the missing transverse energy, E_T^{miss} .

After the object reconstruction and the overlap removal, the events are selected if they contain a $\tau\tau$ pair in one of the channels being studied: $\tau_e\tau_\mu$, $\tau_{\text{lep}}\tau_{\text{had}}$ or $\tau_{\text{had}}\tau_{\text{had}}$. For each channel, additional selections based on topological criteria such as angular distances, the transverse mass m_T of the lepton and E_T^{miss} defined as $m_T^2 = 2p_T^\ell E_T^{\text{miss}}(1 - \cos(\Delta\phi(\ell, E_T^{\text{miss}})))$, and the fraction of each τ -lepton's momentum carried by its visible decay products in the collinear approximation [113] (x_1 and x_2) are applied to enhance the sensitivity to the Higgs boson signal and reject background events. The collinear approximation assumes that the neutrinos from the τ -lepton decays propagate in the same direction as the visible decay products. Additionally, a requirement of at least one jet in the event is added to the selection for each channel. These selection criteria are summarized in Table 3.

The invariant mass ($m_{\tau\tau}$) of the two τ -leptons is calculated using a likelihood-based technique, called the Missing Mass Calculator (MMC) [114], which relies on information about the τ -lepton candidates' momenta, the presence of additional jets, the \vec{p}_T^{miss} and the type of τ -lepton decay. In cases where the likelihood does not converge, the invariant mass is estimated in the collinear approximation, denoted by $m_{\tau\tau}^{\text{coll}}$. The mass reconstruction techniques assume that the missing transverse momentum in the event is solely due to neutrinos from the τ -lepton decays. These mass reconstruction techniques are important in separating the signal from the $Z(\rightarrow \tau\tau)$ background. In addition, $m_{\tau\tau}^{\text{coll}}$ is used to separate the phase space of the $\tau_e\tau_\mu$ channel from the $H \rightarrow WW$ analysis.

5 Event categorization

After the baseline event selection reported in Table 3, an additional event categorization is performed to select Higgs boson events in different STXS production modes and in a signal region targeting the VBF production mode for the differential fiducial measurement. The applied requirements are summarized in Table 4. Subsequently, within each STXS signal region, a further event splitting is performed to provide sensitivity to the targeted STXS bins. The requirements applied for this splitting are unchanged from those in Ref. [3] for the Boost and VH categories. To target additional STXS bins, finer requirements are made for VBF categories as well for those targeting $t\bar{t}H$ production with fully hadronic top-quark and τ -lepton decays (denoted by $t\bar{t}(0\ell)H \rightarrow \tau_{\text{had}}\tau_{\text{had}}$ in the following), as described in more detail in the next part of this section. Most of these selections do not rely on the invariant mass of the two τ -leptons, as the distribution of this variable is subsequently used in a likelihood fit to extract the signal as described in Section 8.

5.1 VBF categorization

The VBF inclusive region is designed to select events with a Higgs boson produced in association with two jets originating from the hard scattering. These events can be distinguished from those from other Higgs boson production modes, and also from $Z(\rightarrow \tau\tau) + \text{jets}$ events, because they contain two high- p_T jets with a large rapidity gap and a large dijet invariant mass (m_{jj}). In order to further reduce the ggF contamination for the differential fiducial measurement, requirements on m_{jj} and $|\Delta\eta_{jj}|$ are increased and

Table 3: Summary of the event selection. In the $\tau_e\tau_\mu$ channel, events recorded with the electron trigger must satisfy $p_T(e) > 27$ GeV and $p_T(\mu) > 10$ GeV, events recorded with the muon trigger must satisfy $p_T(e) > 15$ GeV and $p_T(\mu) > 27.3$ GeV, and events recorded with the electron–muon trigger must satisfy $p_T(e) > 18$ GeV and $p_T(\mu) > 14.7$ GeV.

	$\tau_e\tau_\mu$	$\tau_{\text{lep}}\tau_{\text{had}}$ $e\tau_{\text{had}} \quad \quad \mu\tau_{\text{had}}$	$\tau_{\text{had}}\tau_{\text{had}}$
Preselection			
Object counting	$N_e = 1, N_\mu = 1, N_{\tau_{\text{had-vis}}} = 0$	$N_{e/\mu} = 1, N_{\tau_{\text{had-vis}}} = 1$	$N_{e/\mu} = 0, N_{\tau_{\text{had-vis}}} = 2$
p_T cut	e/μ : p_T cut 10 to 27.3 GeV	e/μ : p_T cut 21 to 27.3 GeV, $\tau_{\text{had-vis}}$: $p_T > 30$ GeV	$\tau_{\text{had-vis}}$: $p_T > 40, 30$ GeV
ID, Isolation, and e -veto	e/μ : Medium e : Loose; μ : Tight	e/μ : Medium, $\tau_{\text{had-vis}}$: Medium e : Loose; μ : Tight 1-prong $\tau_{\text{had-vis}}$: eBDT e -veto	$\tau_{\text{had-vis}}$: Medium
Charge product	Opposite charge	Opposite charge	Opposite charge
Kinematics	$m_{\tau\tau}^{\text{coll}} > m_Z - 25$ GeV $30 < m_{e\mu} < 100$ GeV	$m_T < 70$ GeV	
b -veto	$N_{b\text{-jets}} = 0$ DL1r 85% WP	$N_{b\text{-jets}} = 0$ DL1r 85% WP	$N_{b\text{-jets}} = 0$ DL1r 70% WP not applied in $t\bar{t}(0L)H \rightarrow \tau_{\text{had}}\tau_{\text{had}}$
E_T^{miss}	$E_T^{\text{miss}} > 20$ GeV	$E_T^{\text{miss}} > 20$ GeV	$E_T^{\text{miss}} > 20$ GeV
Leading jet	$p_T > 40$ GeV	$p_T > 40$ GeV	$p_T > 70$ GeV, $ \eta < 3.2$
Angular	$\Delta R_{e\mu} < 2.0, \Delta\eta_{e\mu} < 1.5$	$\Delta R_{\ell\tau_{\text{had-vis}}} < 2.5, \Delta\eta_{\ell\tau_{\text{had-vis}}} < 1.5$	$0.6 < \Delta R_{\tau_{\text{had-vis}}\tau_{\text{had-vis}}} < 2.5$ $ \Delta\eta_{\tau_{\text{had-vis}}\tau_{\text{had-vis}}} < 1.5$
x_1 and x_2	$0.1 < x_1 < 1.0, 0.1 < x_2 < 1.0$	$0.1 < x_1 < 1.4, 0.1 < x_2 < 1.2$	$0.1 < x_1 < 1.4, 0.1 < x_2 < 1.4$

Table 4: Summary of the inclusive signal region selection for the STXS measurement and the fiducial differential measurement. The p_T^H computation used in the Boost category is the same as in Ref. [3] and denoted by $p_T^{\text{reco}}(H)$, and is not the NN-based p_T^H introduced in Section 5.1 for the VBF and ttH categories. The leading and sub-leading jets are denoted by j_0 and j_1 , respectively.

VBF inclusive STXS	$N_{\text{jets}} \geq 2, \text{ sub-leading jet } p_T > 30 \text{ GeV}$ $m_{jj} > 350 \text{ GeV}, \Delta\eta_{jj} > 3$ $\eta(j_0) \times \eta(j_1) < 0$ lepton centrality: visible decay products of the τ -leptons between VBF jets
VBF inclusive differential	$N_{\text{jets}} \geq 2, \text{ sub-leading jet } p_T > 30 \text{ GeV}$ $m_{jj} > 600 \text{ GeV}, \Delta\eta_{jj} > 3.4, p_T(jj) > 30 \text{ GeV}$ $\eta(j_0) \times \eta(j_1) < 0$ lepton centrality: visible decay products of the τ -leptons between VBF jets $p_T(Hjj) < 50 \text{ GeV}$
VH inclusive	$N_{\text{jets}} \geq 2, \text{ sub-leading jet } p_T > 30 \text{ GeV}$ $60 \text{ GeV} < m_{jj} < 120 \text{ GeV}$
tt(0ℓ)$H \rightarrow \tau_{\text{had}}\tau_{\text{had}}$	$N_{\text{jets}} \geq 6 \text{ and } N_{b\text{-jets}} \geq 1$ or $N_{\text{jets}} \geq 5 \text{ and } N_{b\text{-jets}} \geq 2$
Boost inclusive	Not VBF inclusive Not VH inclusive $p_T^{\text{reco}}(H) > 100 \text{ GeV}$

additional requirements on the dijet transverse momentum ($p_T(jj)$) and the transverse momentum of the Higgs boson decay products and the two jets ($p_T(Hjj)$) are introduced in the VBF inclusive region.

Following the convention of the STXS framework, events in the VBF inclusive region are split into eight bins according to $m_{jj} \in [350, 700, 1000, 1500, \infty)$ GeV and $p_T^H \geq 200$ GeV. A novel technique based on a neural network (NN) is adopted to estimate p_T^H for the VBF and tt(0ℓ) $H \rightarrow \tau_{\text{had}}\tau_{\text{had}}$ categories. This NN is trained on ggF production events, using as input variables the ΔR and $\Delta\phi$ separation between the two τ -leptons, the p_T of the system formed by the four-momenta of the two τ -leptons and the E_T^{miss} ($p_T^{\text{reco}}(H)$), and $m_{\tau\tau}^{\text{coll}}$ information. Since this NN exploits the invariant mass of the system and assumes $H \rightarrow \tau\tau$ decays, it improves the p_T^H resolution in signal events – by 50% compared to that obtained with $p_T^{\text{reco}}(H)$ alone – but leads to misreconstruction of the p_T for processes like $Z(\rightarrow \tau\tau) + \text{jets}$.

A boosted decision tree (BDT) discriminant, trained using the dijet system’s kinematic variables as described in Table 5, is used to enhance the VBF $H \rightarrow \tau\tau$ signal relative to ggF $H \rightarrow \tau\tau$ production and the $Z(\rightarrow \tau\tau) + \text{jets}$ background. This BDT was also used in Ref. [3], where more details about it can be found, but the selection criteria applied to the BDT score have been optimized in each of the eight VBF

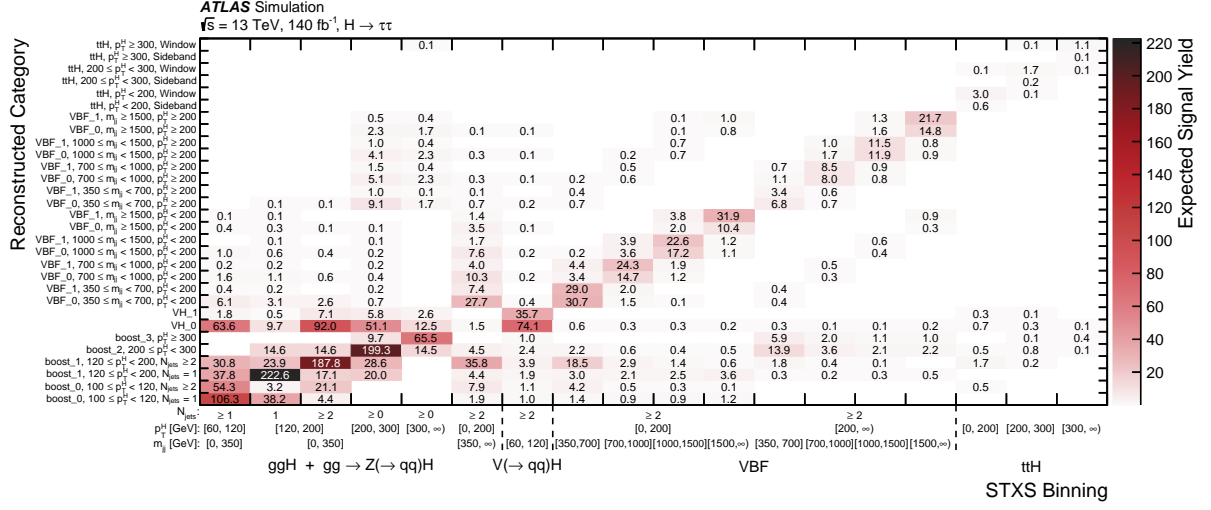
STXS bins and in the differential VBF inclusive region. Based on the discriminant output, additional event splitting into two subcategories, VBF_0 enriched in background and VBF_1 enriched in signal events, is defined.

Table 5: Variables used in the two multivariate taggers employed in the analysis. For each tagger, the presence or absence of a • indicates whether the variable is used or not. The symbol τ stands for any reconstructed τ -lepton candidate (electron, muon or $\tau_{\text{had-vis}}$) as appropriate in each channel. The symbols $p_{\text{T}}(\tau\tau)$ and $p_{\text{T}}(jj)$ indicate the vectorial sums of the momenta of two visible τ -lepton candidates and of the two leading jets, respectively. The Higgs boson candidate is formed by the vector sum of the two visible τ -lepton candidates' momenta and $\vec{p}_{\text{T}}^{\text{miss}}$. The W -boson candidate in an event is built as the pair of non- b -tagged jets with invariant mass closest to m_W . The top-quark candidate in an event is built as the system of the W -boson candidate and a b -tagged jet with invariant mass closest to m_{top} .

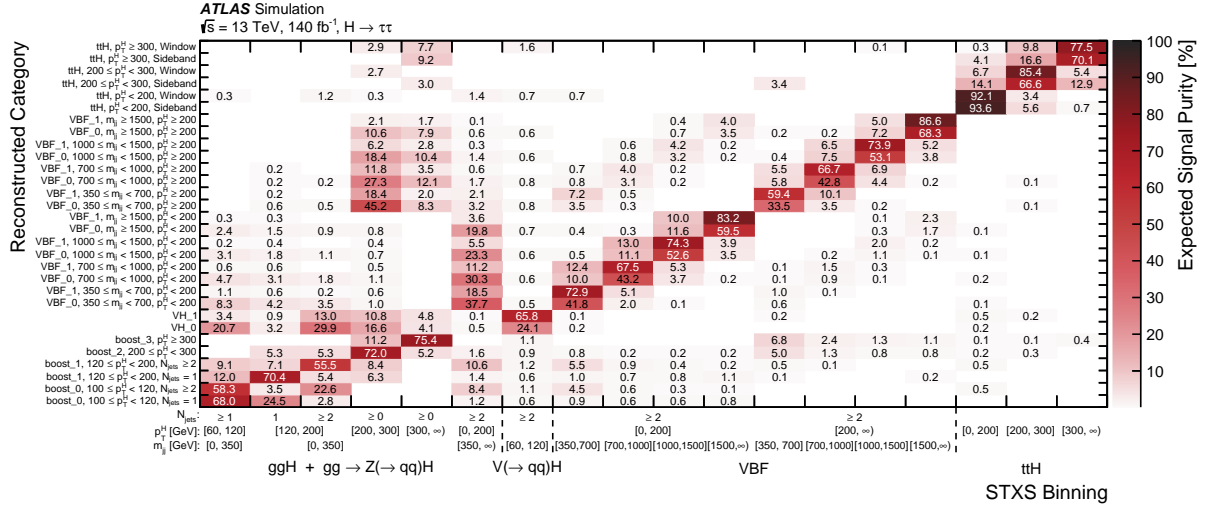
	Variable	VBF	ttH multiclass
Jet properties	Invariant mass of the two leading jets	•	
	$p_{\text{T}}(jj)$	•	
	Product of η of the two leading jets	•	
	Sub-leading jet p_{T}	•	
	η of the 5 leading jets		•
	Scalar sum of all jets p_{T}		•
	Scalar sum of all b -tagged jets p_{T}		•
	Best W -boson candidate dijet invariant mass		•
Angular distances	Best top-quark candidate three-jet invariant mass		•
	$\Delta\phi$ between the two leading jets	•	
	$\Delta\eta$ between the two leading jets	•	
	Minimum ΔR between two jets		•
	Minimum ΔR between a b -tagged jet and a $\tau_{\text{had-vis}}$		•
	$ \Delta\eta(\tau, \tau) $		•
τ -lepton properties	$\Delta R(\tau, \tau)$		•
	$p_{\text{T}}(\tau\tau)$		•
	Sub-leading τ p_{T}		•
H candidate plus jets system	Leading τ η		•
	$p_{\text{T}}(Hjj)$	•	
$\vec{p}_{\text{T}}^{\text{miss}}$	Missing transverse energy $E_{\text{T}}^{\text{miss}}$		•
	Smallest $\Delta\phi(\tau, \vec{p}_{\text{T}}^{\text{miss}})$		•

The threshold values for the BDT output are optimized to maximize the figure of merit $\sigma_{\text{tot}} = \sqrt{\sigma_0^2 + \sigma_1^2}$, where $\sigma_i = S_i/\sqrt{S_i + B_i}$ with S_i and B_i being the numbers of signal and background events in the VBF_0 ($i = 0$) and VBF_1 ($i = 1$) categories. This results in the VBF inclusive STXS region being split into a total of 16 signal regions. The signal yield expected in each of these signal regions is shown in Figure 1(a), while Figure 1(b) illustrates the relative signal population in each signal region.

The differential fiducial measurement has two signal regions: VBF_0 enriched in background and VBF_1 enriched in signal events.



(a)



(b)

Figure 1: (a) Expected SM $H \rightarrow \tau\tau$ signal yield and (b) expected signal purity in each signal region of the analysis (y -axis). Yields are summed over the three $\tau\tau$ channels ($\tau_e\tau_\mu$, $\tau_{lep}\tau_{had}$, $\tau_{had}\tau_{had}$). Only entries with a value above 0.1 are shown in the plots.

5.2 $t\bar{t}(0\ell)H \rightarrow \tau_{had}\tau_{had}$ categorization

The $t\bar{t}(0\ell)H \rightarrow \tau_{had}\tau_{had}$ region is designed to enhance the contribution from $t\bar{t}H$ production. Events are required to have at least six jets including at least one b -tagged jet, or five jets including at least two b -tagged jets. Events within this category are split into several regions based on a multiclass BDT trained to discriminate the $t\bar{t}H$ signal events from the $Z(\rightarrow \tau\tau)$ and $t\bar{t}$ background events. A detailed description of the kinematic variables used for the multiclass BDT training is given in Table 5. Regions enhanced in signal events are defined by combining requirements on the BDT scores; the threshold values for the scores are optimized using the same figure of merit as the one used for VBF categorization. By inverting the

requirement on the score, separate control regions for the $Z(\rightarrow \tau\tau)$ and $t\bar{t}$ backgrounds are also defined. According to the prescription of the STXS framework, three signal regions enriched in signal events are defined according to $p_T^H \in [0, 200, 300, \infty)$ GeV. The NN-based $p_T^{\text{NN}}(H)$ described in Section 5.1 is used to make this splitting. Each signal region is also required to have $m_{\tau\tau} \in [100, 150]$ GeV, while events outside this window are assigned to a sideband region that is used to control the backgrounds. The signal yield expected in each of these regions is shown in Figure 1(a), while Figure 1(b) illustrates the relative signal population in each signal region.

5.3 V(had)H categorization

To match the STXS $qq \rightarrow V(\rightarrow qq)H$ particle-level p_T^{jet} requirement and m_{jj} binning, events selected in the V(had) categories must satisfy $60 \text{ GeV} < m_{jj} < 120 \text{ GeV}$ and the p_T of the sub-leading jet must be greater than 30 GeV. Events in this category are split into two subcategories using a dedicated tagger. The V(had)H tagger was trained by treating all Higgs boson events produced by processes other than VH as background. The BDT score requirement used to define the two categories was optimized to give the smallest uncertainty for the V(had)H cross-section, and provides a selection where the expected fraction of V(had)H among all Higgs boson events is 66% (24%) in the VH_1 (VH_0) category. The signal yield expected in each of these regions is shown in Figure 1(a), while Figure 1(b) illustrates the relative signal population in each signal region.

5.4 Boost categorization

Events failing to meet the criteria of the VBF, V(had)H and ttH categories but having a high- p_T Higgs boson candidate are considered for the ‘Boost’ categories targeting ggF events with large Higgs boson transverse momentum. Events in the Boost category must satisfy $p_T^H > 100 \text{ GeV}$. The reconstructed Higgs boson’s transverse momentum, p_T^H , is estimated using $p_T^{\tau\tau}$ since no significant improvement was found in this Boost category by using the NN-based p_T^H reconstruction. Following the convention of the STXS framework, events are further categorized by p_T^H value and by the total number of jets with p_T greater than 30 GeV ($N_{\text{jets}}(p_T > 30 \text{ GeV})$). Events with $p_T^H < 200 \text{ GeV}$ are separated into 1-jet and ≥ 2 -jet categories, while events with $p_T^H > 200 \text{ GeV}$ and at least one jet are considered without further categorization based on jet multiplicity. The signal yield expected in each of these regions is shown in Figure 1(a), while Figure 1(b) illustrates the relative signal population in each signal region.

6 Background estimation

The dominant backgrounds after the event selection are irreducible backgrounds from $Z(\rightarrow \tau\tau) + \text{jets}$ and $t\bar{t}$ production, and reducible backgrounds from processes where at least one jet is misidentified as a τ_{had} or a light lepton. The contributions from these processes are evaluated using a mixture of simulations and data-driven techniques, following the strategy described extensively in Ref. [3].

Events from the $Z(\rightarrow \tau\tau) + \text{jets}$ process form the dominant background and they are estimated using MC simulated samples constrained using data. The yields predicted from $Z(\rightarrow \tau\tau) + \text{jets}$ MC samples are corrected using dedicated control regions defined by selecting events with kinematic properties similar to those in the corresponding signal regions, as described in detail in Ref. [3]. The selection used to

define these control regions starts from $Z(\rightarrow \ell\ell) + \text{jets}$ data and MC events which are modified through a simplified implementation of the *embedding* procedure [115], rescaling the transverse momentum of each reconstructed lepton through parameterizations to account for the differences in the trigger efficiencies, the kinematics of prompt leptons and the decay products of τ -leptons. After the rescaling, all the relevant kinematic quantities in the analysis are recomputed. This also includes accounting for the additional E_T^{miss} from the neutrinos from the decay of the τ -leptons. These control regions are included in the fit to help constrain the normalization of $Z(\rightarrow \tau\tau) + \text{jets}$ MC events in the signal regions. The uncertainties affecting the reconstructed objects used in the embedding are propagated through the entire procedure, and include those associated with the parameterizations. Dedicated uncertainties affecting each control region are assigned to account for the modelling differences observed between the $Z(\rightarrow \tau\tau)$ and embedded $Z \rightarrow \ell\ell$ MC predictions because of the approximations associated with the simplified embedding procedure. For the fiducial differential measurement an additional shape modelling uncertainty is assigned to the variable under study by comparing the embedded data and MC samples for each variable in each control region.

Processes with at least one jet misidentified as an electron, muon or τ_{had} are collectively referred to as misidentified τ background. They are evaluated using data-driven techniques in the three channels considered in the analysis, following the same methodology as in Ref. [3].

In the $\tau_e\tau_\mu$ channel, the misidentified τ background is estimated using the matrix method [116]. Data events are selected using the same criteria as in Table 3, but without the lepton isolation criteria and with loosened identification criteria for the electrons. The expected number of fake leptons in each signal region is computed from a system of equations relating the efficiencies for real and fake leptons to the observed event yields. The real-lepton efficiencies are estimated using simulations corrected with data-based scale factors, while the fake-lepton efficiencies are measured using data events which have two leptons of the same charge. Uncertainties are assigned to this background, taking into account the statistical uncertainties in the derived efficiencies, the dependency on the number of jets in the final state, the different MC samples used to derive the efficiencies, and the normalization of the real-lepton component subtracted in the efficiency estimation.

In the $\tau_{\text{lep}}\tau_{\text{had}}$ channel, the misidentified τ background is evaluated using the fake-factor technique [116]. Data events are selected if they satisfy a very loose requirement on the $\tau_{\text{had-vis}}$ identification score but do not satisfy the ‘Medium’ working point criteria. Residual contributions from processes with real $\tau_{\text{had-vis}}$ satisfying this requirement are evaluated using simulations and subtracted. The distribution of the misidentified τ background component in each signal region is obtained by multiplying the contribution of data events selected with the inverted identification criterion by a fake-factor defined as the ratio of misidentified $\tau_{\text{had-vis}}$ that respectively pass or fail the ‘Medium’ working point of the $\tau_{\text{had-vis}}$ identification algorithm. Uncertainties are assigned to this background, taking into account the statistical uncertainties in the fake-factors, the uncertainties associated with the subtraction of the residual contributions from processes with real $\tau_{\text{had-vis}}$, and the uncertainties in the flavour composition estimate.

In the $\tau_{\text{had}}\tau_{\text{had}}$ channel, the misidentified τ background is also determined using a fake-factor approach. The method is similar to the one used in the $\tau_{\text{lep}}\tau_{\text{had}}$ channel, and it takes into account the processes with one or two jets misidentified as $\tau_{\text{had-vis}}$ and the trigger matching. Uncertainties are assigned to this background, taking into account the statistical uncertainties in the fake-factors, differences between fake-factors calculated in different validation regions, and different fake-factor parameterizations.

Other minor backgrounds arising from an electron or a muon misidentified as a τ_{had} are estimated from simulation and, in the case of electrons, corrected for the efficiency measured in data.

Event contributions from the $t\bar{t}$ process are sizeable in the $\tau_e\tau_\mu$ and $\tau_{\text{lep}}\tau_{\text{had}}$ channels, and control regions enriched in top-quark events are defined by replacing the b -jet veto in the event selection (see Table 3) with a requirement of at least one b -tagged jet. This allows the $t\bar{t}$ MC simulation to be validated, and the $t\bar{t}$ process normalization to be determined using data.

7 Systematic uncertainties

Systematic uncertainties affect the yields in the various signal and control regions as well as the distribution shape of the main fit observable ($m_{\tau\tau}$). They can be assigned to three main groups: the experimental uncertainties, the theoretical uncertainties for the backgrounds and the theoretical uncertainties for the signal. Overall, the systematic uncertainties having largest impact on the measurement are similar to those in Ref. [3].

The experimental systematic uncertainties include those affecting the trigger, reconstruction, identification and isolation efficiencies for all the considered particles in the final state, as well as their energy scale and resolution [93, 94, 102, 103, 108–111]. These uncertainties also affect the shape of the $m_{\tau\tau}$ distribution, the background yields and the signal cross-section through their effects on the acceptance and the migration between different event categories. Among the experimental uncertainties, the jet-related uncertainties in the energy scale and resolution are the ones having largest impact on the results discussed in Section 8. The jet energy scale uncertainty includes components related to the in situ calibration of jets as well as pile-up, the extrapolation to higher transverse momentum, and uncertainties in the different responses to quark- and gluon-initiated jets. The jet energy scale uncertainty for central jets ($|\eta| < 1.2$) varies from 1% for a wide range of jet p_T ($250 \text{ GeV} < p_T < 2000 \text{ GeV}$) to 5% for very low p_T jets (20 GeV) and to 3.5% for very high p_T jets ($> 2.5 \text{ TeV}$). The jet energy resolution is measured in a dedicated analysis [102] and ranges from $(24 \pm 5)\%$ at 20 GeV to $(6.0 \pm 0.5)\%$ at 300 GeV.

The uncertainties in the $\tau_{\text{had-vis}}$ identification efficiency range from 2% to 6% and are parameterized as a function of the $\tau_{\text{had-vis}}$ p_T and number of associated tracks. The eBDT efficiency uncertainties are of the order of 1% to 2% and are parameterized as a function of the $\tau_{\text{had-vis}}$ p_T , $\tau_{\text{had-vis}}$ η and τ -lepton decay mode. Since the analysis is sensitive to the $\tau_{\text{had-vis}}$ reconstruction efficiency uncertainty through the usage of the kinematic embedding, this efficiency is left as a free parameter in the fit and measured in situ. The total uncertainty of the $\tau_{\text{had-vis}}$ energy scale ranges from 1% to 4%, and is estimated by combining a direct measurement with $Z \rightarrow \tau\tau \rightarrow \mu\tau_{\text{had-vis}} + 3\nu$ events, measurements of the calorimeter response to single particles, and comparisons between simulations using different detector geometries or GEANT4 physics lists. This uncertainty is also parameterized as a function of the $\tau_{\text{had-vis}}$ p_T and number of associated tracks [111].

For the theoretical uncertainties in the background, the largest impact on the results is due to the uncertainties associated with the Z +jets and $t\bar{t}$ samples. For Z +jets, uncertainties were considered for the renormalization scale (μ_r), factorization scale (μ_f) and resummation scale (μ_q), for the jet-to-parton matching scheme (CKKW), for the choice of α_s value, and for the choice of PDFs. The effects of uncertainties in μ_r and μ_f due to missing higher orders and non-perturbative effects were evaluated using six scale variations in the matrix elements by factors of 0.5 and 2, excluding the extreme variations in opposite directions [117]. The effects of μ_q and CKKW uncertainties were estimated from a comparison with alternative samples generated with a varied resummation scale or jet-to-parton matching scheme, respectively, while the effects of other uncertainties were evaluated from internal-weight variations in simulated samples. For $t\bar{t}$, uncertainties were considered for the choice of matrix element and parton shower generators, the choice

of model for initial- and final-state radiation (ISR and FSR respectively), and the choice of PDFs. The effects of PDF uncertainties were estimated using the PDF4LHC15_{NLO} set of eigenvectors, while the other uncertainties were obtained from a comparison with alternative samples generated using the same settings as the default sample apart from the variation of the parameter for which the uncertainty is estimated.

Several sources of theoretical uncertainty in the signal are considered. For all production modes, uncertainties are considered for the PDF and α_s , the parton shower and hadronization model, and missing higher orders in the matrix element calculation. The effects of PDF and α_s uncertainties were estimated from the PDF4LHC15_{NLO} set of eigenvectors. The impact of using a different parton shower and hadronization model is evaluated by comparing the nominal sample with an event sample generated using HERWIG 7 [118] instead of PYTHIA 8. The impact of using a different matrix element generator for the signal sample is evaluated by comparing the nominal signal sample with an alternative sample generated with MADGRAPH5_AMC@NLO [119] instead of POWHEG BOX, while keeping the same parton shower model.

For the ggF production process, 18 sources of uncertainty related to the ggF kinematics and the cross-section were considered, following the prescription in Ref. [120]. Two uncertainties are assigned for the overall fixed-order and resummation effects. Two uncertainties cover the migrations between different jet-multiplicity bins. Seven uncertainties are associated with the modelling the Higgs boson p_T in different phase-space regions. Four uncertainties take into account dijet mass migrations across the STXS bin boundaries. One uncertainty covers the modelling of the Higgs boson plus two leading jets transverse momentum (p_T^{Hjj}) distribution in the ≥ 2 -jet region. One uncertainty is assigned to the modelling of the distribution of the Higgs boson plus one jet transverse momentum (p_T^{Hj}) divided by p_T^H in the high- p_T^H region. The last uncertainty takes into account the uncertainty from the choice of top-quark mass scheme.

For the VBF and VH processes, ten uncertainties related to the STXS categorization were considered: one related to the inclusive cross-section of the process, one related to the two-jet requirement, one related to the Higgs boson p_T selection at 200 GeV, one related to the p_T balance between the Higgs boson and the dijet system in events with two or three jets, and six which take into account dijet mass migrations across the STXS bin boundaries.

For the $t\bar{t}H$ process, six other uncertainties are included: one related to the inclusive cross-section of the process, and five migration uncertainties related to Higgs boson p_T boundaries in the STXS scheme.

8 Simplified template cross-section measurement results

The statistical analysis for the measurements in this paper is based on a likelihood function constructed as the product of Poisson probability terms over the bins of the input distributions. The systematic uncertainties (described in Section 7) are incorporated in the likelihood function through nuisance parameters that are constrained by Gaussian probability terms that multiply the Poisson probability terms. Poisson terms also describe the expected event counts in each bin of the input distributions. The parameters of interest (POIs) of the model are estimated by maximizing the likelihood. The test statistic is constructed from the profile likelihood ratio, and the confidence intervals for the parameters of interest are derived using the asymptotic approximation [121].

8.1 Simplified template cross-section measurement fit model

For the STXS measurement, the likelihood function is built with the following signal regions (SRs) and control regions (CRs):

- Six SRs for the Boost category in each channel; the SRs are defined starting from the Boost inclusive category defined in Table 4 and further split according to the number of jets and p_T^H . For each SR and channel, a corresponding $Z(\rightarrow \tau\tau) + \text{jets}$ CR is defined using the kinematic embedding described in Section 6. Moreover, a CR enriched in the $t\bar{t}$ process is defined for each inclusive category in the $\tau_e\tau_\mu$ and $\tau_{\text{lep}}\tau_{\text{had}}$ channels. Summing over the SRs, $Z(\rightarrow \tau\tau) + \text{jets}$ CRs and $t\bar{t}$ CRs, and considering the three channels, this leads to 38 Boost categories.
- Two SRs for the VH category in each channel; the SRs are defined starting from the VH inclusive category defined in Table 4 and further split into regions of high and low scores of a BDT trained to distinguish the VH production mode from the other Higgs boson production modes. For each SR and channel, a corresponding $Z(\rightarrow \tau\tau) + \text{jets}$ CR is defined using the kinematic embedding. Moreover, a CR enriched in the $t\bar{t}$ process is defined for each inclusive category in the $\tau_e\tau_\mu$ and $\tau_{\text{lep}}\tau_{\text{had}}$ channels. Summing over the SRs, $Z(\rightarrow \tau\tau) + \text{jets}$ CRs and $t\bar{t}$ CRs, and considering the three channels, 14 VH categories are included in the fit.
- Sixteen SRs for the VBF category in each channel, as described in Section 5.1. For each SR and channel, a corresponding $Z(\rightarrow \tau\tau) + \text{jets}$ CR is defined using the kinematic embedding. Moreover, a CR enriched in the $t\bar{t}$ process is defined for each inclusive category in the $\tau_e\tau_\mu$ and $\tau_{\text{lep}}\tau_{\text{had}}$ channels. Summing over the SRs, $Z(\rightarrow \tau\tau) + \text{jets}$ CRs and $t\bar{t}$ CRs, and considering the three channels, this leads to 98 VBF categories.
- Six SRs and two CRs for the ttH category in the $\tau_{\text{had}}\tau_{\text{had}}$ channel, as described in Section 5.2.

In the SRs, the binned $m_{\tau\tau}$ distribution is used to obtain information about the cross-section relative to the SM prediction. In the Boost and VH SRs, $m_{\tau\tau}$ is reconstructed using only the MMC technique, while in the VBF and ttH SRs $m_{\tau\tau}^{\text{coll}}$ is used for events where the MMC technique failed to estimate the invariant mass. CRs are employed to constrain the event yield of specific background processes with a single-bin histogram containing the number of events in the corresponding CR. In particular, the $Z(\rightarrow \tau\tau) + \text{jets}$ CR provides additional constraining power for the $Z(\rightarrow \tau\tau) + \text{jets}$ background uncertainties, being complementary to the mass distribution in a region centred around the Z boson peak. Three different measurements are performed:

1. *$pp \rightarrow H \rightarrow \tau\tau$ total cross-section*: a single POI, corresponding to the $pp \rightarrow H \rightarrow \tau\tau$ cross-section, is estimated by the fit. In the likelihood function, the signal yields in each category are parameterized as the product of the $pp \rightarrow H \rightarrow \tau\tau$ cross-section, the integrated luminosity and the efficiency (including the acceptance of the ATLAS detector) of the selection for a SM Higgs boson with a mass of 125.09 GeV. In this measurement, the relative contributions to the $pp \rightarrow H \rightarrow \tau\tau$ cross-section from the various production modes are fixed to the SM predictions.
2. *Cross-section per production mode*: four POIs, corresponding to the cross-sections of the four dominant production modes (ggF, VBF, VH, $t\bar{t}H$) of the Higgs boson, are estimated by the fit. In this configuration, the event yields in the likelihood function are the sum of those from each individual production mode, parameterized as a function of the POI similarly to the way for the total cross-section measurement described above.

3. *Simplified Template Cross-Section*: eighteen POIs, corresponding to the cross-sections for different bins of the STXS *stage 1.2* framework, are determined by the fit. The cross-sections are measured for six ggF bins, three $t\bar{t}H$ bins and nine VBF + $qq \rightarrow V(\rightarrow qq)H$ bins. These bins were chosen by combining some of the STXS bins proposed in Ref. [4], taking into account the available signal sample size and the expected sensitivity of the analysis. The $qq \rightarrow V(\rightarrow qq)H$ contribution is measured for events with particle-level dijet mass m_{jj} between 60 GeV and 120 GeV, while the VBF contribution is measured in events with m_{jj} above 350 GeV.

8.2 Simplified template cross-section results

The results of the statistical analysis performed for the total cross-section measurement are presented in Figures 2 to 4. Figures 2 and 3 show the $\tau\tau$ invariant mass distributions, split into low and high ranges of p_T^H and m_{jj} respectively, in VBF_0 and VBF_1 for a subset of the categories used in the analysis. The signal from $H \rightarrow \tau\tau$ is clearly visible on top of the background originating mostly from $Z(\rightarrow \tau\tau)$. Figure 4 shows the expected and observed event yields in the $t\bar{t}H$ categories.

The measurements of the total cross-section and per-production-mode cross-sections are shown in Figure 5. Table 6 shows the impact of the different uncertainty sources on the measurements, while the cross-section measured for each production mode is reported in Table 7. Good agreement with the SM predictions is found, with p -values of 65% and 99% for compatibility of the measurements with the SM for the total cross-section and per-production-mode cross-sections, respectively. The VBF production cross-section normalized to the SM prediction is measured to be $0.93^{+0.17}_{-0.15}$, with slightly better precision than in Ref. [3] ($0.90^{+0.20}_{-0.17}$) due to the improved categorization used in the present analysis. The $t\bar{t}H$ cross-section normalized to the SM prediction is measured to be $0.77^{+1.01}_{-0.92}$, using a more refined multivariate analysis strategy which improves the expected precision by roughly 25% relative to the result in Ref. [3] ($1.06^{+1.28}_{-1.08}$).

Figure 6 shows the results of the STXS measurement. The measurements in the inclusive ggF and VH regions are in good agreement with the SM and are similar to those in Ref. [3] as the selections for these regions have not changed, although some of the theoretical uncertainties have been updated. The eight bins used for VBF production show no significant deviation from the SM. In the phase space with higher p_T^H and/or higher m_{jj} the precision of the results is improved due to the smaller SM backgrounds in these regions, leading to a ratio of the measured cross-section to the SM expectation when $p_T^H > 200$ GeV ($p_T^H < 200$ GeV) and $m_{jj} > 1.5$ TeV of $1.29^{+0.39}_{-0.34}$ ($0.12^{+0.34}_{-0.33}$). This is the first measurement for the higher- p_T^H criteria, and the most precise for the lower- p_T^H criteria, in this corner of phase space. As shown in Figure 7, several VBF production POIs at low p_T^H are strongly anti-correlated with a single POI describing ggF production plus two jets, causing the negative values obtained for the VBF bins at $p_T^H < 200$ GeV. Overall, the p -value for compatibility of this result with the SM is 6%.

The results for $t\bar{t}H$ production are limited by statistical uncertainties, and they are used to derive cross-section upper limits at 95% confidence level (CL) for $t\bar{t}H$ production in the STXS framework, using the CL_s method [122, 123], as shown in Figure 8.

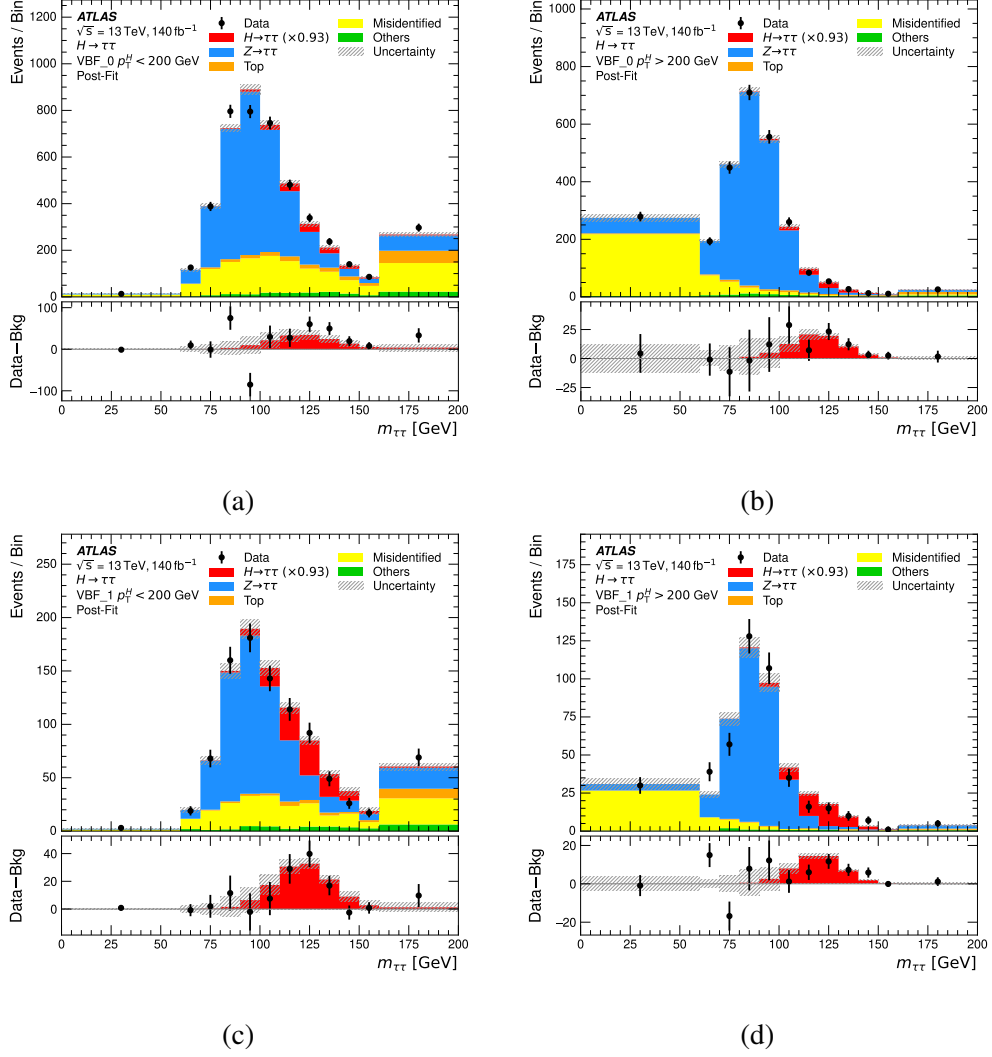


Figure 2: Distribution of the reconstructed $\tau\tau$ invariant mass ($m_{\tau\tau}$) for all events in the (a,b) VBF_0 and (c,d) VBF_1 signal regions for (a,c) $p_T^H < 200$ GeV and (b,d) $p_T^H > 200$ GeV. The bottom panel shows the differences between observed data events and expected background events (black points). The observed Higgs boson signal, corresponding to $(\sigma \times B)/(\sigma \times B)_{\text{SM}} = 0.93$, is shown with a filled red histogram. Entries with values above the x -axis range are shown in the last bin of each distribution. The prediction for each sample is determined from the likelihood fit performed to measure the total $pp \rightarrow H \rightarrow \tau\tau$ cross-section.

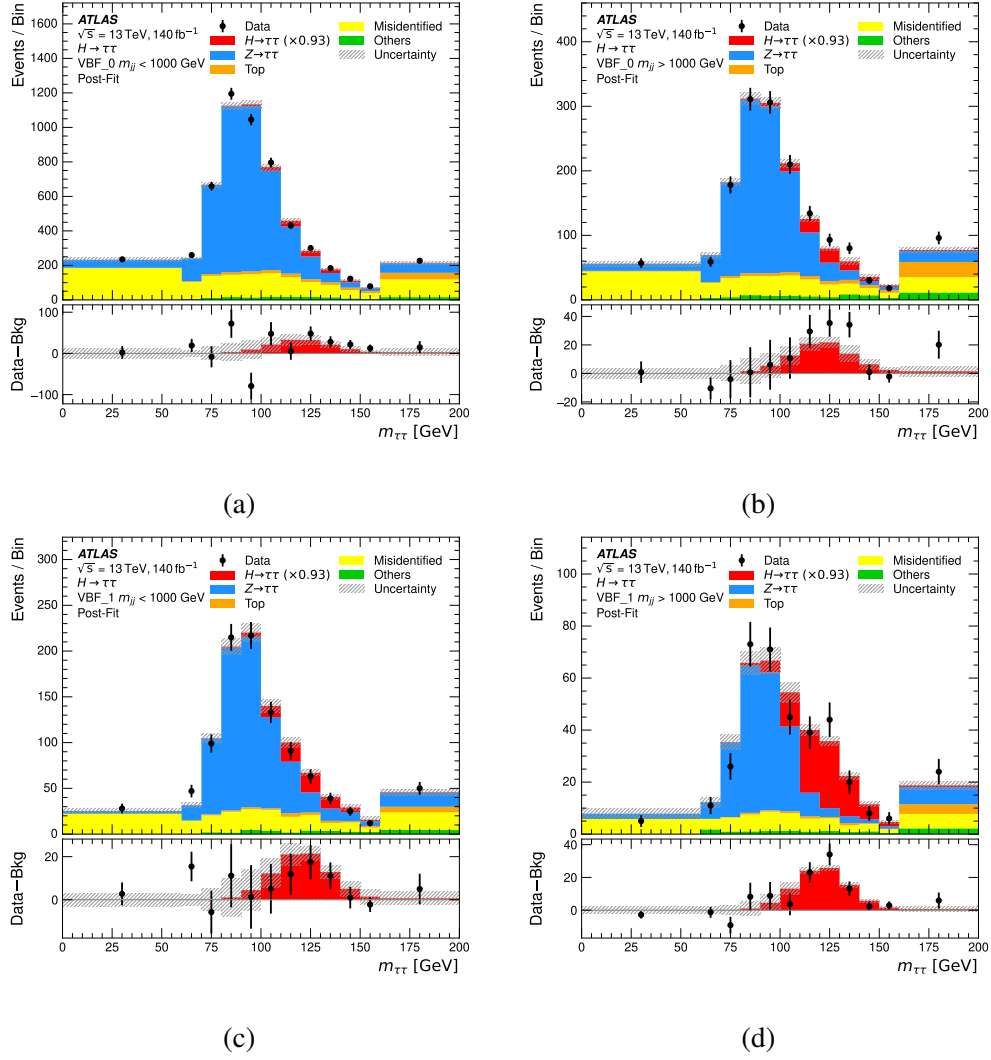


Figure 3: Distribution of the reconstructed $\tau\tau$ invariant mass ($m_{\tau\tau}$) for all events in the (a,b) VBF_0 and (c,d) VBF_1 signal regions for (a,c) $m_{jj} < 1$ TeV and (b,d) $m_{jj} > 1$ TeV. The bottom panel shows the differences between observed data events and expected background events (black points). The observed Higgs boson signal, corresponding to $(\sigma \times B)/(\sigma \times B)_{\text{SM}} = 0.93$, is shown with a filled red histogram. Entries with values above the x -axis range are shown in the last bin of each distribution. The prediction for each sample is determined from the likelihood fit performed to measure the total $pp \rightarrow H \rightarrow \tau\tau$ cross-section.

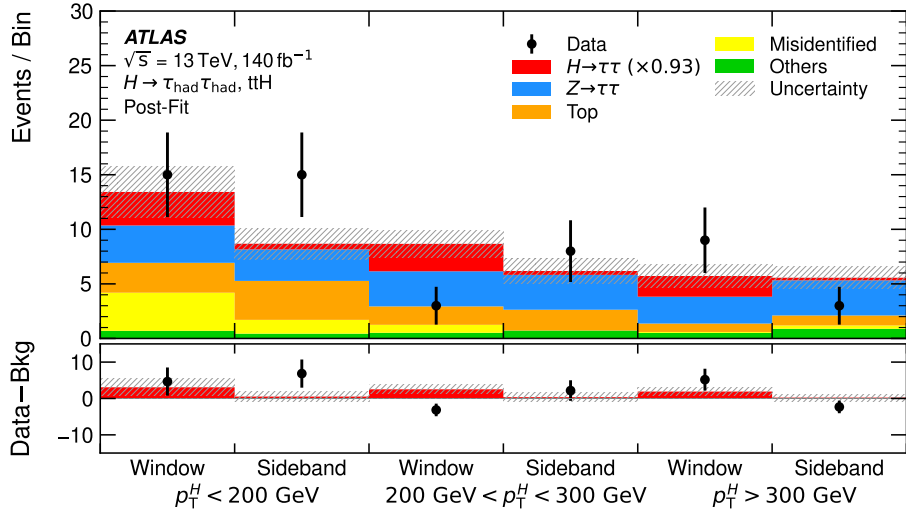


Figure 4: Comparison of the observed and expected event yields in the $t\bar{t}H$ categories. The *window* category contains events with $m_{\tau\tau} \in [100, 150]$ GeV, while events outside of this mass region are included in the *sideband* region. The bottom panel shows the differences between observed data events and expected background events (black points). The observed Higgs boson signal, corresponding to $(\sigma \times B)/(\sigma \times B)_{\text{SM}} = 0.93$, is shown with a filled red histogram. The prediction for each sample is determined from the likelihood fit performed to measure the total $pp \rightarrow H \rightarrow \tau\tau$ cross-section.

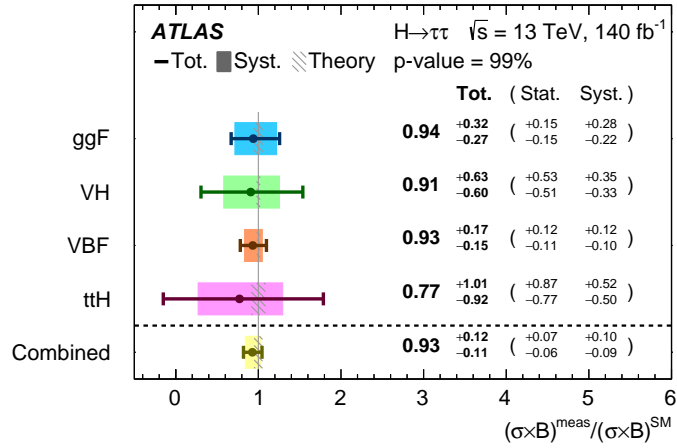


Figure 5: The measured values of $\sigma_H \times B(H \rightarrow \tau\tau)$ relative to the SM expectations in the total (labelled as ‘Combined’) and per-production-mode fit. The total $\pm 1\sigma$ uncertainty in each measurement is indicated by the error bar, with the contribution from the systematic uncertainty indicated by the coloured band.

Table 6: Summary of the different sources of uncertainty in the ratio of $\sigma_H \times B(H \rightarrow \tau\tau)$ to the SM expectation for each production mode. Experimental uncertainties for reconstructed objects combine efficiency and energy/momentum scale and resolution uncertainties. Samples size includes the bin-by-bin statistical uncertainties in the simulated backgrounds as well as statistical uncertainties in misidentified τ backgrounds, which are estimated using data. Entries with no significant impact on the measurement are denoted by ‘-’.

Production mode	ggF	ttH	VBF	VH
Best-fit value	0.94	0.77	0.93	0.91
Total uncertainty	± 0.30	± 0.97	± 0.16	± 0.62
Statistical uncertainty	± 0.15	± 0.82	± 0.12	± 0.52
Total systematic uncertainty	± 0.26	± 0.51	± 0.11	± 0.34
Samples size	± 0.09	± 0.32	± 0.03	± 0.25
Theoretical uncertainty in signal	± 0.19	± 0.14	± 0.10	± 0.13
Jet and E_T^{miss}	± 0.12	± 0.14	± 0.03	± 0.11
Hadronic τ -lepton decays	± 0.05	± 0.09	± 0.01	± 0.04
Misidentified τ -lepton background	± 0.05	± 0.05	± 0.02	± 0.11
Luminosity	± 0.01	± 0.01	± 0.01	± 0.02
Theoretical uncertainty in top-quark processes	± 0.01	± 0.30	-	± 0.02
Theoretical uncertainty in Z + jets processes	± 0.03	± 0.07	-	± 0.02
Flavour tagging	± 0.02	± 0.05	± 0.01	± 0.01
Electrons and muons	± 0.02	± 0.01	± 0.01	± 0.02

Table 7: Best-fit values and uncertainties of the $\sigma_H \times B(H \rightarrow \tau\tau)$ for the four dominant production modes. The uncertainties include both the statistical and systematic components. The SM predictions for each region, computed using the inclusive cross-section calculations and the simulated event samples, are also shown.

Production mode	$\sigma_H \times B(H \rightarrow \tau\tau)$ [pb]	
	SM prediction	Measurement
ggF	2.77 ± 0.09	2.6 ± 0.9
VH	0.117 ± 0.003	0.11 ± 0.07
VBF	0.220 ± 0.005	0.20 ± 0.04
$t\bar{t}H$	0.031 ± 0.003	0.02 ± 0.03

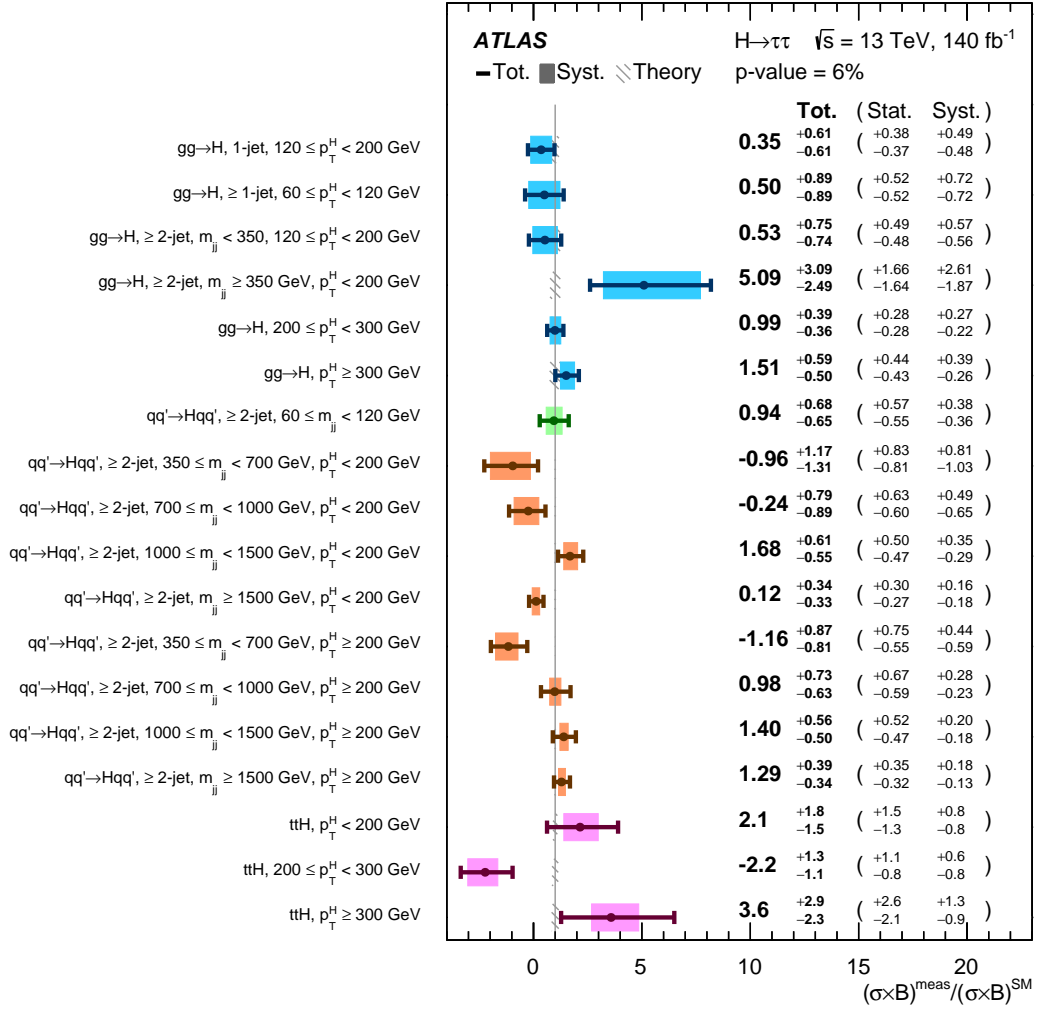


Figure 6: The measured values for $\sigma_H \times B(H \rightarrow \tau\tau)$ relative to the SM expectations in the simplified template cross-section measurement. The error bars and shaded areas show the total uncertainty and systematic uncertainty in the measurements, respectively.

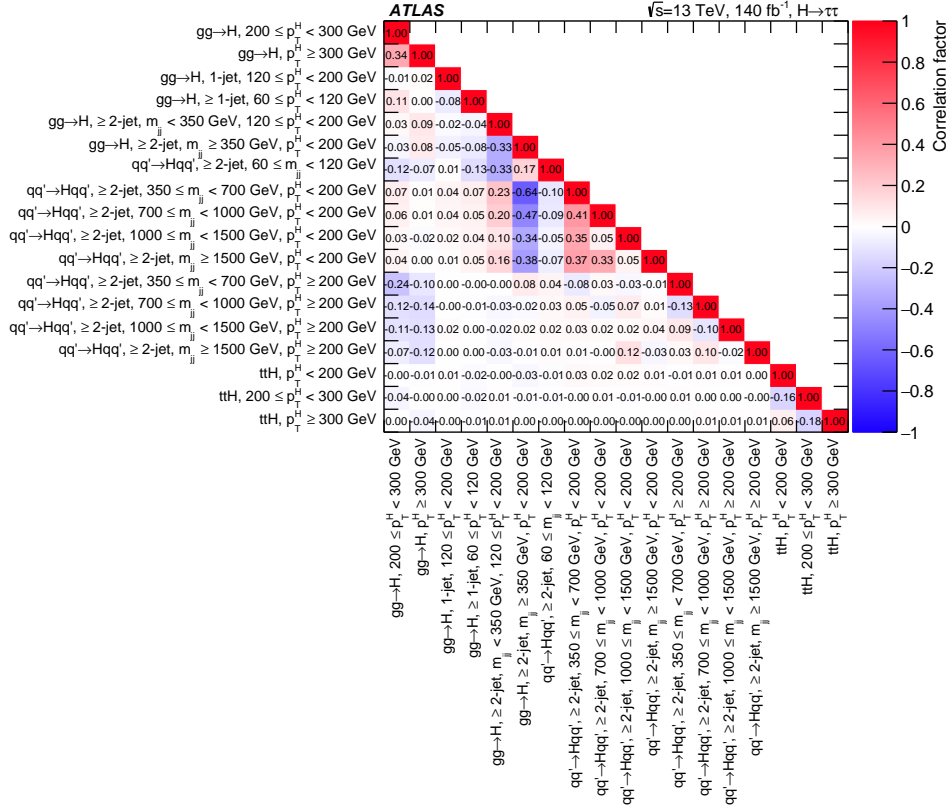


Figure 7: Measured linear correlation factors between each pair of parameters of interest in the simplified template cross-section measurement.

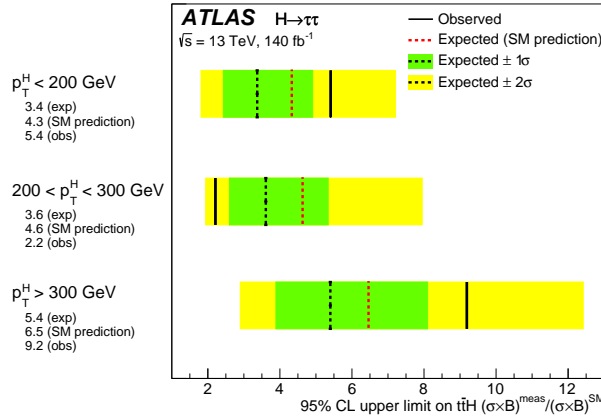


Figure 8: Upper limits at 95% CL on simplified template cross-sections in the individual $t\bar{t}H$ p_T^H bins relative to their SM expectation in the $H \rightarrow \tau\tau$ decay channel, derived using the CL_s method. The observed upper limits (solid black lines) are shown, together with the expected limits both in the background-only hypothesis (dotted black lines) and in the SM hypothesis (dotted red lines). In the case of the expected limits in the background-only hypothesis, one- and two-standard-deviation uncertainty bands are also shown.

9 Unfolded fiducial differential cross-section measurement results

Another way to study the properties of VBF Higgs boson production is to measure its cross-section in a fiducial phase space that targets the VBF phase space defined by detector acceptance and selection requirements. The measured cross-sections are inclusive in the production process, thus minimizing SM assumptions. The measurements are corrected for detector effects and efficiencies (unfolded) using the combined SM MC prediction of VBF, ggF, VH and $t\bar{t}H$ production.

The fiducial differential cross-section is defined in each particle-level kinematic bin, i , of the variable under study as shown in Eq. (1):

$$\sigma_i^{\text{fid}} = \frac{1}{\mathcal{L}\epsilon_i} \sum_j \mathcal{M}_{ij}^{-1} f_j (N_j^{\text{data}} - N_j^{\text{bkg}}), \quad (1)$$

where j is the reconstruction-level bin index, \mathcal{L} is the integrated luminosity, and \mathcal{M} is the migration matrix for events passing both reconstruction- and fiducial-level selections. \mathcal{M} gives the probability that an event in particle-level bin i is reconstructed in reconstruction-level bin j . The selection efficiency ϵ_i is defined as the number of events passing both the fiducial- and reconstruction-level selections divided by the number of events passing the fiducial-level selection. The out-of-acceptance correction f_j is defined as the number of events passing both the fiducial- and reconstruction-level selections divided by the number of events that pass the reconstruction-level selection. This is multiplied by the number of signal events in the SRs, defined as the number of events observed in data (N_j^{data}) after the estimated total number of background events (N_j^{bkg}) is subtracted. \mathcal{M} , ϵ_i , and f_j are determined using the SM signal MC prediction.

In the following, the fiducial phase space is defined, the measured variables are introduced, the likelihood fit model is discussed, and the results of the fiducial differential cross-section measurement are presented.

9.1 Fiducial phase space

The fiducial differential cross-sections are evaluated in a fiducial phase space. This phase space is defined by particle-level kinematic criteria which closely follow the differential inclusive VBF selection applied at reconstruction level and are defined in Tables 3 and 4. The fiducial phase space, in which VBF production constitutes approximately 83% of the Higgs boson signal, and ggF production approximately 17%, is defined in Table 8. The VBF, ggF, VH , and $t\bar{t}H$ Higgs boson production modes are combined as signal, and their relative contributions are fixed to the SM predictions.

For the object definition, only stable final-state particles (with a mean lifetime $c\tau > 10$ mm) are considered at particle level. Electrons and muons are required to not originate from hadrons or hadronic decay products. Their four-momenta are corrected by adding the momenta of final-state radiation photons emitted in a cone of size $\Delta R = 0.1$ around the lepton direction. Hadronically decaying τ -leptons (denoted by τ_{truth} at particle level) are reconstructed by identifying all stable τ -lepton decay particles except for neutrinos and summing their four-momenta. All leptons are required to have $|\eta| < 2.5$, and electrons are excluded from the LAr transition region $1.37 < |\eta| < 1.52$. Jets are defined by clustering all stable particles using the anti- k_r algorithm with a radius parameter of $R = 0.4$. The clustering algorithm excludes prompt leptons and Higgs boson decay products. Jets are required to be separated from τ_{truth} ($\Delta R > 0.4$) and light leptons ($\Delta R > 0.2$), and are required to have $|\eta| < 4.5$. The missing transverse momentum is defined as the vector sum of the transverse momenta of all neutrinos that do not originate from the decay of a hadron.

Table 8: Summary of the fiducial particle-level event selection for all channels. The requirements on light-lepton p_T and $\tau_{\text{truth}} p_T$ follow those reported in Table 3.

	$\tau_e \tau_\mu$	$\tau_{\text{lep}} \tau_{\text{had}}$	$\tau_{\text{had}} \tau_{\text{had}}$
Per Channel			
Object counting	$N_e = 1, N_\mu = 1, N_{\tau_{\text{truth}}} = 0$	$N_{e/\mu} = 1, N_{\tau_{\text{truth}}} = 1$	$N_{e/\mu} = 0, N_{\tau_{\text{truth}}} = 2$
p_T cut	e/μ : p_T cut 10 to 27.3 GeV	e/μ : p_T cut 27.0 to 27.3 GeV, τ_{truth} : $p_T > 30$ GeV	τ_{truth} : $p_T > 40, 30$ GeV
Kinematics	$m_{\tau\tau}^{\text{coll}} > m_Z - 25$ GeV $30 < m_{e\mu} < 100$ GeV	$m_T < 70$ GeV	
Angular	$\Delta R_{e\mu} < 2.0, \Delta\eta_{e\mu} < 1.5$	$\Delta R_{\ell\tau_{\text{truth}}} < 2.5, \Delta\eta_{\ell\tau_{\text{truth}}} < 1.5$	$0.6 < \Delta R_{\tau_{\text{truth}}\tau_{\text{truth}}} < 2.5$ $ \Delta\eta_{\tau_{\text{truth}}\tau_{\text{truth}}} < 1.5$
x_1 and x_2	$0.1 < x_1 < 1.0, 0.1 < x_2 < 1.0$	$0.1 < x_1 < 1.4, 0.1 < x_2 < 1.2$	$0.1 < x_1 < 1.4, 0.1 < x_2 < 1.4$
Common selection	leading jet $p_T > 40$ GeV, sub-leading jet $p_T > 30$ GeV $E_T^{\text{miss}} > 20$ GeV Opposite charge of τ -decay products $m_{jj} > 600$ GeV, $ \Delta\eta_{jj} > 3.4, p_T(jj) > 30$ GeV $\eta(j_0) \times \eta(j_1) < 0$ lepton centrality: visible decay products of the τ -leptons between VBF jets $p_T(Hjj) < 50$ GeV		

9.2 Differential variables

The differential cross-sections are measured in the fiducial phase space as a function of variables sensitive to the kinematics of VBF Higgs boson production, with the goal of validating the SM as well as providing sensitivity to physics beyond the SM. The variables related to jets are the transverse momentum of the leading jet, $p_T(j_0)$, and the signed angle (sorted by rapidity of the jets) in the transverse plane of the two jets, $\Delta\phi_{jj}^{\text{signed}}$, which also provides a way to test of the charge (C) and parity (P) of the Higgs boson. The kinematics of the Higgs boson is tested by measuring its transverse momentum (p_T^H). As in the STXS measurement, the NN reconstruction of p_T^H , introduced in Section 5.1, is used at reconstruction level. To increase the sensitivity to the CP property of the Higgs boson, $\Delta\phi_{jj}^{\text{signed}}$ is also measured as a function of p_T^H . The binning of each differential distribution is driven by the size of the available data sample and is reported in Table 9.

Table 9: Binning of the differential variables.

	$p_T(j_0)$ [GeV]	p_T^H [GeV]	$\Delta\phi_{jj}^{\text{signed}}$	$\Delta\phi_{jj}^{\text{signed}}$ vs p_T^H [GeV]
Bin 1	[40, 95]	[0, 110]	$[-\pi, -\pi/2]$	$\Delta\phi_{jj}^{\text{signed}} < 0$ & $p_T^H < 200$
Bin 2	[95, 130]	[110, 150]	$[-\pi/2, 0]$	$\Delta\phi_{jj}^{\text{signed}} > 0$ & $p_T^H < 200$
Bin 3	[130, 180]	[150, 200]	$[0, \pi/2]$	$\Delta\phi_{jj}^{\text{signed}} < 0$ & $p_T^H > 200$
Bin 4	[180, 500]	[200, 550]	$[\pi/2, \pi]$	$\Delta\phi_{jj}^{\text{signed}} > 0$ & $p_T^H > 200$

The migration matrix is highly diagonal for all variables considered, with values above 75%, 85%, 95% and 90% for the $p_T(j_0)$, p_T^H , $\Delta\phi_{jj}^{\text{signed}}$, and $\Delta\phi_{jj}^{\text{signed}}$ vs p_T^H distributions. This is due to the binning being coarse compared to experimental resolution effects. The selection efficiency, ϵ_i , includes the effect of object reconstruction efficiencies and event-level selections. These are 25%, 15%, and 43% for the $\tau_{\text{lep}}\tau_{\text{had}}$, $\tau_{\text{had}}\tau_{\text{had}}$, and $\tau_e\tau_\mu$ channels respectively. The out-of-acceptance corrections, f_j , range from 74% to 83% across the channels.

9.3 Differential cross-section measurement fit model

For the differential cross-section measurement, the likelihood function is built with the following SRs and CRs:

- Eight SRs for the VBF category in each channel, based on the BDT-based splitting, as described in Section 5.1, plus the different bins reported in Table 9.
- Two $Z(\rightarrow \tau\tau) + \text{jets}$ control regions in each channel, one for each inclusive VBF_0 and VBF_1 SR, defined using the kinematic embedding.
- A CR enriched in the $t\bar{t}$ process, defined for each inclusive category in the $\tau_e\tau_\mu$ and $\tau_{\text{lep}}\tau_{\text{had}}$ channels.

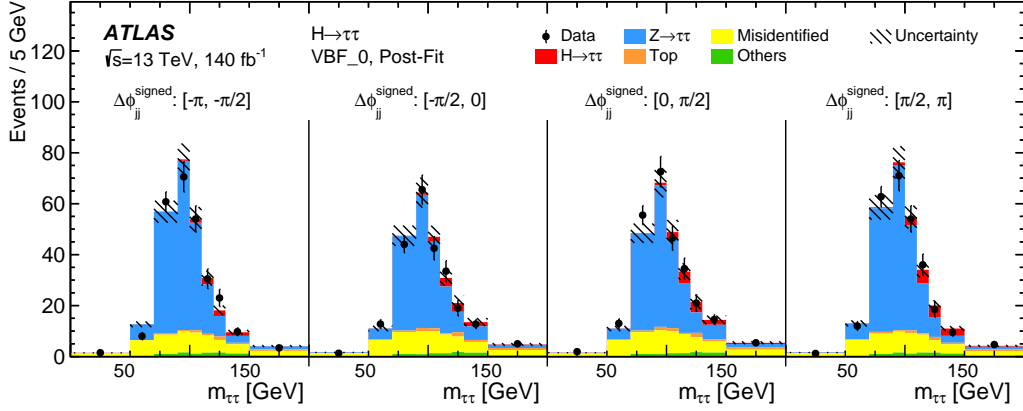
Similarly to the STXS cross-section measurement set-up, the $m_{\tau\tau}$ distribution is used to obtain information about the cross-section relative to the SM prediction, and a single-bin histogram is used for each CR to constrain the background normalization. The detector-level $m_{\tau\tau}$ distributions for each bin of the $\Delta\phi_{jj}^{\text{signed}}$ observable (specified in Table 9) are shown in Figure 9 and compared with the MC templates after the likelihood fit. In these distributions, all three analysis channels are combined in the VBF_0 and VBF_1 SRs.

The differential measurements are performed by using the profile-likelihood unfolding [124] in the signal regions. The free parameters of the fit are the Higgs boson production cross-sections in each bin of the distribution at particle level. No regularization is applied, due to the small bin-to-bin migrations for all variables considered. The performance of the unfolding procedure is tested for possible biases from the choice of MC model. It is verified that it reproduces altered shapes well within the statistical precision of the measurements.

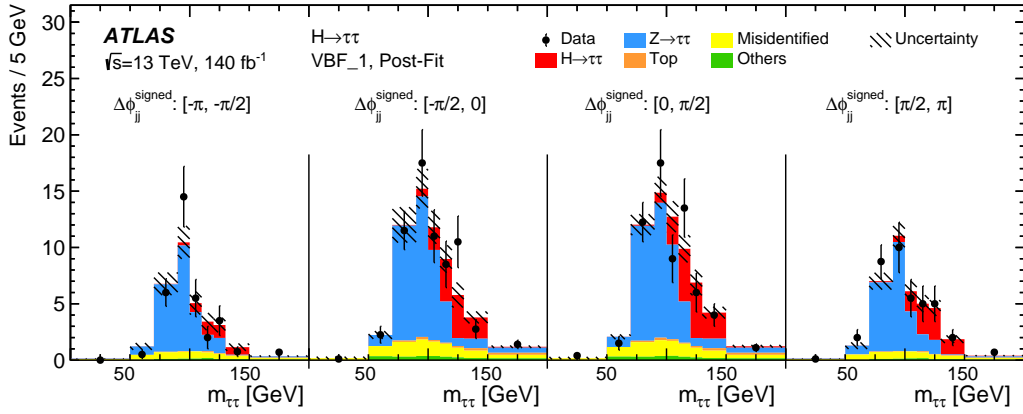
9.4 Differential cross-section measurement results

The fiducial differential cross-sections as a function of the variables of interest are shown in Figure 10. The per-bin precision of the differential cross-section measurements is typically 25%–50%, except for the lowest p_T^H bin, where it reaches 300%. The experimental precision is dominated by the statistical uncertainties in most of the bins, particularly at high values of p_T^H and $p_T(j_0)$. Leading systematic uncertainties, depending on the measured bin, are the limited statistics of the background model, experimental uncertainties for jets and τ -leptons, and uncertainties in the fake-lepton background estimation.

The data are compared with SM predictions from the POWHEG+PYTHIA 8, POWHEG+HERWIG 7 and MADGRAPH5_AMC@NLO+PYTHIA 8 generators for the VBF, ggF, VH , and $t\bar{t}H$ Higgs boson production modes, which are combined according to their SM branching ratios. The theoretical uncertainty in these predictions is much smaller than the experimental uncertainty in the measurements. The RIVET analysis library [125] is used to apply the fiducial selections and calculate the observables to obtain the differential



(a)



(b)

Figure 9: Distribution of the reconstructed $\tau\tau$ invariant mass ($m_{\tau\tau}$) for all events in the (a) VBF_0 and (b) VBF_1 signal regions, shown for each bin of the $\Delta\phi_{jj}^{\text{signed}}$ observable. The observed Higgs boson signal is scaled by the cross-section measured in each bin. Entries with values outside the x -axis range are shown in the last bin of each distribution. The prediction for each sample is determined from the likelihood fit performed to measure the fiducial differential cross-section.

cross-section predictions. Overall, there is good agreement between measured cross-sections and the SM predictions from all generators, with only a few bins showing discrepancies of more than one standard deviation.

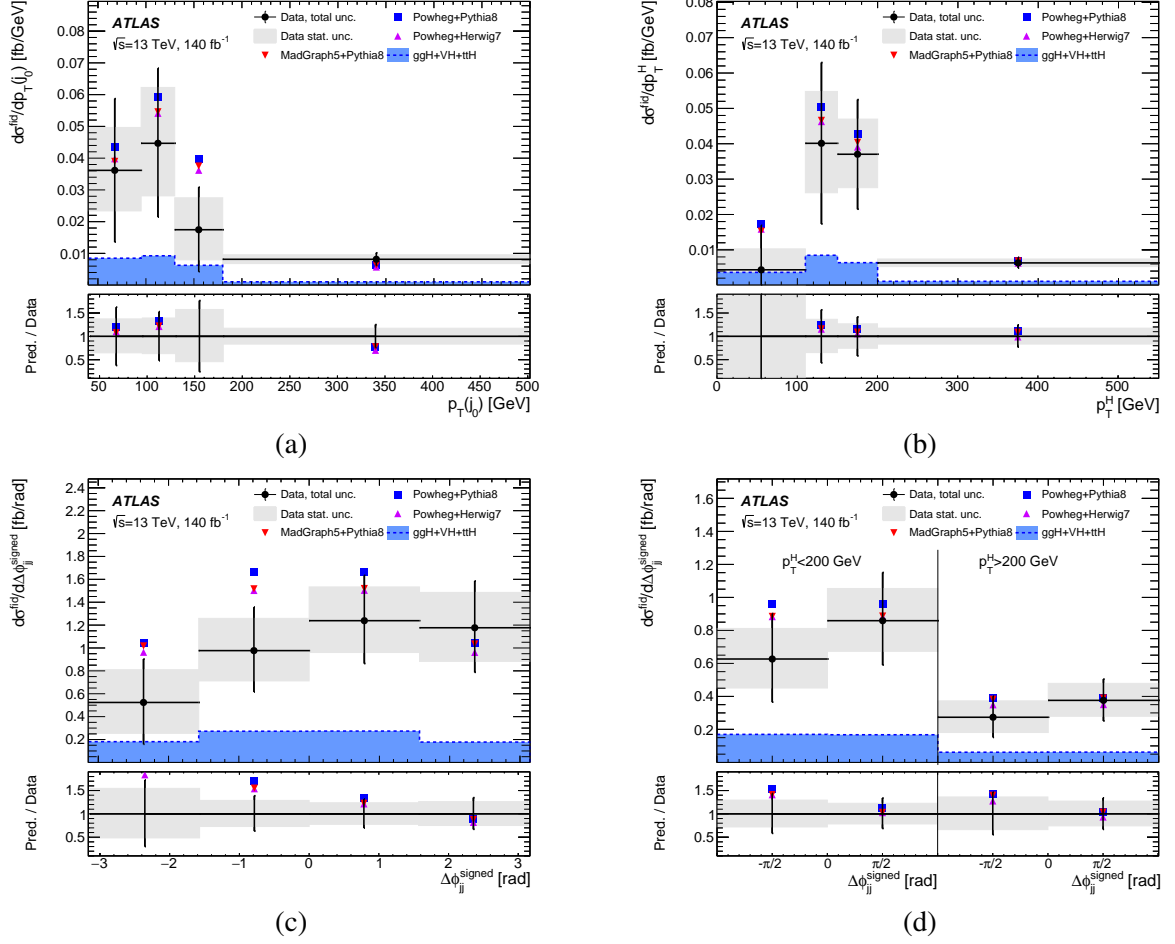


Figure 10: Measured fiducial differential cross-sections for (a) $p_T(j_0)$, (b) p_T^H , (c) $\Delta\phi_{jj}^{\text{signed}}$, and (d) $\Delta\phi_{jj}^{\text{signed}}$ vs p_T^H . The measurements are compared with particle-level SM predictions from the POWHEG+PYTHIA 8, POWHEG+HERWIG 7 and MADGRAPH5_AMC@NLO+PYTHIA 8 generators for the combined VBF, ggF, VH , and $t\bar{t}H$ Higgs boson production modes. The shaded box around each data point shows the statistical uncertainty, while the total uncertainty is indicated by the error bar. The contribution from the ggF, VH , and $t\bar{t}H$ production modes as predicted by POWHEG+PYTHIA 8 is also shown. The bottom panel shows the ratio of different predictions to the data, with the error bars and shaded bands representing the total and statistical uncertainties of the measurements, respectively.

9.5 Interpretation of the differential cross-section measurement in an Effective Field Theory

The unfolded distributions are sensitive to effects beyond-the-SM (BSM) contributions in VBF Higgs boson production. This motivates the interpretation of the results in a generic *Effective Field Theory* (EFT) that parameterizes these potential BSM effects. Anomalous higher-dimensional operators are added to the SM Lagrangian to encapsulate the effects of BSM physics at higher scales, as shown in Eq. (2):

$$\mathcal{L}_{\text{EFT}} = \mathcal{L}_{\text{SM}} + \sum_d \sum_i \frac{c_i^{(d)}}{\Lambda^{d-4}} \mathcal{O}_i^{(d)}, \text{ for } d > 4. \quad (2)$$

The parameters $c_i^{(d)}$, referred to as Wilson coefficients, specify the strength of the anomalous interactions introduced by their corresponding operators, $\mathcal{O}_i^{(d)}$, where the index i runs over all possible operators, and Λ sets the scale of the BSM physics. Only dimension-six operators are considered since the dimension-five and dimension-seven operators violate lepton- or baryon-number conservation, and the impact of higher-dimensional operators is expected to be further suppressed [126]. In this scenario, only the ratio $c_i^{(d=6)}/\Lambda^2$ determines the strength of the BSM physics and Λ is chosen to be 1 TeV by convention.

In the Warsaw basis [127] of the *Standard Model Effective Field Theory* (SMEFT) formalism [128], there are three CP-even and three CP-odd operators that directly affect the interactions between the Higgs boson and the vector bosons; they are listed alongside their corresponding Wilson coefficients in Table 10. The change in the cross-section for each kinematic bin as a function of the Wilson coefficients follows a second-order polynomial as there is an interference term which depends linearly on the Wilson coefficient and a quadratic term that is purely from BSM physics as shown in Eq. (3):

$$\sigma_{\text{SM+EFT}} \propto |\mathcal{M}_{\text{SM}} + \sum_i \frac{c_i}{\Lambda^2} \mathcal{M}_i|^2 = |\mathcal{M}_{\text{SM}}|^2 + 2 \sum_i \frac{c_i}{\Lambda^2} \mathcal{R}(\mathcal{M}_{\text{SM}}^* \mathcal{M}_i) + \sum_{i,j} \frac{c_i c_j}{\Lambda^4} \mathcal{R}(\mathcal{M}_i^* \mathcal{M}_j). \quad (3)$$

Therefore, for each Wilson coefficient, the dependence in each kinematic bin, k , can be parameterized using the form

$$\sigma_{\text{SM+EFT}}^k = \sigma_{\text{SM}}^k \left(1 + \alpha_{ik} \frac{c_i}{\Lambda^2} + \beta_{ik} \left(\frac{c_i}{\Lambda^2} \right)^2 \right). \quad (4)$$

The coefficients α_{ik} and β_{ik} are determined from simulated samples with different values of c_i produced using MADGRAPH5_AMC@NLO 2.9.5 with the SMEFTsim [128, 129] model in the $U(3)^5$ flavour-symmetric limit with $\Lambda = 1$ TeV. The events were generated at LO using the NNPDF3.0_{NLO} PDF set and were showered using PYTHIA 8.245 with the A14 tune. The dependence was determined relative to a SM sample produced using the same set-up and validated against the sample described in Section 3. These fractional changes determined from these BSM samples are then applied to the VBF cross-section predictions from the POWHEG Box v2 sample showered with PYTHIA 8.230 also described in Section 3. For the small contributions from Higgs boson production processes other than VBF, the various other samples described in Section 3 are used.

The linear term that is determined by α comes from the interference of the new physics with the SM matrix element and enters at the lowest order in $\mathcal{O}(\Lambda^{-2})$. The second, quadratic, term is purely from the new-physics contribution and enters at $\mathcal{O}(\Lambda^{-4})$. However, potential terms from dimension-8 operators interfering with the SM would also enter at the same order in $1/\Lambda$. Therefore, for the validity of the EFT approach only considering dimension-6 operators, it is desirable that the contribution from the quadratic term is small and the results are dominated by the contributions from the linear term which enters at

Table 10: The three CP-even and three CP-odd operators and their corresponding Wilson coefficients which directly impact the interactions between the Higgs boson and vector bosons.

	CP-even		
Operator $O_i^{(d=6)}$	$H^\dagger HW_{\mu\nu}^n W^{n\mu\nu}$	$H^\dagger HB_{\mu\nu} B^{\mu\nu}$	$H^\dagger \tau^n HW_{\mu\nu}^n B^{\mu\nu}$
Wilson coefficient	c_{HW}	c_{HB}	c_{HWB}
	CP-odd		
Operator $O_i^{(d=6)}$	$H^\dagger H\tilde{W}_{\mu\nu}^n W^{n\mu\nu}$	$H^\dagger H\tilde{B}_{\mu\nu} B^{\mu\nu}$	$H^\dagger \tau^n H\tilde{W}_{\mu\nu}^n B^{\mu\nu}$
Wilson coefficient	$c_{H\tilde{W}}$	$c_{H\tilde{B}}$	$c_{H\tilde{W}B}$

$O(\Lambda^{-2})$. To assess this, when considering each of the operators in Table 10, measurements are made considering the full form of Eq. (4), and also excluding the quadratic term.

Figure 11 shows the impact of several values of c_{HW} and $c_{H\tilde{W}}$ on the distributions of $\Delta\phi_{jj}^{\text{signed}}$, p_T^H , and $\Delta\phi_{jj}^{\text{signed}}$ vs p_T^H , demonstrating that these variables are sensitive to BSM effects. Due to the CP-odd nature of the operator associated with $c_{H\tilde{W}}$, an asymmetric impact is seen in $\Delta\phi_{jj}^{\text{signed}}$ and additionally it is seen that the relative magnitude of the effect is enhanced by the cut on p_T^H in the two-dimensional distribution. For c_{HW} , effects are seen in both the $\Delta\phi_{jj}^{\text{signed}}$ and p_T^H distributions and, contrary to $c_{H\tilde{W}}$, the effects are symmetric in $\Delta\phi_{jj}^{\text{signed}}$ due to the CP-even nature of the associated operator.

Firstly considered is the scenario where only one of the Wilson coefficients is non-zero and the rest are neglected. The unfolded data are used along with the theoretical dependence of the cross-section on the Wilson coefficients to extract the best-fit value of each of the six considered Wilson coefficients. The same profile-likelihood formalism as presented in Section 9.3 is used with only one degree of freedom introduced, corresponding to the floating Wilson coefficient, and all other Wilson coefficients are set to zero. A scan of the negative log-likelihood described in Section 9.3 is performed for different values of each Wilson coefficient, with the cross-section in each bin fixed to the value predicted by the SMEFT. By considering the change in the negative log-likelihood from its minimum value, the 95% confidence interval for each Wilson coefficient is found. This is done for only the linear term as well as for both the linear and quadratic terms. For the Wilson coefficients associated with CP-even operators the $\Delta\phi_{jj}^{\text{signed}}$ distribution is used, while for those associated with CP-odd operators the $\Delta\phi_{jj}^{\text{signed}}$ vs p_T^H distribution is used. These are the distributions that give the best expected precision. Figure 12 shows the expected and observed confidence intervals for each of the six coefficients individually. Other than for the c_{HWB} coefficient, the intervals considering only the linear term are very similar to the one when both the linear and quadratic terms are considered. Therefore, the approach of using an EFT only considering dimension-six operators is valid for most of the operators considered in the analysis. The observed (expected) intervals for c_{HW} and $c_{H\tilde{W}}$ are $[-1.85, +0.57]$ ($[-1.17, +1.23]$) and $[-0.31, +0.88]$ ($[-0.60, +0.60]$) in the linear scenario and are the most stringent among the considered coefficients. The constraints on $c_{H\tilde{W}}$ are the tightest to date.

The operators considered are closely related and new physics could result in contributions from multiple operators [130] such that it is also interesting to explore the case where two of the operators are non-zero. This proceeds in the same way by scanning the change in negative log-likelihood across a plane of two of the Wilson coefficients while the others are set to zero. Only terms which enter at $O(\Lambda^{-2})$ are considered. The first plane considered, in Figure 13(a), is c_{HW} vs c_{HB} where the $\Delta\phi_{jj}^{\text{signed}}$ distribution is used to perform the measurement. The effects of these two coefficients are very similar such that there is a ‘flat direction’ where the effects of the two Wilson coefficients cancel each other out and there is no sensitivity

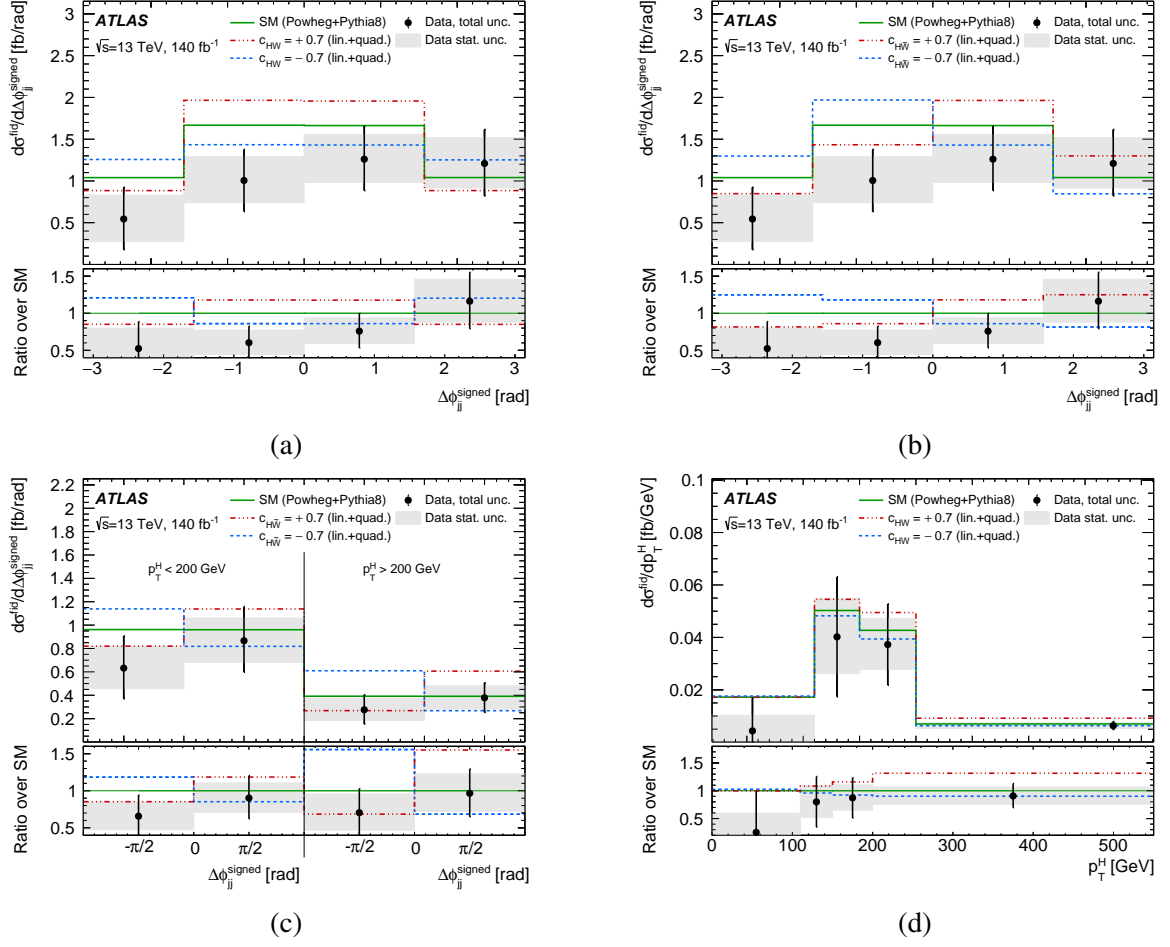


Figure 11: The unfolded data compared with the nominal SM predictions from POWHEG+PYTHIA 8, as well as the predictions for several values of Wilson coefficients in the SMEFT, for (a,b) $\Delta\phi_{jj}^{\text{signed}}$, (c) $\Delta\phi_{jj}^{\text{signed}}$ vs p_T^H and (d) p_T^H .

from the analysis. As one moves away from this direction the analysis gains sensitivity and can constrain the allowed values of the coefficients. In Ref. [131] a fit across multiple Higgs analyses measured the Higgs boson's decay width into two photons or into a Z boson and a photon. These two decay channels only proceed through loop diagrams in the SM so they are very sensitive to BSM physics contributions which have been calculated at NLO [132, 133]. These channels also have ‘flat directions’ where the $O(\Lambda^{-2})$ contributions from the two operators cancel each other out. However, these are different from the ‘flat direction’ in this analysis, showing the complementarity of the different types of measurement and that multiple measurements are required to constrain the multi-dimensional EFT parameter space. It should also be noted that while in the displayed plane c_{HWB} is set to zero, both this analysis and the two decay widths also have a dependence on this parameter such that in three dimensions any two measurements will still have a direction in which neither is sensitive. The second considered plane, in Figure 13(b), is $c_{H\bar{W}}$ vs $c_{H\bar{B}}$, where the $\Delta\phi_{jj}^{\text{signed}}$ vs p_T^H distribution is used. This also shows a ‘flat direction’ and also tighter constraints than the first plane because of the two-dimensional distribution used. There are no constraints from Higgs boson decay widths in this case, due to the CP-odd nature of the operators. Finally, the plane of c_{HW} vs $c_{H\bar{W}}$ in Figure 13(c) is considered using the $\Delta\phi_{jj}^{\text{signed}}$ distribution. In this case the two operators

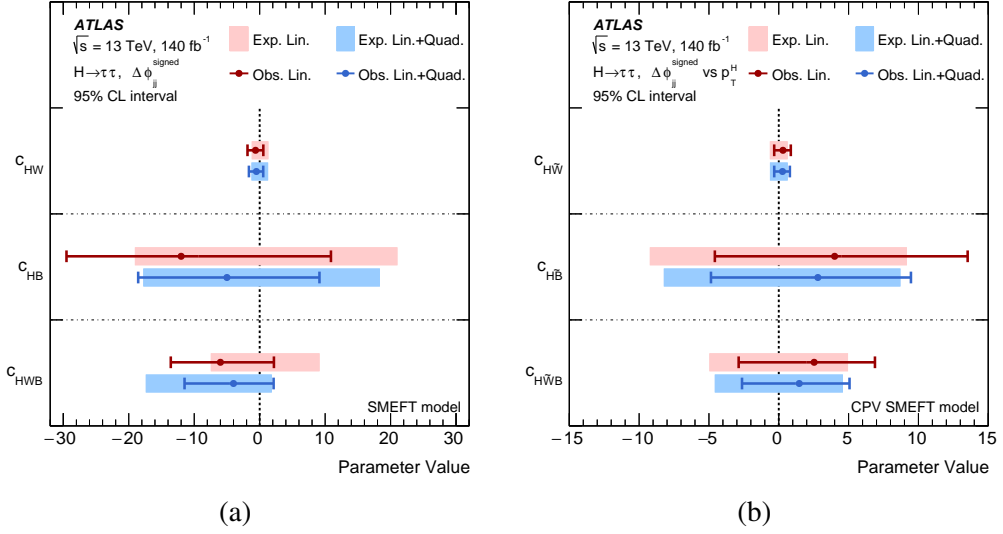


Figure 12: The 95% expected and observed confidence intervals for each of the six considered Wilson coefficients. Each coefficient is treated individually and both the linear and linear + quadratic models are considered when evaluating the sensitivity to the terms that enter at $\mathcal{O}(\Lambda^{-4})$. For the (a) CP-even operators the $\Delta\phi_{jj}^{\text{signed}}$ distribution is used to extract the confidence interval, while for (b) the CP-odd operators the $\Delta\phi_{jj}^{\text{signed}}$ vs p_T^H distribution is used. The limits are computed at a new-physics scale $\Lambda = 1$ TeV.

introduce distinct shape differences to the distribution such that there are no ‘flat directions’. In all cases the observed 95% confidence limits agree well with the expected confidence limits such that there is no evidence of BSM physics.

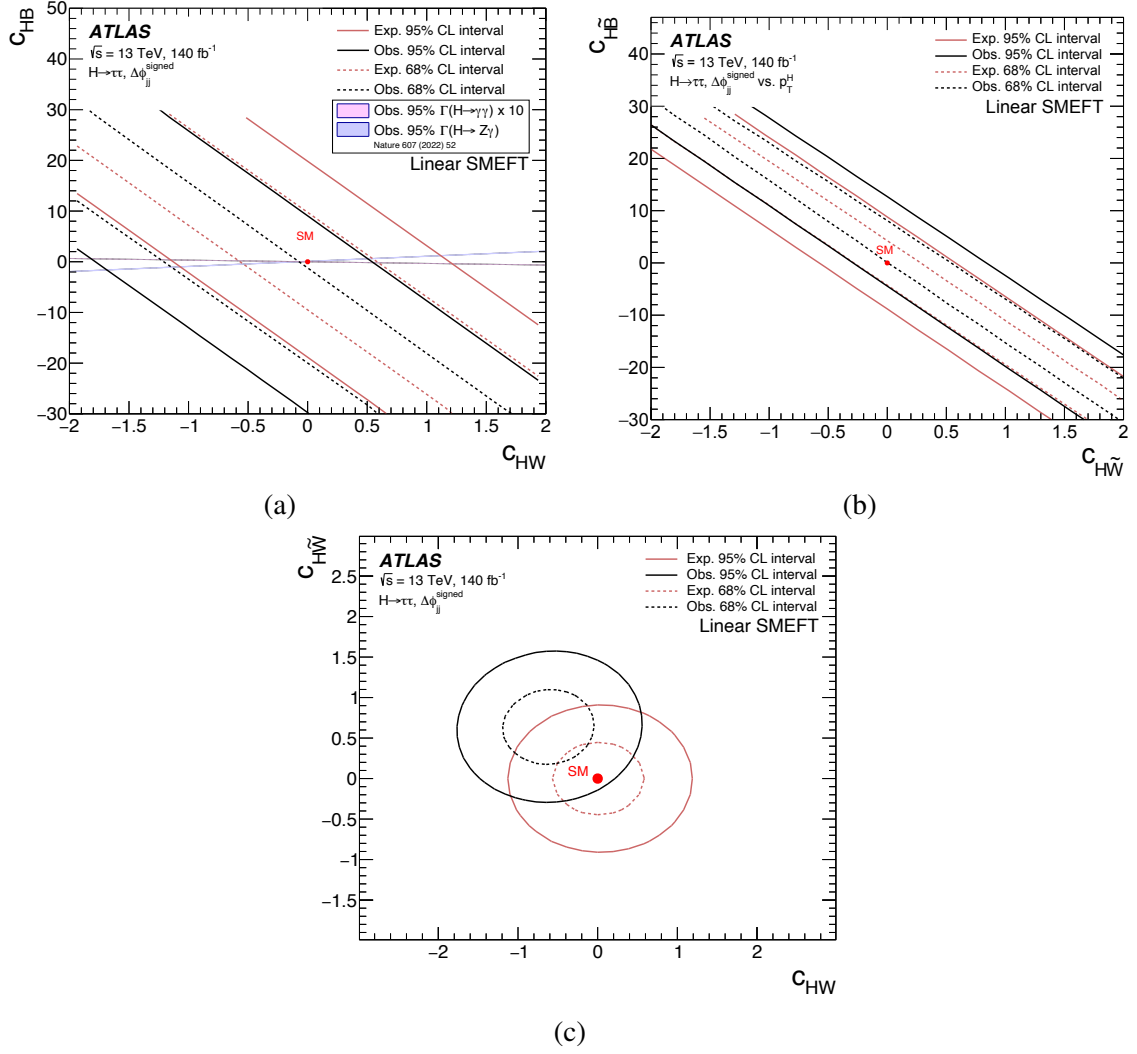


Figure 13: Two-dimensional observed and expected limits at 68% and 95% confidence level obtained from various combinations of two Wilson coefficients using only the SM–dimension-6 interference in the SMEFT basis: (a) c_{HW} vs c_{HB} , (b) $c_{H\tilde{W}}$ vs c_{HB} and (c) c_{HW} vs $c_{H\tilde{W}}$. The limits are computed at a new-physics scale $\Lambda = 1$ TeV. In (a) and (c), the $\Delta\phi_{jj}^{\text{signed}}$ distribution is used, while in the purely CP-odd case (b), the $\Delta\phi_{jj}^{\text{signed}}$ vs p_T^H distribution is used. To illustrate the complementarity of this measurement with other Higgs boson studies, in (a) the limits from measurements in the $H \rightarrow \gamma\gamma$ and $H \rightarrow Z\gamma$ [131] interpreted in the SMEFT [132, 133] are also shown. The interval resulting from the $H \rightarrow \gamma\gamma$ measurement has been increased by a factor of ten for visibility.

10 Conclusion

Measurements of Higgs boson production cross-sections in the τ -lepton-pair decay channel are presented. The analysis uses 140 fb^{-1} of proton–proton collisions at $\sqrt{s} = 13$ TeV recorded by the ATLAS detector at the LHC and supersedes the previous analysis of the same dataset. Two different types of measurement were performed: cross-section measurements of the four main production processes in the STXS framework, including eight kinematic bins for VBF production, and unfolded differential measurements in a region of phase space enhanced in VBF production. The latter are also used to derive 95% confidence intervals for

dimension-six operators in the SMEFT formalism. Many of these measurements are limited by the size of the analyzed data sample.

Cross-section measurements for the four main Higgs boson production modes (gluon–gluon fusion, vector-boson fusion, associated production with a vector boson, and associated production with a top–antitop quark pair) are found to agree well with the SM predictions. In particular, the ratio of the measured cross-section to the SM prediction for VBF Higgs boson production is found to be $0.93^{+0.17}_{-0.15}$, representing the most precise measurement of this production mode across all Higgs boson results.

Eighteen bins of the STXS framework were measured, with an overall p -value of 6% for compatibility with the SM prediction, demonstrating reasonable agreement. For VBF production, higher precision is achieved in the higher p_T^H and higher m_{jj} regions because of their higher signal purity. The ratio of the measured cross-section to the SM prediction for VBF production with $p_T^H > 200$ GeV ($p_T^H < 200$ GeV) and $m_{jj} > 1.5$ TeV is $1.29^{+0.39}_{-0.34}$ ($0.12^{+0.34}_{-0.33}$). This is the first measurement for the higher p_T^H range, and the most precise for the lower p_T^H range, in this corner of phase space.

Unfolded differential cross-sections for Higgs boson production in a region of phase space dominated by VBF production are also presented. Four distributions are unfolded to particle level: p_T^H , $p_T(j_0)$, $\Delta\phi_{jj}^{\text{signed}}$, and $\Delta\phi_{jj}^{\text{signed}}$ vs p_T^H . All of these distributions show good agreement with the SM predictions, with typical uncertainties of 30%–50%, dominated by the statistical uncertainty of the data.

These distributions are sensitive to BSM physics and a SMEFT interpretation is presented. Six operators were considered, all affecting the VBF Higgs boson production vertex, and the associated Wilson coefficients are c_{HW} , c_{HB} , c_{HWB} , and their CP-odd counterparts. For each coefficient, 95% confidence intervals were derived for the interference term alone and for both the interference and purely BSM contributions. The constraints on the CP-odd Wilson coefficient $c_{H\tilde{W}}$ in the former case, $[-0.31, +0.88]$, are the strongest to date from any channel. Two-dimensional 95% confidence intervals were also derived, demonstrating unique sensitivity for these operators compared to other Higgs boson analyses.

Acknowledgements

We thank CERN for the very successful operation of the LHC and its injectors, as well as the support staff at CERN and at our institutions worldwide without whom ATLAS could not be operated efficiently.

The crucial computing support from all WLCG partners is acknowledged gratefully, in particular from CERN, the ATLAS Tier-1 facilities at TRIUMF/SFU (Canada), NDGF (Denmark, Norway, Sweden), CC-IN2P3 (France), KIT/GridKA (Germany), INFN-CNAF (Italy), NL-T1 (Netherlands), PIC (Spain), RAL (UK) and BNL (USA), the Tier-2 facilities worldwide and large non-WLCG resource providers. Major contributors of computing resources are listed in Ref. [134].

We gratefully acknowledge the support of ANPCyT, Argentina; YerPhI, Armenia; ARC, Australia; BMWFW and FWF, Austria; ANAS, Azerbaijan; CNPq and FAPESP, Brazil; NSERC, NRC and CFI, Canada; CERN; ANID, Chile; CAS, MOST and NSFC, China; Minciencias, Colombia; MEYS CR, Czech Republic; DNRF and DNSRC, Denmark; IN2P3-CNRS and CEA-DRF/IRFU, France; SRNSFG, Georgia; BMBF, HGF and MPG, Germany; GSRI, Greece; RGC and Hong Kong SAR, China; ISF and Benozziyo Center, Israel; INFN, Italy; MEXT and JSPS, Japan; CNRST, Morocco; NWO, Netherlands; RCN, Norway; MNiSW, Poland; FCT, Portugal; MNE/IFA, Romania; MESTD, Serbia; MSSR, Slovakia; ARRS and MIZŠ, Slovenia; DSI/NRF, South Africa; MICINN, Spain; SRC and Wallenberg Foundation, Sweden;

SERI, SNSF and Cantons of Bern and Geneva, Switzerland; NSTC, Taipei; TENMAK, Türkiye; STFC, United Kingdom; DOE and NSF, United States of America.

Individual groups and members have received support from BCKDF, CANARIE, CRC and DRAC, Canada; CERN-CZ, FORTE and PRIMUS, Czech Republic; COST, ERC, ERDF, Horizon 2020, ICSC-NextGenerationEU and Marie Skłodowska-Curie Actions, European Union; Investissements d'Avenir Labex, Investissements d'Avenir Idex and ANR, France; DFG and AvH Foundation, Germany; Herakleitos, Thales and Aristeia programmes co-financed by EU-ESF and the Greek NSRF, Greece; BSF-NSF and MINERVA, Israel; NCN and NAWA, Poland; La Caixa Banking Foundation, CERCA Programme Generalitat de Catalunya and PROMETEO and GenT Programmes Generalitat Valenciana, Spain; Göran Gustafssons Stiftelse, Sweden; The Royal Society and Leverhulme Trust, United Kingdom.

In addition, individual members wish to acknowledge support from Armenia: Yerevan Physics Institute (FAPERJ); CERN: European Organization for Nuclear Research (CERN PJAS); Chile: Agencia Nacional de Investigación y Desarrollo (FONDECYT 1230812, FONDECYT 1230987, FONDECYT 1240864); China: Chinese Ministry of Science and Technology (MOST-2023YFA1605700), National Natural Science Foundation of China (NSFC - 12175119, NSFC 12275265, NSFC-12075060); Czech Republic: Czech Science Foundation (GACR - 24-11373S), Ministry of Education Youth and Sports (FORTE CZ.02.01.01/00/22_008/0004632), PRIMUS Research Programme (PRIMUS/21/SCI/017); EU: H2020 European Research Council (ERC - 101002463); European Union: European Research Council (ERC - 948254, ERC 101089007), Horizon 2020 Framework Programme (MUCCA - CHIST-ERA-19-XAI-00), European Union, Future Artificial Intelligence Research (FAIR-NextGenerationEU PE00000013), Italian Center for High Performance Computing, Big Data and Quantum Computing (ICSC, NextGenerationEU); France: Agence Nationale de la Recherche (ANR-20-CE31-0013, ANR-21-CE31-0013, ANR-21-CE31-0022, ANR-22-EDIR-0002), Investissements d'Avenir Labex (ANR-11-LABX-0012); Germany: Baden-Württemberg Stiftung (BW Stiftung-Postdoc Eliteprogramme), Deutsche Forschungsgemeinschaft (DFG - 469666862, DFG - CR 312/5-2); Italy: Istituto Nazionale di Fisica Nucleare (ICSC, NextGenerationEU), Ministero dell'Università e della Ricerca (PRIN - 20223N7F8K - PNRR M4.C2.1.1); Japan: Japan Society for the Promotion of Science (JSPS KAKENHI JP22H01227, JSPS KAKENHI JP22H04944, JSPS KAKENHI JP22KK0227, JSPS KAKENHI JP23KK0245); Netherlands: Netherlands Organisation for Scientific Research (NWO Veni 2020 - VI.Veni.202.179); Norway: Research Council of Norway (RCN-314472); Poland: Polish National Agency for Academic Exchange (PPN/PPO/2020/1/00002/U/00001), Polish National Science Centre (NCN 2021/42/E/ST2/00350, NCN OPUS nr 2022/47/B/ST2/03059, NCN UMO-2019/34/E/ST2/00393, UMO-2020/37/B/ST2/01043, UMO-2021/40/C/ST2/00187, UMO-2022/47/O/ST2/00148, UMO-2023/49/B/ST2/04085, UMO-2023/51/B/ST2/00920); Slovenia: Slovenian Research Agency (ARIS grant J1-3010); Spain: Generalitat Valenciana (Artemisa, FEDER, IDIFEDER/2018/048), Ministry of Science and Innovation (MCIN & NextGenEU PCI2022-135018-2, MICIN & FEDER PID2021-125273NB, RYC2019-028510-I, RYC2020-030254-I, RYC2021-031273-I, RYC2022-038164-I), PROMETEO and GenT Programmes Generalitat Valenciana (CIDEAGENT/2019/027); Sweden: Swedish Research Council (Swedish Research Council 2023-04654, VR 2018-00482, VR 2022-03845, VR 2022-04683, VR 2023-03403, VR grant 2021-03651), Knut and Alice Wallenberg Foundation (KAW 2018.0157, KAW 2018.0458, KAW 2019.0447, KAW 2022.0358); Switzerland: Swiss National Science Foundation (SNSF - PCEFP2_194658); United Kingdom: Leverhulme Trust (Leverhulme Trust RPG-2020-004), Royal Society (NIF-R1-231091); United States of America: U.S. Department of Energy (ECA DE-AC02-76SF00515), Neubauer Family Foundation.

References

- [1] ATLAS Collaboration, *Observation of a new particle in the search for the Standard Model Higgs boson with the ATLAS detector at the LHC*, *Phys. Lett. B* **716** (2012) 1, arXiv: [1207.7214 \[hep-ex\]](#).
- [2] CMS Collaboration, *Observation of a new boson at a mass of 125 GeV with the CMS experiment at the LHC*, *Phys. Lett. B* **716** (2012) 30, arXiv: [1207.7235 \[hep-ex\]](#).
- [3] ATLAS Collaboration, *Measurements of Higgs boson production cross-sections in the $H \rightarrow \tau^+ \tau^-$ decay channel in pp collisions at $\sqrt{s} = 13$ TeV with the ATLAS detector*, *JHEP* **08** (2022) 175, arXiv: [2201.08269 \[hep-ex\]](#).
- [4] D. de Florian et al., *Handbook of LHC Higgs Cross Sections: 4. Deciphering the Nature of the Higgs Sector*, (2017), arXiv: [1610.07922 \[hep-ph\]](#).
- [5] ATLAS Collaboration, *Higgs boson production cross-section measurements and their EFT interpretation in the 4ℓ decay channel at $\sqrt{s} = 13$ TeV with the ATLAS detector*, *Eur. Phys. J. C* **80** (2020) 957, arXiv: [2004.03447 \[hep-ex\]](#), Erratum: *Eur. Phys. J. C* **81** (2021) 29, Erratum: *Eur. Phys. J. C* **81** (2021) 398.
- [6] ATLAS Collaboration, *Measurement of the properties of Higgs boson production at $\sqrt{s} = 13$ TeV in the $H \rightarrow \gamma\gamma$ channel using 139fb^{-1} of pp collision data with the ATLAS experiment*, *JHEP* **07** (2023) 088, arXiv: [2207.00348 \[hep-ex\]](#).
- [7] ATLAS Collaboration, *Measurements of Higgs boson production by gluon–gluon fusion and vector-boson fusion using $H \rightarrow WW^* \rightarrow e\nu\mu\nu$ decays in pp collisions at $\sqrt{s} = 13$ TeV with the ATLAS detector*, *Phys. Rev. D* **108** (2023) 032005, arXiv: [2207.00338 \[hep-ex\]](#).
- [8] CMS Collaboration, *Measurements of Higgs boson production in the decay channel with a pair of τ leptons in proton–proton collisions at $\sqrt{s} = 13$ TeV*, *Eur. Phys. J. C* **83** (2023) 562, arXiv: [2204.12957 \[hep-ex\]](#).
- [9] CMS Collaboration, *Measurements of production cross sections of the Higgs boson in the four-lepton final state in proton–proton collisions at $\sqrt{s} = 13$ TeV*, *Eur. Phys. J. C* **81** (2021) 488, arXiv: [2103.04956 \[hep-ex\]](#).
- [10] CMS Collaboration, *Measurements of Higgs boson production cross sections and couplings in the diphoton decay channel at $\sqrt{s} = 13$ TeV*, *JHEP* **07** (2021) 027, arXiv: [2103.06956 \[hep-ex\]](#).
- [11] CMS Collaboration, *Measurements of the Higgs boson production cross section and couplings in the W boson pair decay channel in proton–proton collisions at $\sqrt{s} = 13$ TeV*, *Eur. Phys. J. C* **83** (2023) 667, arXiv: [2206.09466 \[hep-ex\]](#).
- [12] ATLAS Collaboration, *Measurements of the Higgs boson inclusive and differential fiducial cross-sections in the diphoton decay channel with pp collisions at $\sqrt{s} = 13$ TeV with the ATLAS detector*, *JHEP* **08** (2022) 027, arXiv: [2202.00487 \[hep-ex\]](#).
- [13] ATLAS Collaboration, *Integrated and differential fiducial cross-section measurements for the vector boson fusion production of the Higgs boson in the $H \rightarrow WW^* \rightarrow e\nu\mu\nu$ decay channel at 13 TeV with the ATLAS detector*, *Phys. Rev. D* **108** (2023) 072003, arXiv: [2304.03053 \[hep-ex\]](#).

- [14] ATLAS Collaboration, *The ATLAS Experiment at the CERN Large Hadron Collider*, [JINST 3 \(2008\) S08003](#).
- [15] ATLAS Collaboration, *ATLAS Insertable B-Layer: Technical Design Report*, ATLAS-TDR-19; CERN-LHCC-2010-013, 2010, URL: <https://cds.cern.ch/record/1291633>, Addendum: ATLAS-TDR-19-ADD-1; CERN-LHCC-2012-009, 2012, URL: <https://cds.cern.ch/record/1451888>.
- [16] B. Abbott et al., *Production and integration of the ATLAS Insertable B-Layer*, [JINST 13 \(2018\) T05008](#), arXiv: [1803.00844 \[physics.ins-det\]](#).
- [17] G. Avoni et al., *The new LUCID-2 detector for luminosity measurement and monitoring in ATLAS*, [JINST 13 \(2018\) P07017](#).
- [18] ATLAS Collaboration, *Performance of the ATLAS trigger system in 2015*, [Eur. Phys. J. C 77 \(2017\) 317](#), arXiv: [1611.09661 \[hep-ex\]](#).
- [19] ATLAS Collaboration, *Software and computing for Run 3 of the ATLAS experiment at the LHC*, (2024), arXiv: [2404.06335 \[hep-ex\]](#).
- [20] ATLAS Collaboration, *ATLAS data quality operations and performance for 2015–2018 data-taking*, [JINST 15 \(2020\) P04003](#), arXiv: [1911.04632 \[physics.ins-det\]](#).
- [21] ATLAS Collaboration, *Luminosity determination in pp collisions at $\sqrt{s} = 13$ TeV using the ATLAS detector at the LHC*, [Eur. Phys. J. C 83 \(2023\) 982](#), arXiv: [2212.09379 \[hep-ex\]](#).
- [22] S. Frixione, G. Ridolfi and P. Nason, *A positive-weight next-to-leading-order Monte Carlo for heavy flavour hadroproduction*, [JHEP 09 \(2007\) 126](#), arXiv: [0707.3088 \[hep-ph\]](#).
- [23] P. Nason, *A new method for combining NLO QCD with shower Monte Carlo algorithms*, [JHEP 11 \(2004\) 040](#), arXiv: [hep-ph/0409146](#).
- [24] S. Frixione, P. Nason and C. Oleari, *Matching NLO QCD computations with parton shower simulations: the POWHEG method*, [JHEP 11 \(2007\) 070](#), arXiv: [0709.2092 \[hep-ph\]](#).
- [25] S. Alioli, P. Nason, C. Oleari and E. Re, *A general framework for implementing NLO calculations in shower Monte Carlo programs: the POWHEG BOX*, [JHEP 06 \(2010\) 043](#), arXiv: [1002.2581 \[hep-ph\]](#).
- [26] H. B. Hartanto, B. Jäger, L. Reina and D. Wackerth, *Higgs boson production in association with top quarks in the POWHEG BOX*, [Phys. Rev. D 91 \(2015\) 094003](#), arXiv: [1501.04498 \[hep-ph\]](#).
- [27] C. Anastasiou et al., *High precision determination of the gluon fusion Higgs boson cross-section at the LHC*, [JHEP 05 \(2016\) 058](#), arXiv: [1602.00695 \[hep-ph\]](#).
- [28] C. Anastasiou, C. Duhr, F. Dulat, F. Herzog and B. Mistlberger, *Higgs Boson Gluon-Fusion Production in QCD at Three Loops*, [Phys. Rev. Lett. 114 \(2015\) 212001](#), arXiv: [1503.06056 \[hep-ph\]](#).
- [29] F. Dulat, A. Lazopoulos and B. Mistlberger, *iHixs 2 – Inclusive Higgs cross sections*, [Comput. Phys. Commun. 233 \(2018\) 243](#), arXiv: [1802.00827 \[hep-ph\]](#).

- [30] R. V. Harlander and K. J. Ozeren,
Finite top mass effects for hadronic Higgs production at next-to-next-to-leading order,
[JHEP **11** \(2009\) 088](#), arXiv: [0909.3420 \[hep-ph\]](#).
- [31] R. V. Harlander and K. J. Ozeren,
Top mass effects in Higgs production at next-to-next-to-leading order QCD: Virtual corrections,
[Phys. Lett. B **679** \(2009\) 467](#), arXiv: [0907.2997 \[hep-ph\]](#).
- [32] R. V. Harlander, H. Mantler, S. Marzani and K. J. Ozeren,
Higgs production in gluon fusion at next-to-next-to-leading order QCD for finite top mass,
[Eur. Phys. J. C **66** \(2010\) 359](#), arXiv: [0912.2104 \[hep-ph\]](#).
- [33] A. Pak, M. Rogal and M. Steinhauser,
Finite top quark mass effects in NNLO Higgs boson production at LHC, [JHEP **02** \(2010\) 025](#),
arXiv: [0911.4662 \[hep-ph\]](#).
- [34] S. Actis, G. Passarino, C. Sturm and S. Uccirati,
NLO electroweak corrections to Higgs boson production at hadron colliders,
[Phys. Lett. B **670** \(2008\) 12](#), arXiv: [0809.1301 \[hep-ph\]](#).
- [35] S. Actis, G. Passarino, C. Sturm and S. Uccirati,
NNLO computational techniques: The cases $H \rightarrow \gamma\gamma$ and $H \rightarrow gg$, [Nucl. Phys. B **811** \(2009\) 182](#),
arXiv: [0809.3667 \[hep-ph\]](#).
- [36] M. Bonetti, K. Melnikov and L. Tancredi, *Higher order corrections to mixed QCD-EW contributions to Higgs boson production in gluon fusion*, [Phys. Rev. D **97** \(2018\) 056017](#),
arXiv: [1801.10403 \[hep-ph\]](#), Erratum: [Phys. Rev. D **97** \(2018\) 099906\(E\)](#).
- [37] J. Butterworth et al., *PDF4LHC recommendations for LHC Run II*, [J. Phys. G **43** \(2016\) 023001](#),
arXiv: [1510.03865 \[hep-ph\]](#).
- [38] T. Sjöstrand et al., *An introduction to PYTHIA 8.2*, [Comput. Phys. Commun. **191** \(2015\) 159](#),
arXiv: [1410.3012 \[hep-ph\]](#).
- [39] ATLAS Collaboration, *Measurement of the Z/γ^* boson transverse momentum distribution in pp collisions at $\sqrt{s} = 7$ TeV with the ATLAS detector*, [JHEP **09** \(2014\) 145](#),
arXiv: [1406.3660 \[hep-ex\]](#).
- [40] M. Ciccolini, A. Denner and S. Dittmaier, *Strong and Electroweak Corrections to the Production of a Higgs Boson + 2 Jets via Weak Interactions at the Large Hadron Collider*,
[Phys. Rev. Lett. **99** \(2007\) 161803](#), arXiv: [0707.0381 \[hep-ph\]](#).
- [41] M. Ciccolini, A. Denner and S. Dittmaier,
Electroweak and QCD corrections to Higgs production via vector-boson fusion at the CERN LHC,
[Phys. Rev. D **77** \(2008\) 013002](#), arXiv: [0710.4749 \[hep-ph\]](#).
- [42] P. Bolzoni, F. Maltoni, S.-O. Moch and M. Zaro,
Higgs Boson Production via Vector-Boson Fusion at Next-to-Next-to-Leading Order in QCD,
[Phys. Rev. Lett. **105** \(2010\) 011801](#), arXiv: [1003.4451 \[hep-ph\]](#).
- [43] M. L. Ciccolini, S. Dittmaier and M. Krämer,
Electroweak radiative corrections to associated WH and ZH production at hadron colliders,
[Phys. Rev. D **68** \(2003\) 073003](#), arXiv: [hep-ph/0306234 \[hep-ph\]](#).
- [44] O. Brein, A. Djouadi and R. Harlander,
NNLO QCD corrections to the Higgs-strahlung processes at hadron colliders,
[Phys. Lett. B **579** \(2004\) 149](#), arXiv: [hep-ph/0307206](#).

- [45] O. Brein, R. V. Harlander, M. Wiesemann and T. Zirke, *Top-quark mediated effects in hadronic Higgs-Strahlung*, *Eur. Phys. J. C* **72** (2012) 1868, arXiv: [1111.0761 \[hep-ph\]](#).
- [46] L. Altenkamp, S. Dittmaier, R. V. Harlander, H. Rzehak and T. J. E. Zirke, *Gluon-induced Higgs-strahlung at next-to-leading order QCD*, *JHEP* **02** (2013) 078, arXiv: [1211.5015 \[hep-ph\]](#).
- [47] A. Denner, S. Dittmaier, S. Kallweit and A. Mück, *HAWK 2.0: A Monte Carlo program for Higgs production in vector-boson fusion and Higgs strahlung at hadron colliders*, *Comput. Phys. Commun.* **195** (2015) 161, arXiv: [1412.5390 \[hep-ph\]](#).
- [48] O. Brein, R. V. Harlander and T. J. E. Zirke, *vh@nnlo – Higgs Strahlung at hadron colliders*, *Comput. Phys. Commun.* **184** (2013) 998, arXiv: [1210.5347 \[hep-ph\]](#).
- [49] R. V. Harlander, A. Kulesza, V. Theeuwes and T. Zirke, *Soft gluon resummation for gluon-induced Higgs Strahlung*, *JHEP* **11** (2014) 082, arXiv: [1410.0217 \[hep-ph\]](#).
- [50] D. J. Lange, *The EvtGen particle decay simulation package*, *Nucl. Instrum. Meth. A* **462** (2001) 152.
- [51] W. Beenakker, S. Dittmaier, M. Krämer, B. Plumper, M. Spira et al., *NLO QCD corrections to $t\bar{t}H$ production in hadron collisions*, *Nucl. Phys. B* **653** (2003) 151, arXiv: [hep-ph/0211352 \[hep-ph\]](#).
- [52] S. Dawson, C. Jackson, L. Orr, L. Reina and D. Wackerroth, *Associated Higgs boson production with top quarks at the CERN Large Hadron Collider: NLO QCD corrections*, *Phys. Rev. D* **68** (2003) 034022, arXiv: [hep-ph/0305087 \[hep-ph\]](#).
- [53] Y. Zhang, W.-G. Ma, R.-Y. Zhang, C. Chen and L. Guo, *QCD NLO and EW NLO corrections to $t\bar{t}H$ production with top quark decays at hadron collider*, *Phys. Lett. B* **738** (2014) 1, arXiv: [1407.1110 \[hep-ph\]](#).
- [54] S. Frixione, V. Hirschi, D. Pagani, H. -. Shao and M. Zaro, *Weak corrections to Higgs hadroproduction in association with a top-quark pair*, *JHEP* **09** (2014) 065, arXiv: [1407.0823 \[hep-ph\]](#).
- [55] NNPDF Collaboration, R. D. Ball et al., *Parton distributions for the LHC run II*, *JHEP* **04** (2015) 040, arXiv: [1410.8849 \[hep-ph\]](#).
- [56] ATLAS Collaboration, *ATLAS Pythia 8 tunes to 7 TeV data*, ATL-PHYS-PUB-2014-021, 2014, URL: <https://cds.cern.ch/record/1966419>.
- [57] A. Djouadi, J. Kalinowski and M. Spira, *HDECAY: a program for Higgs boson decays in the Standard Model and its supersymmetric extension*, *Comput. Phys. Commun.* **108** (1998) 56, arXiv: [hep-ph/9704448](#).
- [58] M. Spira, *QCD Effects in Higgs Physics*, *Fortsch. Phys.* **46** (1998) 203, arXiv: [hep-ph/9705337](#).
- [59] A. Djouadi, M. M. Mühlleitner and M. Spira, *Decays of Supersymmetric Particles: the Program SUSY-HIT (SUSpect-SdecaY-Hdecay-InTerface)*, *Acta Phys. Polon. B* **38** (2007) 635, arXiv: [hep-ph/0609292](#).
- [60] A. Bredenstein, A. Denner, S. Dittmaier and M. M. Weber, *Radiative corrections to the semileptonic and hadronic Higgs-boson decays $H \rightarrow WW/ZZ \rightarrow 4$ fermions*, *JHEP* **02** (2007) 080, arXiv: [hep-ph/0611234](#).

- [61] A. Bredenstein, A. Denner, S. Dittmaier and M. M. Weber, *Precise predictions for the Higgs-boson decay $H \rightarrow WW/ZZ \rightarrow 4$ leptons*, [Phys. Rev. D **74** \(2006\) 013004](#), arXiv: [hep-ph/0604011 \[hep-ph\]](#).
- [62] A. Bredenstein, A. Denner, S. Dittmaier and M. M. Weber, *Precision calculations for the Higgs decays $H \rightarrow ZZ/WW \rightarrow 4$ leptons*, [Nucl. Phys. B Proc. Suppl. **160** \(2006\) 131](#), arXiv: [hep-ph/0607060 \[hep-ph\]](#).
- [63] E. Bothmann et al., *Event generation with Sherpa 2.2*, [SciPost Phys. **7** \(2019\) 034](#), arXiv: [1905.09127 \[hep-ph\]](#).
- [64] T. Gleisberg and S. Höche, *Comix, a new matrix element generator*, [JHEP **12** \(2008\) 039](#), arXiv: [0808.3674 \[hep-ph\]](#).
- [65] F. Buccioni et al., *OpenLoops 2*, [Eur. Phys. J. C **79** \(2019\) 866](#), arXiv: [1907.13071 \[hep-ph\]](#).
- [66] F. Cascioli, P. Maierhöfer and S. Pozzorini, *Scattering Amplitudes with Open Loops*, [Phys. Rev. Lett. **108** \(2012\) 111601](#), arXiv: [1111.5206 \[hep-ph\]](#).
- [67] A. Denner, S. Dittmaier and L. Hofer, *COLLIER: A fortran-based complex one-loop library in extended regularizations*, [Comput. Phys. Commun. **212** \(2017\) 220](#), arXiv: [1604.06792 \[hep-ph\]](#).
- [68] S. Schumann and F. Krauss, *A parton shower algorithm based on Catani–Seymour dipole factorisation*, [JHEP **03** \(2008\) 038](#), arXiv: [0709.1027 \[hep-ph\]](#).
- [69] S. Höche, F. Krauss, M. Schönherr and F. Siegert, *A critical appraisal of NLO+PS matching methods*, [JHEP **09** \(2012\) 049](#), arXiv: [1111.1220 \[hep-ph\]](#).
- [70] S. Höche, F. Krauss, M. Schönherr and F. Siegert, *QCD matrix elements + parton showers. The NLO case*, [JHEP **04** \(2013\) 027](#), arXiv: [1207.5030 \[hep-ph\]](#).
- [71] S. Catani, F. Krauss, B. R. Webber and R. Kuhn, *QCD Matrix Elements + Parton Showers*, [JHEP **11** \(2001\) 063](#), arXiv: [hep-ph/0109231](#).
- [72] S. Höche, F. Krauss, S. Schumann and F. Siegert, *QCD matrix elements and truncated showers*, [JHEP **05** \(2009\) 053](#), arXiv: [0903.1219 \[hep-ph\]](#).
- [73] C. Anastasiou, L. Dixon, K. Melnikov and F. Petriello, *High-precision QCD at hadron colliders: Electroweak gauge boson rapidity distributions at next-to-next-to leading order*, [Phys. Rev. D **69** \(2004\) 094008](#), arXiv: [hep-ph/0312266](#).
- [74] ATLAS Collaboration, *Measurement of the cross-section for electroweak production of dijets in association with a Z boson in pp collisions at $\sqrt{s} = 13$ TeV with the ATLAS detector*, [Phys. Lett. B **775** \(2017\) 206](#), arXiv: [1709.10264 \[hep-ex\]](#).
- [75] ATLAS Collaboration, *Test of CP invariance in vector-boson fusion production of the Higgs boson in the $H \rightarrow \tau\tau$ channel in proton–proton collisions at $\sqrt{s} = 13$ TeV with the ATLAS detector*, [Phys. Lett. B **805** \(2020\) 135426](#), arXiv: [2002.05315 \[hep-ex\]](#).
- [76] ATLAS Collaboration, *Studies on top-quark Monte Carlo modelling for Top2016*, ATL-PHYS-PUB-2016-020, 2016, URL: <https://cds.cern.ch/record/2216168>.

- [77] M. Beneke, P. Falgari, S. Klein and C. Schwinn, *Hadronic top-quark pair production with NNLL threshold resummation*, *Nucl. Phys. B* **855** (2012) 695, arXiv: [1109.1536 \[hep-ph\]](#).
- [78] M. Cacciari, M. Czakon, M. Mangano, A. Mitov and P. Nason, *Top-pair production at hadron colliders with next-to-next-to-leading logarithmic soft-gluon resummation*, *Phys. Lett. B* **710** (2012) 612, arXiv: [1111.5869 \[hep-ph\]](#).
- [79] P. Bärnreuther, M. Czakon and A. Mitov, *Percent-Level-Precision Physics at the Tevatron: Next-to-Next-to-Leading Order QCD Corrections to $q\bar{q} \rightarrow t\bar{t} + X$* , *Phys. Rev. Lett.* **109** (2012) 132001, arXiv: [1204.5201 \[hep-ph\]](#).
- [80] M. Czakon and A. Mitov, *NNLO corrections to top-pair production at hadron colliders: the all-fermionic scattering channels*, *JHEP* **12** (2012) 054, arXiv: [1207.0236 \[hep-ph\]](#).
- [81] M. Czakon and A. Mitov, *NNLO corrections to top pair production at hadron colliders: the quark-gluon reaction*, *JHEP* **01** (2013) 080, arXiv: [1210.6832 \[hep-ph\]](#).
- [82] M. Czakon, P. Fiedler and A. Mitov, *Total Top-Quark Pair-Production Cross Section at Hadron Colliders Through $O(\alpha_S^4)$* , *Phys. Rev. Lett.* **110** (2013) 252004, arXiv: [1303.6254 \[hep-ph\]](#).
- [83] M. Czakon and A. Mitov, *Top++: A program for the calculation of the top-pair cross-section at hadron colliders*, *Comput. Phys. Commun.* **185** (2014) 2930, arXiv: [1112.5675 \[hep-ph\]](#).
- [84] T. Sjöstrand, S. Mrenna and P. Skands, *A brief introduction to PYTHIA 8.1*, *Comput. Phys. Commun.* **178** (2008) 852, arXiv: [0710.3820 \[hep-ph\]](#).
- [85] ATLAS Collaboration, *The Pythia 8 A3 tune description of ATLAS minimum bias and inelastic measurements incorporating the Donnachie–Landshoff diffractive model*, ATL-PHYS-PUB-2016-017, 2016, URL: <https://cds.cern.ch/record/2206965>.
- [86] A. D. Martin, W. J. Stirling, R. S. Thorne and G. Watt, *Parton distributions for the LHC*, *Eur. Phys. J. C* **63** (2009) 189, arXiv: [0901.0002 \[hep-ph\]](#).
- [87] ATLAS Collaboration, *The ATLAS Simulation Infrastructure*, *Eur. Phys. J. C* **70** (2010) 823, arXiv: [1005.4568 \[physics.ins-det\]](#).
- [88] S. Agostinelli et al., *GEANT4 – a simulation toolkit*, *Nucl. Instrum. Meth. A* **506** (2003) 250.
- [89] ATLAS Collaboration, *Performance of electron and photon triggers in ATLAS during LHC Run 2*, *Eur. Phys. J. C* **80** (2020) 47, arXiv: [1909.00761 \[hep-ex\]](#).
- [90] ATLAS Collaboration, *Performance of the ATLAS muon triggers in Run 2*, *JINST* **15** (2020) P09015, arXiv: [2004.13447 \[physics.ins-det\]](#).
- [91] ATLAS Collaboration, *The ATLAS inner detector trigger performance in pp collisions at 13 TeV during LHC Run 2*, *Eur. Phys. J. C* **82** (2022) 206, arXiv: [2107.02485 \[hep-ex\]](#).
- [92] ATLAS Collaboration, *Performance of the ATLAS Level-1 topological trigger in Run 2*, *Eur. Phys. J. C* **82** (2022) 7, arXiv: [2105.01416 \[hep-ex\]](#).
- [93] ATLAS Collaboration, *Electron and photon efficiencies in LHC Run 2 with the ATLAS experiment*, *JHEP* **05** (2024) 162, arXiv: [2308.13362 \[hep-ex\]](#).

- [94] ATLAS Collaboration, *Muon reconstruction and identification efficiency in ATLAS using the full Run 2 pp collision data set at $\sqrt{s} = 13$ TeV*, *Eur. Phys. J. C* **81** (2021) 578, arXiv: [2012.00578](https://arxiv.org/abs/2012.00578) [[hep-ex](#)].
- [95] ATLAS Collaboration, *2015 start-up trigger menu and initial performance assessment of the ATLAS trigger using Run-2 data*, ATL-DAQ-PUB-2016-001, 2016, URL: <https://cds.cern.ch/record/2136007>.
- [96] ATLAS Collaboration, *Trigger Menu in 2016*, ATL-DAQ-PUB-2017-001, 2017, URL: <https://cds.cern.ch/record/2242069>.
- [97] ATLAS Collaboration, *Trigger Menu in 2017*, ATL-DAQ-PUB-2018-002, 2018, URL: <https://cds.cern.ch/record/2625986>.
- [98] ATLAS Collaboration, *Trigger Menu in 2018*, ATL-DAQ-PUB-2019-001, 2019, URL: <https://cds.cern.ch/record/2693402>.
- [99] M. Cacciari, G. P. Salam and G. Soyez, *The anti- k_t jet clustering algorithm*, *JHEP* **04** (2008) 063, arXiv: [0802.1189](https://arxiv.org/abs/0802.1189) [[hep-ph](#)].
- [100] M. Cacciari, G. P. Salam and G. Soyez, *FastJet user manual*, *Eur. Phys. J. C* **72** (2012) 1896, arXiv: [1111.6097](https://arxiv.org/abs/1111.6097) [[hep-ph](#)].
- [101] ATLAS Collaboration, *Jet reconstruction and performance using particle flow with the ATLAS Detector*, *Eur. Phys. J. C* **77** (2017) 466, arXiv: [1703.10485](https://arxiv.org/abs/1703.10485) [[hep-ex](#)].
- [102] ATLAS Collaboration, *Jet energy scale and resolution measured in proton–proton collisions at $\sqrt{s} = 13$ TeV with the ATLAS detector*, *Eur. Phys. J. C* **81** (2021) 689, arXiv: [2007.02645](https://arxiv.org/abs/2007.02645) [[hep-ex](#)].
- [103] ATLAS Collaboration, *Performance of pile-up mitigation techniques for jets in pp collisions at $\sqrt{s} = 8$ TeV using the ATLAS detector*, *Eur. Phys. J. C* **76** (2016) 581, arXiv: [1510.03823](https://arxiv.org/abs/1510.03823) [[hep-ex](#)].
- [104] ATLAS Collaboration, *Identification and rejection of pile-up jets at high pseudorapidity with the ATLAS detector*, *Eur. Phys. J. C* **77** (2017) 580, arXiv: [1705.02211](https://arxiv.org/abs/1705.02211) [[hep-ex](#)], Erratum: *Eur. Phys. J. C* **77** (2017) 712.
- [105] ATLAS Collaboration, *ATLAS flavour-tagging algorithms for the LHC Run 2 pp collision dataset*, *Eur. Phys. J. C* **83** (2023) 681, arXiv: [2211.16345](https://arxiv.org/abs/2211.16345) [[physics.data-an](#)].
- [106] ATLAS Collaboration, *Reconstruction, Energy Calibration, and Identification of Hadronically Decaying Tau Leptons in the ATLAS Experiment for Run-2 of the LHC*, ATL-PHYS-PUB-2015-045, 2015, URL: <https://cds.cern.ch/record/2064383>.
- [107] ATLAS Collaboration, *Identification of hadronic tau lepton decays using neural networks in the ATLAS experiment*, ATL-PHYS-PUB-2019-033, 2019, URL: <https://cds.cern.ch/record/2688062>.
- [108] ATLAS Collaboration, *ATLAS b-jet identification performance and efficiency measurement with $t\bar{t}$ events in pp collisions at $\sqrt{s} = 13$ TeV*, *Eur. Phys. J. C* **79** (2019) 970, arXiv: [1907.05120](https://arxiv.org/abs/1907.05120) [[hep-ex](#)].
- [109] ATLAS Collaboration, *Measurement of the c-jet mistagging efficiency in $t\bar{t}$ events using pp collision data at $\sqrt{s} = 13$ TeV collected with the ATLAS detector*, *Eur. Phys. J. C* **82** (2022) 95, arXiv: [2109.10627](https://arxiv.org/abs/2109.10627) [[hep-ex](#)].

- [110] ATLAS Collaboration, *Calibration of the light-flavour jet mistagging efficiency of the b -tagging algorithms with Z +jets events using 139fb^{-1} of ATLAS proton–proton collision data at $\sqrt{s} = 13\text{ TeV}$* , *Eur. Phys. J. C* **83** (2023) 728, arXiv: 2301.06319 [hep-ex].
- [111] ATLAS Collaboration, *Measurement of the tau lepton reconstruction and identification performance in the ATLAS experiment using pp collisions at $\sqrt{s} = 13\text{ TeV}$* , ATLAS-CONF-2017-029, 2017, URL: <https://cds.cern.ch/record/2261772>.
- [112] ATLAS Collaboration, *The performance of missing transverse momentum reconstruction and its significance with the ATLAS detector using 140fb^{-1} of $\sqrt{s} = 13\text{ TeV}$ pp collisions*, (2024), arXiv: 2402.05858 [hep-ex].
- [113] R. Ellis, I. Hinchliffe, M. Soldate and J. van der Bij, *Higgs decay to $\tau^+\tau^-$: A possible signature of intermediate mass Higgs bosons at high energy hadron colliders*, *Nucl. Phys. B* **297** (1988) 221.
- [114] A. Elagin, P. Murat, A. Pranko and A. Safonov, *A new mass reconstruction technique for resonances decaying to $\tau\tau$* , *Nucl. Instrum. Meth. A* **654** (2011) 481, arXiv: 1012.4686 [hep-ex].
- [115] ATLAS Collaboration, *Modelling $Z \rightarrow \tau\tau$ processes in ATLAS with τ -embedded $Z \rightarrow \mu\mu$ data*, *JINST* **10** (2015) P09018, arXiv: 1506.05623 [hep-ex].
- [116] ATLAS Collaboration, *Tools for estimating fake/non-prompt lepton backgrounds with the ATLAS detector at the LHC*, *JINST* **18** (2023) T11004, arXiv: 2211.16178 [hep-ex].
- [117] E. Bothmann, M. Schönherr and S. Schumann, *Reweighting QCD matrix-element and parton-shower calculations*, *Eur. Phys. J. C* **76** (2016) 590, arXiv: 1606.08753 [hep-ph].
- [118] J. Bellm et al., *Herwig 7.1 Release Note*, (2017), arXiv: 1705.06919 [hep-ph].
- [119] J. Alwall et al., *The automated computation of tree-level and next-to-leading order differential cross sections, and their matching to parton shower simulations*, *JHEP* **07** (2014) 079, arXiv: 1405.0301 [hep-ph].
- [120] ATLAS Collaboration, *Evaluation of QCD uncertainties for Higgs boson production through gluon fusion and in association with two top quarks for simplified template cross-section measurements*, ATL-PHYS-PUB-2023-031, 2023, URL: <https://cds.cern.ch/record/2878797>.
- [121] G. Cowan, K. Cranmer, E. Gross and O. Vitells, *Asymptotic formulae for likelihood-based tests of new physics*, *Eur. Phys. J. C* **71** (2011) 1554, arXiv: 1007.1727 [physics.data-an], Erratum: *Eur. Phys. J. C* **73** (2013) 2501.
- [122] T. Junk, *Confidence level computation for combining searches with small statistics*, *Nucl. Instrum. Meth. A* **434** (1999) 435, arXiv: hep-ex/9902006.
- [123] A. L. Read, *Presentation of search results: the CL_s technique*, *J. Phys. G* **28** (2002) 2693.
- [124] ATLAS Collaboration, *Inclusive and differential cross-section measurements of $t\bar{t}Z$ production in pp collisions at $\sqrt{s} = 13\text{ TeV}$ with the ATLAS detector, including EFT and spin-correlation interpretations*, (2023), arXiv: 2312.04450 [hep-ex].

- [125] A. Buckley et al., *Rivet user manual*, *Comput. Phys. Commun.* **184** (2013) 2803, arXiv: [1003.0694 \[hep-ph\]](#).
- [126] C. Hays, A. Martin, V. Sanz and J. Setford, *On the impact of dimension-eight SMEFT operators on Higgs measurements*, *JHEP* **02** (2019) 123, arXiv: [1808.00442 \[hep-ph\]](#).
- [127] B. Grzadkowski, M. Iskrzyński, M. Misiak and J. Rosiek, *Dimension-Six Terms in the Standard Model Lagrangian*, *JHEP* **10** (2010) 085, arXiv: [1008.4884 \[hep-ph\]](#).
- [128] I. Brivio, Y. Jiang and M. Trott, *The SMEFTsim package, theory and tools*, *JHEP* **12** (2017) 070, arXiv: [1709.06492 \[hep-ph\]](#).
- [129] I. Brivio, *SMEFTsim 3.0 — a practical guide*, *JHEP* **04** (2021) 073, arXiv: [2012.11343 \[hep-ph\]](#).
- [130] J. de Blas, J. C. Criado, M. Perez-Victoria and J. Santiago, *Effective description of general extensions of the Standard Model: the complete tree-level dictionary*, *JHEP* **03** (2018) 109, arXiv: [1711.10391 \[hep-ph\]](#).
- [131] ATLAS Collaboration, *A detailed map of Higgs boson interactions by the ATLAS experiment ten years after the discovery*, *Nature* **607** (2022) 52, arXiv: [2207.00092 \[hep-ex\]](#), Erratum: *Nature* **612** (2022) E24.
- [132] S. Dawson and P. P. Giardino, *Electroweak corrections to Higgs boson decays to $\gamma\gamma$ and W^+W^- in standard model EFT*, *Phys. Rev. D* **98** (2018) 095005, arXiv: [1807.11504 \[hep-ph\]](#).
- [133] S. Dawson and P. P. Giardino, *Higgs decays to ZZ and $Z\gamma$ in the standard model effective field theory: An NLO analysis*, *Phys. Rev. D* **97** (2018) 093003, arXiv: [1801.01136 \[hep-ph\]](#).
- [134] ATLAS Collaboration, *ATLAS Computing Acknowledgements*, ATL-SOFT-PUB-2023-001, 2023, URL: <https://cds.cern.ch/record/2869272>.

The ATLAS Collaboration

G. Aad ¹⁰⁴, E. Aakvaag ¹⁷, B. Abbott ¹²³, S. Abdelhameed ^{119a}, K. Abeling ⁵⁶, N.J. Abicht ⁵⁰, S.H. Abidi ³⁰, M. Aboeela ⁴⁵, A. Aboulhorma ^{36e}, H. Abramowicz ¹⁵⁴, H. Abreu ¹⁵³, Y. Abulaiti ¹²⁰, B.S. Acharya ^{70a,70b,k}, A. Ackermann ^{64a}, C. Adam Bourdarios ⁴, L. Adamczyk ^{87a}, S.V. Addepalli ²⁷, M.J. Addison ¹⁰³, J. Adelman ¹¹⁸, A. Adiguzel ^{22c}, T. Adye ¹³⁷, A.A. Affolder ¹³⁹, Y. Afik ⁴⁰, M.N. Agaras ¹³, J. Agarwala ^{74a,74b}, A. Aggarwal ¹⁰², C. Agheorghiesei ^{28c}, F. Ahmadov ^{39,x}, W.S. Ahmed ¹⁰⁶, S. Ahuja ⁹⁷, X. Ai ^{63e}, G. Aielli ^{77a,77b}, A. Aikot ¹⁶⁶, M. Ait Tamlihat ^{36e}, B. Aitbenkikh ^{36a}, M. Akbiyik ¹⁰², T.P.A. Åkesson ¹⁰⁰, A.V. Akimov ³⁸, D. Akiyama ¹⁷¹, N.N. Akolkar ²⁵, S. Aktas ^{22a}, K. Al Houry ⁴², G.L. Alberghi ^{24b}, J. Albert ¹⁶⁸, P. Albicocco ⁵⁴, G.L. Albouy ⁶¹, S. Alderweireldt ⁵³, Z.L. Alegria ¹²⁴, M. Aleksa ³⁷, I.N. Aleksandrov ³⁹, C. Alexa ^{28b}, T. Alexopoulos ¹⁰, F. Alfonsi ^{24b}, M. Algren ⁵⁷, M. Alhroob ¹⁷⁰, B. Ali ¹³⁵, H.M.J. Ali ^{93,r}, S. Ali ³², S.W. Alibocus ⁹⁴, M. Aliev ^{34c}, G. Alimonti ^{72a}, W. Alkahi ⁵⁶, C. Allaire ⁶⁷, B.M.M. Allbrooke ¹⁴⁹, J.S. Allen ¹⁰³, J.F. Allen ⁵³, C.A. Allendes Flores ^{140f}, P.P. Allport ²¹, A. Aloisio ^{73a,73b}, F. Alonso ⁹², C. Alpigiani ¹⁴¹, Z.M.K. Alsolami ⁹³, M. Alvarez Estevez ¹⁰¹, A. Alvarez Fernandez ¹⁰², M. Alves Cardoso ⁵⁷, M.G. Alvigi ^{73a,73b}, M. Aly ¹⁰³, Y. Amaral Coutinho ^{84b}, A. Ambler ¹⁰⁶, C. Amelung ³⁷, M. Amerl ¹⁰³, C.G. Ames ¹¹¹, D. Amidei ¹⁰⁸, B. Amini ⁵⁵, K.J. Amirie ¹⁵⁸, S.P. Amor Dos Santos ^{133a}, K.R. Amos ¹⁶⁶, D. Amperiadou ¹⁵⁵, S. An ⁸⁵, V. Ananiev ¹²⁸, C. Anastopoulos ¹⁴², T. Andeen ¹¹, J.K. Anders ³⁷, A.C. Anderson ⁶⁰, S.Y. Andrean ^{48a,48b}, A. Andreazza ^{72a,72b}, S. Angelidakis ⁹, A. Angerami ⁴², A.V. Anisenkov ³⁸, A. Annovi ^{75a}, C. Antel ⁵⁷, E. Antipov ¹⁴⁸, M. Antonelli ⁵⁴, F. Anulli ^{76a}, M. Aoki ⁸⁵, T. Aoki ¹⁵⁶, M.A. Aparo ¹⁴⁹, L. Aperio Bella ⁴⁹, C. Appelt ¹⁹, A. Apyan ²⁷, S.J. Arbiol Val ⁸⁸, C. Arcangeletti ⁵⁴, A.T.H. Arce ⁵², J-F. Arguin ¹¹⁰, S. Argyropoulos ¹⁵⁵, J.-H. Arling ⁴⁹, O. Arnaez ⁴, H. Arnold ¹⁴⁸, G. Artoni ^{76a,76b}, H. Asada ¹¹³, K. Asai ¹²¹, S. Asai ¹⁵⁶, N.A. Asbah ³⁷, R.A. Ashby Pickering ¹⁷⁰, K. Assamagan ³⁰, R. Astalos ^{29a}, K.S.V. Astrand ¹⁰⁰, S. Atashi ¹⁶², R.J. Atkin ^{34a}, M. Atkinson ¹⁶⁵, H. Atmani ^{36f}, P.A. Atmasiddha ¹³¹, K. Augsten ¹³⁵, S. Auricchio ^{73a,73b}, A.D. Auriol ²¹, V.A. Austrup ¹⁰³, G. Avolio ³⁷, K. Axiotis ⁵⁷, G. Azuelos ^{110,ac}, D. Babal ^{29b}, H. Bachacou ¹³⁸, K. Bachas ^{155,o}, A. Bachi ³⁵, F. Backman ^{48a,48b}, A. Badea ⁴⁰, T.M. Baer ¹⁰⁸, P. Bagnaia ^{76a,76b}, M. Bahmani ¹⁹, D. Bahner ⁵⁵, K. Bai ¹²⁶, J.T. Baines ¹³⁷, L. Baines ⁹⁶, O.K. Baker ¹⁷⁵, E. Bakos ¹⁶, D. Bakshi Gupta ⁸, L.E. Balabram Filho ^{84b}, V. Balakrishnan ¹²³, R. Balasubramanian ⁴, E.M. Baldin ³⁸, P. Balek ^{87a}, E. Ballabene ^{24b,24a}, F. Balli ¹³⁸, L.M. Baltes ^{64a}, W.K. Balunas ³³, J. Balz ¹⁰², I. Bamwidhi ^{119b}, E. Banas ⁸⁸, M. Bandieramonte ¹³², A. Bandyopadhyay ²⁵, S. Bansal ²⁵, L. Barak ¹⁵⁴, M. Barakat ⁴⁹, E.L. Barberio ¹⁰⁷, D. Barberis ^{58b,58a}, M. Barbero ¹⁰⁴, M.Z. Barel ¹¹⁷, T. Barillari ¹¹², M-S. Barisits ³⁷, T. Barklow ¹⁴⁶, P. Baron ¹²⁵, D.A. Baron Moreno ¹⁰³, A. Baroncelli ^{63a}, A.J. Barr ¹²⁹, J.D. Barr ⁹⁸, F. Barreiro ¹⁰¹, J. Barreiro Guimarães da Costa ¹⁴, U. Barron ¹⁵⁴, M.G. Barros Teixeira ^{133a}, S. Barsov ³⁸, F. Bartels ^{64a}, R. Bartoldus ¹⁴⁶, A.E. Barton ⁹³, P. Bartos ^{29a}, A. Basan ¹⁰², M. Baselga ⁵⁰, A. Bassalat ^{67,b}, M.J. Basso ^{159a}, S. Bataju ⁴⁵, R. Bate ¹⁶⁷, R.L. Bates ⁶⁰, S. Batlamous ¹⁰¹, B. Batool ¹⁴⁴, M. Battaglia ¹³⁹, D. Battulga ¹⁹, M. Baucé ^{76a,76b}, M. Bauer ⁸⁰, P. Bauer ²⁵, L.T. Bazzano Hurrell ³¹, J.B. Beacham ⁵², T. Beau ¹³⁰, J.Y. Beaucamp ⁹², P.H. Beauchemin ¹⁶¹, P. Bechtel ²⁵, H.P. Beck ^{20,n}, K. Becker ¹⁷⁰, A.J. Beddall ⁸³, V.A. Bednyakov ³⁹, C.P. Bee ¹⁴⁸, L.J. Beemster ¹⁶, T.A. Beermann ³⁷, M. Begalli ^{84d}, M. Begel ³⁰, A. Behera ¹⁴⁸, J.K. Behr ⁴⁹, J.F. Beirer ³⁷, F. Beisiegel ²⁵, M. Belfkir ^{119b}, G. Bella ¹⁵⁴, L. Bellagamba ^{24b}, A. Bellerive ³⁵, P. Bellos ²¹, K. Beloborodov ³⁸, D. Benckekroun ^{36a}, F. Bendebba ^{36a}, Y. Benhammou ¹⁵⁴,

K.C. Benkendorfer [ID62](#), L. Beresford [ID49](#), M. Beretta [ID54](#), E. Bergeaas Kuutmann [ID164](#), N. Berger [ID4](#),
 B. Bergmann [ID135](#), J. Beringer [ID18a](#), G. Bernardi [ID5](#), C. Bernius [ID146](#), F.U. Bernlochner [ID25](#),
 F. Bernon [ID37](#), A. Berrocal Guardia [ID13](#), T. Berry [ID97](#), P. Berta [ID136](#), A. Berthold [ID51](#), S. Bethke [ID112](#),
 A. Betti [ID76a,76b](#), A.J. Bevan [ID96](#), N.K. Bhalla [ID55](#), S. Bhatta [ID148](#), D.S. Bhattacharya [ID169](#),
 P. Bhattarai [ID146](#), Z.M. Bhatti [ID120](#), K.D. Bhide [ID55](#), V.S. Bhopatkar [ID124](#), R.M. Bianchi [ID132](#),
 G. Bianco [ID24b,24a](#), O. Biebel [ID111](#), R. Bielski [ID126](#), M. Biglietti [ID78a](#), C.S. Billingsley [ID45](#), Y. Bimgdi [ID36f](#),
 M. Bindi [ID56](#), A. Bingul [ID22b](#), C. Bini [ID76a,76b](#), G.A. Bird [ID33](#), M. Birman [ID172](#), M. Biros [ID136](#),
 S. Biryukov [ID149](#), T. Bisanz [ID50](#), E. Bisceglie [ID44b,44a](#), J.P. Biswal [ID137](#), D. Biswas [ID144](#), I. Bloch [ID49](#),
 A. Blue [ID60](#), U. Blumenschein [ID96](#), J. Blumenthal [ID102](#), V.S. Bobrovnikov [ID38](#), M. Boehler [ID55](#),
 B. Boehm [ID169](#), D. Bogavac [ID37](#), A.G. Bogdanchikov [ID38](#), L.S. Boggia [ID130](#), C. Bohm [ID48a](#),
 V. Boisvert [ID97](#), P. Bokan [ID37](#), T. Bold [ID87a](#), M. Bomben [ID5](#), M. Bona [ID96](#), M. Boonekamp [ID138](#),
 C.D. Booth [ID97](#), A.G. Borbély [ID60](#), I.S. Bordulev [ID38](#), G. Borissov [ID93](#), D. Bortoletto [ID129](#),
 D. Boscherini [ID24b](#), M. Bosman [ID13](#), J.D. Bossio Sola [ID37](#), K. Bouaouda [ID36a](#), N. Bouchhar [ID166](#),
 L. Boudet [ID4](#), J. Boudreau [ID132](#), E.V. Bouhova-Thacker [ID93](#), D. Boumediene [ID41](#), R. Bouquet [ID58b,58a](#),
 A. Boveia [ID122](#), J. Boyd [ID37](#), D. Boye [ID30](#), I.R. Boyko [ID39](#), L. Bozianu [ID57](#), J. Bracinek [ID21](#),
 N. Brahimy [ID4](#), G. Brandt [ID174](#), O. Brandt [ID33](#), F. Braren [ID49](#), B. Brau [ID105](#), J.E. Brau [ID126](#),
 R. Brenner [ID172](#), L. Brenner [ID117](#), R. Brenner [ID164](#), S. Bressler [ID172](#), G. Brianti [ID79a,79b](#), D. Britton [ID60](#),
 D. Britzger [ID112](#), I. Brock [ID25](#), G. Brooijmans [ID42](#), E.M. Brooks [ID159b](#), E. Brost [ID30](#), L.M. Brown [ID168](#),
 L.E. Bruce [ID62](#), T.L. Bruckler [ID129](#), P.A. Bruckman de Renstrom [ID88](#), B. Brüers [ID49](#), A. Bruni [ID24b](#),
 G. Bruni [ID24b](#), M. Bruschi [ID24b](#), N. Brusino [ID76a,76b](#), T. Buanes [ID17](#), Q. Buat [ID141](#), D. Buchin [ID112](#),
 A.G. Buckley [ID60](#), O. Bulekov [ID38](#), B.A. Bullard [ID146](#), S. Burdin [ID94](#), C.D. Burgard [ID50](#),
 A.M. Burger [ID37](#), B. Burghgrave [ID8](#), O. Burlayenko [ID55](#), J. Burleson [ID165](#), J.T.P. Burr [ID33](#),
 J.C. Burzynski [ID145](#), E.L. Busch [ID42](#), V. Büscher [ID102](#), P.J. Bussey [ID60](#), J.M. Butler [ID26](#), C.M. Buttar [ID60](#),
 J.M. Butterworth [ID98](#), W. Buttinger [ID137](#), C.J. Buxo Vazquez [ID109](#), A.R. Buzykaev [ID38](#),
 S. Cabrera Urbán [ID166](#), L. Cadamuro [ID67](#), D. Caforio [ID59](#), H. Cai [ID132](#), Y. Cai [ID14,114c](#), Y. Cai [ID114a](#),
 V.M.M. Cairo [ID37](#), O. Cakir [ID3a](#), N. Calace [ID37](#), P. Calafiura [ID18a](#), G. Calderini [ID130](#), P. Calfayan [ID69](#),
 G. Callea [ID60](#), L.P. Caloba [ID84b](#), D. Calvet [ID41](#), S. Calvet [ID41](#), M. Calvetti [ID75a,75b](#), R. Camacho Toro [ID130](#),
 S. Camarda [ID37](#), D. Camarero Munoz [ID27](#), P. Camarri [ID77a,77b](#), M.T. Camerlingo [ID73a,73b](#),
 D. Cameron [ID37](#), C. Camincher [ID168](#), M. Campanelli [ID98](#), A. Camplani [ID43](#), V. Canale [ID73a,73b](#),
 A.C. Canbay [ID3a](#), E. Canonero [ID97](#), J. Cantero [ID166](#), Y. Cao [ID165](#), F. Capocasa [ID27](#), M. Capua [ID44b,44a](#),
 A. Carbone [ID72a,72b](#), R. Cardarelli [ID77a](#), J.C.J. Cardenas [ID8](#), G. Carducci [ID44b,44a](#), T. Carli [ID37](#),
 G. Carlino [ID73a](#), J.I. Carlotto [ID13](#), B.T. Carlson [ID132,p](#), E.M. Carlson [ID168,159a](#), J. Carmignani [ID94](#),
 L. Carminati [ID72a,72b](#), A. Carnelli [ID138](#), M. Carnesale [ID76a,76b](#), S. Caron [ID116](#), E. Carquin [ID140f](#),
 I.B. Carr [ID107](#), S. Carrá [ID72a](#), G. Carratta [ID24b,24a](#), A.M. Carroll [ID126](#), M.P. Casado [ID13,h](#), M. Caspar [ID49](#),
 F.L. Castillo [ID4](#), L. Castillo Garcia [ID13](#), V. Castillo Gimenez [ID166](#), N.F. Castro [ID133a,133e](#),
 A. Catinaccio [ID37](#), J.R. Catmore [ID128](#), T. Cavaliere [ID4](#), V. Cavaliere [ID30](#), N. Cavalli [ID24b,24a](#),
 L.J. Caviedes Betancourt [ID23b](#), Y.C. Cekmecelioglu [ID49](#), E. Celebi [ID83](#), S. Cella [ID37](#),
 M.S. Centonze [ID71a,71b](#), V. Cepaitis [ID57](#), K. Cerny [ID125](#), A.S. Cerqueira [ID84a](#), A. Cerri [ID149](#),
 L. Cerrito [ID77a,77b](#), F. Cerutti [ID18a](#), B. Cervato [ID144](#), A. Cervelli [ID24b](#), G. Cesarini [ID54](#), S.A. Cetin [ID83](#),
 D. Chakraborty [ID118](#), J. Chan [ID18a](#), W.Y. Chan [ID156](#), J.D. Chapman [ID33](#), E. Chapon [ID138](#),
 B. Chargeishvili [ID152b](#), D.G. Charlton [ID21](#), M. Chatterjee [ID20](#), C. Chauhan [ID136](#), Y. Che [ID114a](#),
 S. Chekanov [ID6](#), S.V. Chekulaev [ID159a](#), G.A. Chelkov [ID39,a](#), A. Chen [ID108](#), B. Chen [ID154](#), B. Chen [ID168](#),
 H. Chen [ID114a](#), H. Chen [ID30](#), J. Chen [ID63c](#), J. Chen [ID145](#), M. Chen [ID129](#), S. Chen [ID89](#), S.J. Chen [ID114a](#),
 X. Chen [ID63c](#), X. Chen [ID15,ab](#), Y. Chen [ID63a](#), C.L. Cheng [ID173](#), H.C. Cheng [ID65a](#), S. Cheong [ID146](#),
 A. Cheplakov [ID39](#), E. Cheremushkina [ID49](#), E. Cherepanova [ID117](#), R. Cherkaoui El Moursli [ID36e](#),
 E. Cheu [ID7](#), K. Cheung [ID66](#), L. Chevalier [ID138](#), V. Chiarella [ID54](#), G. Chiarelli [ID75a](#), N. Chiedde [ID104](#),
 G. Chiodini [ID71a](#), A.S. Chisholm [ID21](#), A. Chitan [ID28b](#), M. Chitishvili [ID166](#), M.V. Chizhov [ID39](#),

K. Choi ¹¹, Y. Chou ¹⁴¹, E.Y.S. Chow ¹¹⁶, K.L. Chu ¹⁷², M.C. Chu ^{65a}, X. Chu ^{14,114c},
 Z. Chubinidze ⁵⁴, J. Chudoba ¹³⁴, J.J. Chwastowski ⁸⁸, D. Cieri ¹¹², K.M. Ciesla ^{87a},
 V. Cindro ⁹⁵, A. Ciocio ^{18a}, F. Cirotto ^{73a,73b}, Z.H. Citron ¹⁷², M. Citterio ^{72a}, D.A. Ciubotaru ^{28b},
 A. Clark ⁵⁷, P.J. Clark ⁵³, N. Clarke Hall ⁹⁸, C. Clarry ¹⁵⁸, J.M. Clavijo Columbie ⁴⁹,
 S.E. Clawson ⁴⁹, C. Clement ^{48a,48b}, Y. Coadou ¹⁰⁴, M. Cobal ^{70a,70c}, A. Coccaro ^{58b},
 M.G. Cochran Branson ¹⁴¹, R.F. Coelho Barrue ^{133a}, R. Coelho Lopes De Sa ¹⁰⁵, S. Coelli ^{72a},
 L.S. Colangeli ¹⁵⁸, B. Cole ⁴², J. Collot ⁶¹, P. Conde Muiño ^{133a,133g}, M.P. Connell ^{34c},
 S.H. Connell ^{34c}, E.I. Conroy ¹²⁹, F. Conventi ^{73a,ad}, H.G. Cooke ²¹, A.M. Cooper-Sarkar ¹²⁹,
 F.A. Corchia ^{24b,24a}, A. Cordeiro Oudot Choi ¹³⁰, L.D. Corpe ⁴¹, M. Corradi ^{76a,76b},
 F. Corriveau ^{106,w}, A. Cortes-Gonzalez ¹⁹, M.J. Costa ¹⁶⁶, F. Costanza ⁴, D. Costanzo ¹⁴²,
 B.M. Cote ¹²², J. Couthures ⁴, G. Cowan ⁹⁷, K. Cranmer ¹⁷³, L. Cremer ⁵⁰,
 D. Cremonini ^{24b,24a}, S. Crépe-Renaudin ⁶¹, F. Crescioli ¹³⁰, M. Cristinziani ¹⁴⁴,
 M. Cristoforetti ^{79a,79b}, V. Croft ¹¹⁷, J.E. Crosby ¹²⁴, G. Crosetti ^{44b,44a}, A. Cueto ¹⁰¹, H. Cui ⁹⁸,
 Z. Cui ⁷, W.R. Cunningham ⁶⁰, F. Curcio ¹⁶⁶, J.R. Curran ⁵³, P. Czodrowski ³⁷,
 M.J. Da Cunha Sargedas De Sousa ^{58b,58a}, J.V. Da Fonseca Pinto ^{84b}, C. Da Via ¹⁰³,
 W. Dabrowski ^{87a}, T. Dado ³⁷, S. Dahbi ¹⁵¹, T. Dai ¹⁰⁸, D. Dal Santo ²⁰, C. Dallapiccola ¹⁰⁵,
 M. Dam ⁴³, G. D'amen ³⁰, V. D'Amico ¹¹¹, J. Damp ¹⁰², J.R. Dandoy ³⁵, D. Dannheim ³⁷,
 M. Danninger ¹⁴⁵, V. Dao ¹⁴⁸, G. Darbo ^{58b}, S.J. Das ^{30,ae}, F. Dattola ⁴⁹, S. D'Auria ^{72a,72b},
 A. D'avano ^{73a,73b}, C. David ^{34a}, T. Davidek ¹³⁶, I. Dawson ⁹⁶, H.A. Day-hall ¹³⁵, K. De ⁸,
 R. De Asmundis ^{73a}, N. De Biase ⁴⁹, S. De Castro ^{24b,24a}, N. De Groot ¹¹⁶, P. de Jong ¹¹⁷,
 H. De la Torre ¹¹⁸, A. De Maria ^{114a}, A. De Salvo ^{76a}, U. De Sanctis ^{77a,77b}, F. De Santis ^{71a,71b},
 A. De Santo ¹⁴⁹, J.B. De Vivie De Regie ⁶¹, J. Debevc ⁹⁵, D.V. Dedovich ³⁹, J. Degens ⁹⁴,
 A.M. Deiana ⁴⁵, F. Del Corso ^{24b,24a}, J. Del Peso ¹⁰¹, L. Delagrangé ¹³⁰, F. Deliot ¹³⁸,
 C.M. Delitzsch ⁵⁰, M. Della Pietra ^{73a,73b}, D. Della Volpe ⁵⁷, A. Dell'Acqua ³⁷,
 L. Dell'Asta ^{72a,72b}, M. Delmastro ⁴, P.A. Delsart ⁶¹, S. Demers ¹⁷⁵, M. Demichev ³⁹,
 S.P. Denisov ³⁸, L. D'Eramo ⁴¹, D. Derendarz ⁸⁸, F. Derue ¹³⁰, P. Dervan ⁹⁴, K. Desch ²⁵,
 C. Deutsch ²⁵, F.A. Di Bello ^{58b,58a}, A. Di Ciaccio ^{77a,77b}, L. Di Ciaccio ⁴,
 A. Di Domenico ^{76a,76b}, C. Di Donato ^{73a,73b}, A. Di Girolamo ³⁷, G. Di Gregorio ³⁷,
 A. Di Luca ^{79a,79b}, B. Di Micco ^{78a,78b}, R. Di Nardo ^{78a,78b}, K.F. Di Petrillo ⁴⁰,
 M. Diamantopoulou ³⁵, F.A. Dias ¹¹⁷, T. Dias Do Vale ¹⁴⁵, M.A. Diaz ^{140a,140b},
 F.G. Diaz Capriles ²⁵, A.R. Didenko ³⁹, M. Didenko ¹⁶⁶, E.B. Diehl ¹⁰⁸, S. Díez Cornell ⁴⁹,
 C. Díez Pardos ¹⁴⁴, C. Dimitriadi ¹⁶⁴, A. Dimitrievska ²¹, J. Dingfelder ²⁵, T. Dingley ¹²⁹,
 I-M. Dinu ^{28b}, S.J. Dittmeier ^{64b}, F. Dittus ³⁷, M. Divisek ¹³⁶, B. Dixit ⁹⁴, F. Djama ¹⁰⁴,
 T. Djobava ^{152b}, C. Doglioni ^{103,100}, A. Dohnalova ^{29a}, J. Dolejsi ¹³⁶, Z. Dolezal ¹³⁶,
 K. Domijan ^{87a}, K.M. Dona ⁴⁰, M. Donadelli ^{84d}, B. Dong ¹⁰⁹, J. Donini ⁴¹,
 A. D'Onofrio ^{73a,73b}, M. D'Onofrio ⁹⁴, J. Dopke ¹³⁷, A. Doria ^{73a}, N. Dos Santos Fernandes ^{133a},
 P. Dougan ¹⁰³, M.T. Dova ⁹², A.T. Doyle ⁶⁰, M.A. Draguet ¹²⁹, M.P. Drescher ⁵⁶, E. Dreyer ¹⁷²,
 I. Drivas-koulouris ¹⁰, M. Drnevich ¹²⁰, M. Drozdova ⁵⁷, D. Du ^{63a}, T.A. du Pree ¹¹⁷,
 F. Dubinin ³⁸, M. Dubovsky ^{29a}, E. Duchovni ¹⁷², G. Duckeck ¹¹¹, O.A. Ducu ^{28b}, D. Duda ⁵³,
 A. Dudarev ³⁷, E.R. Duden ²⁷, M. D'uffici ¹⁰³, L. Duflot ⁶⁷, M. Dührssen ³⁷, I. Duminica ^{28g},
 A.E. Dumitriu ^{28b}, M. Dunford ^{64a}, S. Dungs ⁵⁰, K. Dunne ^{48a,48b}, A. Duperrin ¹⁰⁴,
 H. Duran Yildiz ^{3a}, M. Düren ⁵⁹, A. Durglishvili ^{152b}, B.L. Dwyer ¹¹⁸, G.I. Dyckes ^{18a},
 M. Dyndal ^{87a}, B.S. Dziedzic ³⁷, Z.O. Earnshaw ¹⁴⁹, G.H. Eberwein ¹²⁹, B. Eckerova ^{29a},
 S. Eggebrecht ⁵⁶, E. Egidio Purcino De Souza ^{84e}, L.F. Ehrke ⁵⁷, G. Eigen ¹⁷, K. Einsweiler ^{18a},
 T. Ekelof ¹⁶⁴, P.A. Ekman ¹⁰⁰, S. El Farkh ^{36b}, Y. El Ghazali ^{63a}, H. El Jarrari ³⁷,
 A. El Moussaouy ^{36a}, V. Ellajosyula ¹⁶⁴, M. Ellert ¹⁶⁴, F. Ellinghaus ¹⁷⁴, N. Ellis ³⁷,
 J. Elmsheuser ³⁰, M. Elsayy ^{119a}, M. Elsing ³⁷, D. Emeliyanov ¹³⁷, Y. Enari ⁸⁵, I. Ene ^{18a},

S. Epari ¹³, P.A. Erland ⁸⁸, D. Ernani Martins Neto ⁸⁸, M. Errenst ¹⁷⁴, M. Escalier ⁶⁷,
 C. Escobar ¹⁶⁶, E. Etzion ¹⁵⁴, G. Evans ^{133a}, H. Evans ⁶⁹, L.S. Evans ⁹⁷, A. Ezhilov ³⁸,
 S. Ezzarqtouni ^{36a}, F. Fabbri ^{24b,24a}, L. Fabbri ^{24b,24a}, G. Facini ⁹⁸, V. Fadeyev ¹³⁹,
 R.M. Fakhrutdinov ³⁸, D. Fakoudis ¹⁰², S. Falciano ^{76a}, L.F. Falda Ulhoa Coelho ³⁷,
 F. Fallavollita ¹¹², G. Falsetti ^{44b,44a}, J. Faltova ¹³⁶, C. Fan ¹⁶⁵, K.Y. Fan ^{65b}, Y. Fan ¹⁴,
 Y. Fang ^{14,114c}, M. Fanti ^{72a,72b}, M. Faraj ^{70a,70b}, Z. Farazpay ⁹⁹, A. Farbin ⁸, A. Farilla ^{78a},
 T. Farooque ¹⁰⁹, S.M. Farrington ⁵³, F. Fassi ^{36e}, D. Fassouliotis ⁹, M. Faucci Giannelli ^{77a,77b},
 W.J. Fawcett ³³, L. Fayard ⁶⁷, P. Federic ¹³⁶, P. Federicova ¹³⁴, O.L. Fedin ^{38,a}, M. Feickert ¹⁷³,
 L. Feligioni ¹⁰⁴, D.E. Fellers ¹²⁶, C. Feng ^{63b}, Z. Feng ¹¹⁷, M.J. Fenton ¹⁶², L. Ferencz ⁴⁹,
 R.A.M. Ferguson ⁹³, S.I. Fernandez Luengo ^{140f}, P. Fernandez Martinez ¹³, M.J.V. Fernoux ¹⁰⁴,
 J. Ferrando ⁹³, A. Ferrari ¹⁶⁴, P. Ferrari ^{117,116}, R. Ferrari ^{74a}, D. Ferrere ⁵⁷, C. Ferretti ¹⁰⁸,
 D. Fiacco ^{76a,76b}, F. Fiedler ¹⁰², P. Fiedler ¹³⁵, S. Filimonov ³⁸, A. Filipčić ⁹⁵, E.K. Filmer ^{159a},
 F. Filthaut ¹¹⁶, M.C.N. Fiolhais ^{133a,133c,c}, L. Fiorini ¹⁶⁶, W.C. Fisher ¹⁰⁹, T. Fitschen ¹⁰³,
 P.M. Fitzhugh ¹³⁸, I. Fleck ¹⁴⁴, P. Fleischmann ¹⁰⁸, T. Flick ¹⁷⁴, M. Flores ^{34d,z},
 L.R. Flores Castillo ^{65a}, L. Flores Sanz De Acedo ³⁷, F.M. Follega ^{79a,79b}, N. Fomin ³³,
 J.H. Foo ¹⁵⁸, A. Formica ¹³⁸, A.C. Forti ¹⁰³, E. Fortin ³⁷, A.W. Fortman ^{18a}, M.G. Foti ^{18a},
 L. Fountas ^{9,i}, D. Fournier ⁶⁷, H. Fox ⁹³, P. Francavilla ^{75a,75b}, S. Francescato ⁶²,
 S. Franchellucci ⁵⁷, M. Franchini ^{24b,24a}, S. Franchino ^{64a}, D. Francis ³⁷, L. Franco ¹¹⁶,
 V. Franco Lima ³⁷, L. Franconi ⁴⁹, M. Franklin ⁶², G. Frattari ²⁷, Y.Y. Frid ¹⁵⁴, J. Friend ⁶⁰,
 N. Fritzsche ³⁷, A. Froch ⁵⁵, D. Froidevaux ³⁷, J.A. Frost ¹²⁹, Y. Fu ^{63a},
 S. Fuenzalida Garrido ^{140f}, M. Fujimoto ¹⁰⁴, K.Y. Fung ^{65a}, E. Furtado De Simas Filho ^{84e},
 M. Furukawa ¹⁵⁶, J. Fuster ¹⁶⁶, A. Gaa ⁵⁶, A. Gabrielli ^{24b,24a}, A. Gabrielli ¹⁵⁸, P. Gadow ³⁷,
 G. Gagliardi ^{58b,58a}, L.G. Gagnon ^{18a}, S. Gaid ¹⁶³, S. Galantzan ¹⁵⁴, J. Gallagher ¹,
 E.J. Gallas ¹²⁹, B.J. Gallop ¹³⁷, K.K. Gan ¹²², S. Ganguly ¹⁵⁶, Y. Gao ⁵³,
 F.M. Garay Walls ^{140a,140b}, B. Garcia ³⁰, C. García ¹⁶⁶, A. Garcia Alonso ¹¹⁷,
 A.G. Garcia Caffaro ¹⁷⁵, J.E. García Navarro ¹⁶⁶, M. Garcia-Sciveres ^{18a}, G.L. Gardner ¹³¹,
 R.W. Gardner ⁴⁰, N. Garelli ¹⁶¹, D. Garg ⁸¹, R.B. Garg ¹⁴⁶, J.M. Gargan ⁵³, C.A. Garner ¹⁵⁸,
 C.M. Garvey ^{34a}, V.K. Gassmann ¹⁶¹, G. Gaudio ^{74a}, V. Gautam ¹³, P. Gauzzi ^{76a,76b},
 J. Gavranovic ⁹⁵, I.L. Gavrilenko ³⁸, A. Gavrilyuk ³⁸, C. Gay ¹⁶⁷, G. Gaycken ¹²⁶,
 E.N. Gazis ¹⁰, A.A. Geanta ^{28b}, C.M. Gee ¹³⁹, A. Gekow ¹²², C. Gemme ^{58b}, M.H. Genest ⁶¹,
 A.D. Gentry ¹¹⁵, S. George ⁹⁷, W.F. George ²¹, T. Geralis ⁴⁷, P. Gessinger-Befurt ³⁷,
 M.E. Geyik ¹⁷⁴, M. Ghani ¹⁷⁰, K. Ghorbanian ⁹⁶, A. Ghosal ¹⁴⁴, A. Ghosh ¹⁶², A. Ghosh ⁷,
 B. Giacobbe ^{24b}, S. Giagu ^{76a,76b}, T. Giani ¹¹⁷, A. Giannini ^{63a}, S.M. Gibson ⁹⁷, M. Gignac ¹³⁹,
 D.T. Gil ^{87b}, A.K. Gilbert ^{87a}, B.J. Gilbert ⁴², D. Gillberg ³⁵, G. Gilles ¹¹⁷, L. Ginabat ¹³⁰,
 D.M. Gingrich ^{2,ac}, M.P. Giordani ^{70a,70c}, P.F. Giraud ¹³⁸, G. Giugliarelli ^{70a,70c}, D. Giugni ^{72a},
 F. Giuli ^{77a,77b}, I. Gkialas ^{9,i}, L.K. Gladilin ³⁸, C. Glasman ¹⁰¹, G.R. Gledhill ¹²⁶, G. Glemža ⁴⁹,
 M. Glisic ¹²⁶, I. Gnesi ^{44b}, Y. Go ³⁰, M. Goblirsch-Kolb ³⁷, B. Gocke ⁵⁰, D. Godin ¹¹⁰,
 B. Gokturk ^{22a}, S. Goldfarb ¹⁰⁷, T. Golling ⁵⁷, M.G.D. Gololo ^{34g}, D. Golubkov ³⁸,
 J.P. Gombas ¹⁰⁹, A. Gomes ^{133a,133b}, G. Gomes Da Silva ¹⁴⁴, A.J. Gomez Delegido ¹⁶⁶,
 R. Gonçalves ^{133a}, L. Gonella ²¹, A. Gongadze ^{152c}, F. Gonnella ²¹, J.L. Gonski ¹⁴⁶,
 R.Y. González Andana ⁵³, S. González de la Hoz ¹⁶⁶, R. Gonzalez Lopez ⁹⁴,
 C. Gonzalez Renteria ^{18a}, M.V. Gonzalez Rodrigues ⁴⁹, R. Gonzalez Suarez ¹⁶⁴,
 S. Gonzalez-Sevilla ⁵⁷, L. Goossens ³⁷, B. Gorini ³⁷, E. Gorini ^{71a,71b}, A. Gorišek ⁹⁵,
 T.C. Gosart ¹³¹, A.T. Goshaw ⁵², M.I. Gostkin ³⁹, S. Goswami ¹²⁴, C.A. Gottardo ³⁷,
 S.A. Gotz ¹¹¹, M. Goughri ^{36b}, V. Goumarre ⁴⁹, A.G. Goussiou ¹⁴¹, N. Govender ^{34c},
 R.P. Grabarczyk ¹²⁹, I. Grabowska-Bold ^{87a}, K. Graham ³⁵, E. Gramstad ¹²⁸,
 S. Grancagnolo ^{71a,71b}, C.M. Grant ^{1,138}, P.M. Gravila ^{28f}, F.G. Gravili ^{71a,71b}, H.M. Gray ^{18a},

M. Greco ^{71a,71b}, M.J. Green ¹, C. Grefe ²⁵, A.S. Grefsrud ¹⁷, I.M. Gregor ⁴⁹, K.T. Greif ¹⁶²,
P. Grenier ¹⁴⁶, S.G. Grewe ¹¹², A.A. Grillo ¹³⁹, K. Grimm ³², S. Grinstein ^{13,s}, J.-F. Grivaz ⁶⁷,
E. Gross ¹⁷², J. Grosse-Knetter ⁵⁶, L. Guan ¹⁰⁸, J.G.R. Guerrero Rojas ¹⁶⁶, G. Guerrieri ³⁷,
R. Gugel ¹⁰², J.A.M. Guhit ¹⁰⁸, A. Guida ¹⁹, E. Guilloton ¹⁷⁰, S. Guindon ³⁷, F. Guo ^{14,114c},
J. Guo ^{63c}, L. Guo ⁴⁹, L. Guo ¹⁴, Y. Guo ¹⁰⁸, A. Gupta ⁵⁰, R. Gupta ¹³², S. Gurbuz ²⁵,
S.S. Gurdasani ⁵⁵, G. Gustavino ^{76a,76b}, P. Gutierrez ¹²³, L.F. Gutierrez Zagazeta ¹³¹,
M. Gutsche ⁵¹, C. Gutschow ⁹⁸, C. Gwenlan ¹²⁹, C.B. Gwilliam ⁹⁴, E.S. Haaland ¹²⁸,
A. Haas ¹²⁰, M. Habedank ⁶⁰, C. Haber ^{18a}, H.K. Hadavand ⁸, A. Hadeef ⁵¹, S. Hadzic ¹¹²,
A.I. Hagan ⁹³, J.J. Hahn ¹⁴⁴, E.H. Haines ⁹⁸, M. Haleem ¹⁶⁹, J. Haley ¹²⁴, G.D. Hallowell ¹⁰⁴,
L. Halser ²⁰, K. Hamano ¹⁶⁸, M. Hamer ²⁵, E.J. Hampshire ⁹⁷, J. Han ^{63b}, L. Han ^{114a},
L. Han ^{63a}, S. Han ^{18a}, Y.F. Han ¹⁵⁸, K. Hanagaki ⁸⁵, M. Hance ¹³⁹, D.A. Hangal ⁴²,
H. Hanif ¹⁴⁵, M.D. Hank ¹³¹, J.B. Hansen ⁴³, P.H. Hansen ⁴³, D. Harada ⁵⁷, T. Harenberg ¹⁷⁴,
S. Harkusha ¹⁷⁶, M.L. Harris ¹⁰⁵, Y.T. Harris ²⁵, J. Harrison ¹³, N.M. Harrison ¹²²,
P.F. Harrison ¹⁷⁰, N.M. Hartman ¹¹², N.M. Hartmann ¹¹¹, R.Z. Hasan ^{97,137}, Y. Hasegawa ¹⁴³,
F. Haslbeck ¹²⁹, S. Hassan ¹⁷, R. Hauser ¹⁰⁹, C.M. Hawkes ²¹, R.J. Hawkins ³⁷,
Y. Hayashi ¹⁵⁶, D. Hayden ¹⁰⁹, C. Hayes ¹⁰⁸, R.L. Hayes ¹¹⁷, C.P. Hays ¹²⁹, J.M. Hays ⁹⁶,
H.S. Hayward ⁹⁴, F. He ^{63a}, M. He ^{14,114c}, Y. He ⁴⁹, Y. He ⁹⁸, N.B. Heatley ⁹⁶, V. Hedberg ¹⁰⁰,
A.L. Heggelund ¹²⁸, N.D. Hehir ^{96,*}, C. Heidegger ⁵⁵, K.K. Heidegger ⁵⁵, J. Heilman ³⁵,
S. Heim ⁴⁹, T. Heim ^{18a}, J.G. Heinlein ¹³¹, J.J. Heinrich ¹²⁶, L. Heinrich ^{112,aa}, J. Hejbal ¹³⁴,
A. Held ¹⁷³, S. Hellesund ¹⁷, C.M. Helling ¹⁶⁷, S. Hellman ^{48a,48b}, R.C.W. Henderson ⁹³,
L. Henkelmann ³³, A.M. Henriques Correia ³⁷, H. Herde ¹⁰⁰, Y. Hernández Jiménez ¹⁴⁸,
L.M. Herrmann ²⁵, T. Herrmann ⁵¹, G. Herten ⁵⁵, R. Hertenberger ¹¹¹, L. Hervas ³⁷,
M.E. Hesping ¹⁰², N.P. Hessey ^{159a}, J. Hessler ¹¹², M. Hidaoui ^{36b}, N. Hidic ¹³⁶, E. Hill ¹⁵⁸,
S.J. Hillier ²¹, J.R. Hinds ¹⁰⁹, F. Hinterkeuser ²⁵, M. Hirose ¹²⁷, S. Hirose ¹⁶⁰,
D. Hirschbuehl ¹⁷⁴, T.G. Hitchings ¹⁰³, B. Hiti ⁹⁵, J. Hobbs ¹⁴⁸, R. Hobincu ^{28e}, N. Hod ¹⁷²,
M.C. Hodgkinson ¹⁴², B.H. Hodgkinson ¹²⁹, A. Hoecker ³⁷, D.D. Hofer ¹⁰⁸, J. Hofer ¹⁶⁶,
T. Holm ²⁵, M. Holzbock ³⁷, L.B.A.H. Hommels ³³, B.P. Honan ¹⁰³, J.J. Hong ⁶⁹, J. Hong ^{63c},
T.M. Hong ¹³², B.H. Hooberman ¹⁶⁵, W.H. Hopkins ⁶, M.C. Hoppesch ¹⁶⁵, Y. Horii ¹¹³,
M.E. Horstmann ¹¹², S. Hou ¹⁵¹, A.S. Howard ⁹⁵, J. Howarth ⁶⁰, J. Hoya ⁶, M. Hrabovsky ¹²⁵,
A. Hrynevich ⁴⁹, T. Hryn'ova ⁴, P.J. Hsu ⁶⁶, S.-C. Hsu ¹⁴¹, T. Hsu ⁶⁷, M. Hu ^{18a}, Q. Hu ^{63a},
S. Huang ³³, X. Huang ^{14,114c}, Y. Huang ¹⁴², Y. Huang ¹⁰², Y. Huang ¹⁴, Z. Huang ¹⁰³,
Z. Hubacek ¹³⁵, M. Huebner ²⁵, F. Huegging ²⁵, T.B. Huffman ¹²⁹, C.A. Hugli ⁴⁹,
M. Huhtinen ³⁷, S.K. Huiberts ¹⁷, R. Hulsken ¹⁰⁶, N. Huseynov ^{12,f}, J. Huston ¹⁰⁹, J. Huth ⁶²,
R. Hyneman ¹⁴⁶, G. Iacobucci ⁵⁷, G. Iakovidis ³⁰, L. Iconomidou-Fayard ⁶⁷, J.P. Iddon ³⁷,
P. Iengo ^{73a,73b}, R. Iguchi ¹⁵⁶, Y. Iiyama ¹⁵⁶, T. Iizawa ¹²⁹, Y. Ikegami ⁸⁵, N. Ilic ¹⁵⁸,
H. Imam ^{84c}, G. Inacio Goncalves ^{84d}, T. Ingebretsen Carlson ^{48a,48b}, J.M. Inglis ⁹⁶,
G. Introzzi ^{74a,74b}, M. Iodice ^{78a}, V. Ippolito ^{76a,76b}, R.K. Irwin ⁹⁴, M. Ishino ¹⁵⁶, W. Islam ¹⁷³,
C. Issever ¹⁹, S. Istin ^{22a,ag}, H. Ito ¹⁷¹, R. Iuppa ^{79a,79b}, A. Ivina ¹⁷², J.M. Izen ⁴⁶, V. Izzo ^{73a},
P. Jacka ¹³⁴, P. Jackson ¹, C.S. Jagfeld ¹¹¹, G. Jain ^{159a}, P. Jain ⁴⁹, K. Jakobs ⁵⁵,
T. Jakoubek ¹⁷², J. Jamieson ⁶⁰, W. Jang ¹⁵⁶, M. Javurkova ¹⁰⁵, P. Jawahar ¹⁰³, L. Jeanty ¹²⁶,
J. Jejelava ^{152a,y}, P. Jenni ^{55,e}, C.E. Jessiman ³⁵, C. Jia ^{63b}, H. Jia ¹⁶⁷, J. Jia ¹⁴⁸, X. Jia ^{14,114c},
Z. Jia ^{114a}, C. Jiang ⁵³, S. Jiggins ⁴⁹, J. Jimenez Pena ¹³, S. Jin ^{114a}, A. Jinaru ^{28b},
O. Jinnouchi ¹⁵⁷, P. Johansson ¹⁴², K.A. Johns ⁷, J.W. Johnson ¹³⁹, F.A. Jolly ⁴⁹,
D.M. Jones ¹⁴⁹, E. Jones ⁴⁹, K.S. Jones ⁸, P. Jones ³³, R.W.L. Jones ⁹³, T.J. Jones ⁹⁴,
H.L. Joos ^{56,37}, R. Joshi ¹²², J. Jovicevic ¹⁶, X. Ju ^{18a}, J.J. Junggeburth ¹⁰⁵, T. Junkermann ^{64a},
A. Juste Rozas ^{13,s}, M.K. Juzek ⁸⁸, S. Kabana ^{140e}, A. Kaczmarska ⁸⁸, M. Kado ¹¹²,
H. Kagan ¹²², M. Kagan ¹⁴⁶, A. Kahn ¹³¹, C. Kahra ¹⁰², T. Kaji ¹⁵⁶, E. Kajomovitz ¹⁵³,

N. Kakati [id](#)¹⁷², I. Kalaitzidou [id](#)⁵⁵, C.W. Kalderon [id](#)³⁰, N.J. Kang [id](#)¹³⁹, D. Kar [id](#)^{34g}, K. Karava [id](#)¹²⁹,
 M.J. Kareem [id](#)^{159b}, E. Karentzos [id](#)⁵⁵, O. Karkout [id](#)¹¹⁷, S.N. Karpov [id](#)³⁹, Z.M. Karpova [id](#)³⁹,
 V. Kartvelishvili [id](#)⁹³, A.N. Karyukhin [id](#)³⁸, E. Kasimi [id](#)¹⁵⁵, J. Katzy [id](#)⁴⁹, S. Kaur [id](#)³⁵, K. Kawade [id](#)¹⁴³,
 M.P. Kawale [id](#)¹²³, C. Kawamoto [id](#)⁸⁹, T. Kawamoto [id](#)^{63a}, E.F. Kay [id](#)³⁷, F.I. Kaya [id](#)¹⁶¹, S. Kazakos [id](#)¹⁰⁹,
 V.F. Kazanin [id](#)³⁸, Y. Ke [id](#)¹⁴⁸, J.M. Keaveney [id](#)^{34a}, R. Keeler [id](#)¹⁶⁸, G.V. Kehris [id](#)⁶², J.S. Keller [id](#)³⁵,
 J.J. Kempster [id](#)¹⁴⁹, O. Kepka [id](#)¹³⁴, B.P. Kerridge [id](#)¹³⁷, S. Kersten [id](#)¹⁷⁴, B.P. Kerševan [id](#)⁹⁵,
 L. Keszeghova [id](#)^{29a}, S. Ketabchi Haghighat [id](#)¹⁵⁸, R.A. Khan [id](#)¹³², A. Khanov [id](#)¹²⁴,
 A.G. Kharlamov [id](#)³⁸, T. Kharlamova [id](#)³⁸, E.E. Khoda [id](#)¹⁴¹, M. Kholodenko [id](#)^{133a}, T.J. Khoo [id](#)¹⁹,
 G. Khorauli [id](#)¹⁶⁹, J. Khubua [id](#)^{152b,*}, Y.A.R. Khwaira [id](#)¹³⁰, B. Kibirige [id](#)^{34g}, D. Kim [id](#)⁶,
 D.W. Kim [id](#)^{48a,48b}, Y.K. Kim [id](#)⁴⁰, N. Kimura [id](#)⁹⁸, M.K. Kingston [id](#)⁵⁶, A. Kirchhoff [id](#)⁵⁶, C. Kirfel [id](#)²⁵,
 F. Kirfel [id](#)²⁵, J. Kirk [id](#)¹³⁷, A.E. Kiryunin [id](#)¹¹², S. Kita [id](#)¹⁶⁰, C. Kitsaki [id](#)¹⁰, O. Kivernyk [id](#)²⁵,
 M. Klassen [id](#)¹⁶¹, C. Klein [id](#)³⁵, L. Klein [id](#)¹⁶⁹, M.H. Klein [id](#)⁴⁵, S.B. Klein [id](#)⁵⁷, U. Klein [id](#)⁹⁴,
 A. Klimentov [id](#)³⁰, T. Klioutchnikova [id](#)³⁷, P. Kluit [id](#)¹¹⁷, S. Kluth [id](#)¹¹², E. Kneringer [id](#)⁸⁰,
 T.M. Knight [id](#)¹⁵⁸, A. Knue [id](#)⁵⁰, D. Kobylanski [id](#)¹⁷², S.F. Koch [id](#)¹²⁹, M. Kocian [id](#)¹⁴⁶, P. Kodyš [id](#)¹³⁶,
 D.M. Koeck [id](#)¹²⁶, P.T. Koenig [id](#)²⁵, T. Koffas [id](#)³⁵, O. Kolay [id](#)⁵¹, I. Koletsou [id](#)⁴, T. Komarek [id](#)⁸⁸,
 K. Köneke [id](#)⁵⁵, A.X.Y. Kong [id](#)¹, T. Kono [id](#)¹²¹, N. Konstantinidis [id](#)⁹⁸, P. Kontaxakis [id](#)⁵⁷,
 B. Konya [id](#)¹⁰⁰, R. Kopeliansky [id](#)⁴², S. Koperny [id](#)^{87a}, K. Korcyl [id](#)⁸⁸, K. Kordas [id](#)^{155,d}, A. Korn [id](#)⁹⁸,
 S. Korn [id](#)⁵⁶, I. Korolkov [id](#)¹³, N. Korotkova [id](#)³⁸, B. Kortman [id](#)¹¹⁷, O. Kortner [id](#)¹¹², S. Kortner [id](#)¹¹²,
 W.H. Kostecka [id](#)¹¹⁸, V.V. Kostyukhin [id](#)¹⁴⁴, A. Kotsokechagia [id](#)³⁷, A. Kotwal [id](#)⁵², A. Koulouris [id](#)³⁷,
 A. Kourkoumeli-Charalampidi [id](#)^{74a,74b}, C. Kourkoumelis [id](#)⁹, E. Kourlitis [id](#)^{112,aa}, O. Kovanda [id](#)¹²⁶,
 R. Kowalewski [id](#)¹⁶⁸, W. Kozanecki [id](#)¹²⁶, A.S. Kozhin [id](#)³⁸, V.A. Kramarenko [id](#)³⁸, G. Kramberger [id](#)⁹⁵,
 P. Kramer [id](#)¹⁰², M.W. Krasny [id](#)¹³⁰, A. Krasznahorkay [id](#)³⁷, A.C. Kraus [id](#)¹¹⁸, J.W. Kraus [id](#)¹⁷⁴,
 J.A. Kremer [id](#)⁴⁹, T. Kresse [id](#)⁵¹, L. Kretschmann [id](#)¹⁷⁴, J. Kretschmar [id](#)⁹⁴, K. Kreul [id](#)¹⁹,
 P. Krieger [id](#)¹⁵⁸, M. Krivos [id](#)¹³⁶, K. Krizka [id](#)²¹, K. Kroeninger [id](#)⁵⁰, H. Kroha [id](#)¹¹², J. Kroll [id](#)¹³⁴,
 J. Kroll [id](#)¹³¹, K.S. Krowpman [id](#)¹⁰⁹, U. Kruchonak [id](#)³⁹, H. Krüger [id](#)²⁵, N. Krumnack [id](#)⁸², M.C. Kruse [id](#)⁵²,
 O. Kuchinskaia [id](#)³⁸, S. Kuday [id](#)^{3a}, S. Kuehn [id](#)³⁷, R. Kuesters [id](#)⁵⁵, T. Kuhl [id](#)⁴⁹, V. Kukhtin [id](#)³⁹,
 Y. Kulchitsky [id](#)^{38,a}, S. Kuleshov [id](#)^{140d,140b}, M. Kumar [id](#)^{34g}, N. Kumari [id](#)⁴⁹, P. Kumari [id](#)^{159b},
 A. Kupco [id](#)¹³⁴, T. Kupfer [id](#)⁵⁰, A. Kupich [id](#)³⁸, O. Kuprash [id](#)⁵⁵, H. Kurashige [id](#)⁸⁶, L.L. Kurchaninov [id](#)^{159a},
 O. Kurdysh [id](#)⁶⁷, Y.A. Kurochkin [id](#)³⁸, A. Kurova [id](#)³⁸, M. Kuze [id](#)¹⁵⁷, A.K. Kvam [id](#)¹⁰⁵, J. Kvita [id](#)¹²⁵,
 T. Kwan [id](#)¹⁰⁶, N.G. Kyriacou [id](#)¹⁰⁸, L.A.O. Laatu [id](#)¹⁰⁴, C. Lacasta [id](#)¹⁶⁶, F. Lacava [id](#)^{76a,76b},
 H. Lacker [id](#)¹⁹, D. Lacour [id](#)¹³⁰, N.N. Lad [id](#)⁹⁸, E. Ladygin [id](#)³⁹, A. Lafarge [id](#)⁴¹, B. Laforge [id](#)¹³⁰,
 T. Lagouri [id](#)¹⁷⁵, F.Z. Lahbabi [id](#)^{36a}, S. Lai [id](#)⁵⁶, J.E. Lambert [id](#)¹⁶⁸, S. Lammers [id](#)⁶⁹, W. Lampl [id](#)⁷,
 C. Lampoudis [id](#)^{155,d}, G. Lamprinoudis [id](#)¹⁰², A.N. Lancaster [id](#)¹¹⁸, E. Lançon [id](#)³⁰, U. Landgraf [id](#)⁵⁵,
 M.P.J. Landon [id](#)⁹⁶, V.S. Lang [id](#)⁵⁵, O.K.B. Langrekken [id](#)¹²⁸, A.J. Lankford [id](#)¹⁶², F. Lanni [id](#)³⁷,
 K. Lantzsck [id](#)²⁵, A. Lanza [id](#)^{74a}, M. Lanzac Berrocal [id](#)¹⁶⁶, J.F. Laporte [id](#)¹³⁸, T. Lari [id](#)^{72a},
 F. Lasagni Manghi [id](#)^{24b}, M. Lassnig [id](#)³⁷, V. Latonova [id](#)¹³⁴, A. Laurier [id](#)¹⁵³, S.D. Lawlor [id](#)¹⁴²,
 Z. Lawrence [id](#)¹⁰³, R. Lazaridou [id](#)¹⁷⁰, M. Lazzaroni [id](#)^{72a,72b}, B. Le [id](#)¹⁰³, H.D.M. Le [id](#)¹⁰⁹,
 E.M. Le Boulicaut [id](#)¹⁷⁵, L.T. Le Pottier [id](#)^{18a}, B. Leban [id](#)^{24b,24a}, A. Lebedev [id](#)⁸², M. LeBlanc [id](#)¹⁰³,
 F. Ledroit-Guillon [id](#)⁶¹, S.C. Lee [id](#)¹⁵¹, S. Lee [id](#)^{48a,48b}, T.F. Lee [id](#)⁹⁴, L.L. Leeuw [id](#)^{34c}, H.P. Lefebvre [id](#)⁹⁷,
 M. Lefebvre [id](#)¹⁶⁸, C. Leggett [id](#)^{18a}, G. Lehmann Miotto [id](#)³⁷, M. Leigh [id](#)⁵⁷, W.A. Leight [id](#)¹⁰⁵,
 W. Leinonen [id](#)¹¹⁶, A. Leisos [id](#)^{155,q}, M.A.L. Leite [id](#)^{84c}, C.E. Leitgeb [id](#)¹⁹, R. Leitner [id](#)¹³⁶,
 K.J.C. Leney [id](#)⁴⁵, T. Lenz [id](#)²⁵, S. Leone [id](#)^{75a}, C. Leonidopoulos [id](#)⁵³, A. Leopold [id](#)¹⁴⁷, R. Les [id](#)¹⁰⁹,
 C.G. Lester [id](#)³³, M. Levchenko [id](#)³⁸, J. Levêque [id](#)⁴, L.J. Levinson [id](#)¹⁷², G. Levrini [id](#)^{24b,24a},
 M.P. Lewicki [id](#)⁸⁸, C. Lewis [id](#)¹⁴¹, D.J. Lewis [id](#)⁴, L. Lewitt [id](#)¹⁴², A. Li [id](#)³⁰, B. Li [id](#)^{63b}, C. Li [id](#)^{63a},
 C-Q. Li [id](#)¹¹², H. Li [id](#)^{63a}, H. Li [id](#)^{63b}, H. Li [id](#)^{114a}, H. Li [id](#)¹⁵, H. Li [id](#)^{63b}, J. Li [id](#)^{63c}, K. Li [id](#)¹⁴, L. Li [id](#)^{63c},
 M. Li [id](#)^{14,114c}, S. Li [id](#)^{14,114c}, S. Li [id](#)^{63d,63c}, T. Li [id](#)⁵, X. Li [id](#)¹⁰⁶, Z. Li [id](#)¹⁵⁶, Z. Li [id](#)^{14,114c}, Z. Li [id](#)^{63a},
 S. Liang [id](#)^{14,114c}, Z. Liang [id](#)¹⁴, M. Liberatore [id](#)¹³⁸, B. Liberti [id](#)^{77a}, K. Lie [id](#)^{65c}, J. Lieber Marin [id](#)^{84e},

H. Lien ⁶⁹, H. Lin ¹⁰⁸, K. Lin ¹⁰⁹, L. Linden ¹¹¹, R.E. Lindley ⁷, J.H. Lindon ², J. Ling ⁶²,
 E. Lipeles ¹³¹, A. Lipniacka ¹⁷, A. Lister ¹⁶⁷, J.D. Little ⁶⁹, B. Liu ¹⁴, B.X. Liu ^{114b},
 D. Liu ^{63d,63c}, E.H.L. Liu ²¹, J.B. Liu ^{63a}, J.K.K. Liu ³³, K. Liu ^{63d}, K. Liu ^{63d,63c}, M. Liu ^{63a},
 M.Y. Liu ^{63a}, P. Liu ¹⁴, Q. Liu ^{63d,141,63c}, X. Liu ^{63a}, X. Liu ^{63b}, Y. Liu ^{114b,114c}, Y.L. Liu ^{63b},
 Y.W. Liu ^{63a}, S.L. Lloyd ⁹⁶, E.M. Lobodzinska ⁴⁹, P. Loch ⁷, E. Lodhi ¹⁵⁸, T. Lohse ¹⁹,
 K. Lohwasser ¹⁴², E. Loiacono ⁴⁹, J.D. Lomas ²¹, J.D. Long ⁴², I. Longarini ¹⁶², R. Longo ¹⁶⁵,
 I. Lopez Paz ⁶⁸, A. Lopez Solis ⁴⁹, N.A. Lopez-canelas ⁷, N. Lorenzo Martinez ⁴, A.M. Lory ¹¹¹,
 M. Losada ^{119a}, G. Löschecke Centeno ¹⁴⁹, O. Loseva ³⁸, X. Lou ^{48a,48b}, X. Lou ^{14,114c},
 A. Lounis ⁶⁷, P.A. Love ⁹³, G. Lu ^{14,114c}, M. Lu ⁶⁷, S. Lu ¹³¹, Y.J. Lu ⁶⁶, H.J. Lubatti ¹⁴¹,
 C. Luci ^{76a,76b}, F.L. Lucio Alves ^{114a}, F. Luehring ⁶⁹, O. Lukianchuk ⁶⁷, B.S. Lunday ¹³¹,
 O. Lundberg ¹⁴⁷, B. Lund-Jensen ^{147,*}, N.A. Luongo ⁶, M.S. Lutz ³⁷, A.B. Lux ²⁶, D. Lynn ³⁰,
 R. Lysak ¹³⁴, E. Lytken ¹⁰⁰, V. Lyubushkin ³⁹, T. Lyubushkina ³⁹, M.M. Lyukova ¹⁴⁸,
 M.Firdaus M. Soberi ⁵³, H. Ma ³⁰, K. Ma ^{63a}, L.L. Ma ^{63b}, W. Ma ^{63a}, Y. Ma ¹²⁴,
 J.C. MacDonald ¹⁰², P.C. Machado De Abreu Farias ^{84e}, R. Madar ⁴¹, T. Madula ⁹⁸, J. Maeda ⁸⁶,
 T. Maeno ³⁰, H. Maguire ¹⁴², V. Maiboroda ¹³⁸, A. Maio ^{133a,133b,133d}, K. Maj ^{87a},
 O. Majersky ⁴⁹, S. Majewski ¹²⁶, N. Makovec ⁶⁷, V. Maksimovic ¹⁶, B. Malaescu ¹³⁰,
 Pa. Malecki ⁸⁸, V.P. Maleev ³⁸, F. Malek ^{61,m}, M. Mali ⁹⁵, D. Malito ⁹⁷, U. Mallik ⁸¹,
 S. Maltezos ¹⁰, S. Malyukov ³⁹, J. Mamuzic ¹³, G. Mancini ⁵⁴, M.N. Mancini ²⁷, G. Manco ^{74a,74b},
 J.P. Mandalia ⁹⁶, S.S. Mandarray ¹⁴⁹, I. Mandić ⁹⁵, L. Manhaes de Andrade Filho ^{84a},
 I.M. Maniatis ¹⁷², J. Manjarres Ramos ⁹¹, D.C. Mankad ¹⁷², A. Mann ¹¹¹, S. Manzoni ³⁷,
 L. Mao ^{63c}, X. Mapekula ^{34c}, A. Marantis ^{155,q}, G. Marchiori ⁵, M. Marcisovsky ¹³⁴,
 C. Marcon ^{72a}, M. Marinescu ²¹, S. Marium ⁴⁹, M. Marjanovic ¹²³, A. Markhoos ⁵⁵,
 M. Markovitch ⁶⁷, E.J. Marshall ⁹³, Z. Marshall ^{18a}, S. Marti-Garcia ¹⁶⁶, J. Martin ⁹⁸,
 T.A. Martin ¹³⁷, V.J. Martin ⁵³, B. Martin dit Latour ¹⁷, L. Martinelli ^{76a,76b}, M. Martinez ^{13,s},
 P. Martinez Agullo ¹⁶⁶, V.I. Martinez Outschoorn ¹⁰⁵, P. Martinez Suarez ¹³, S. Martin-Haugh ¹³⁷,
 G. Martinovicova ¹³⁶, V.S. Martoiu ^{28b}, A.C. Martyniuk ⁹⁸, A. Marzin ³⁷, D. Mascione ^{79a,79b},
 L. Masetti ¹⁰², J. Masik ¹⁰³, A.L. Maslennikov ³⁸, P. Massarotti ^{73a,73b}, P. Mastrandrea ^{75a,75b},
 A. Mastroberardino ^{44b,44a}, T. Masubuchi ¹²⁷, T.T. Mathew ¹²⁶, T. Mathisen ¹⁶⁴, J. Matousek ¹³⁶,
 D.M. Mattern ⁵⁰, J. Maurer ^{28b}, T. Maurin ⁶⁰, A.J. Maury ⁶⁷, B. Maček ⁹⁵, D.A. Maximov ³⁸,
 A.E. May ¹⁰³, R. Mazini ¹⁵¹, I. Maznas ¹¹⁸, M. Mazza ¹⁰⁹, S.M. Mazza ¹³⁹, E. Mazzeo ^{72a,72b},
 C. Mc Ginn ³⁰, J.P. Mc Gowan ¹⁶⁸, S.P. Mc Kee ¹⁰⁸, C.A. Mc Lean ⁶, C.C. McCracken ¹⁶⁷,
 E.F. McDonald ¹⁰⁷, A.E. McDougall ¹¹⁷, J.A. Mcfayden ¹⁴⁹, R.P. McGovern ¹³¹,
 R.P. Mckenzie ^{34g}, T.C. Mclachlan ⁴⁹, D.J. Mclaughlin ⁹⁸, S.J. McMahon ¹³⁷,
 C.M. Mcpartland ⁹⁴, R.A. McPherson ^{168,w}, S. Mehlhase ¹¹¹, A. Mehta ⁹⁴, D. Melini ¹⁶⁶,
 B.R. Mellado Garcia ^{34g}, A.H. Melo ⁵⁶, F. Meloni ⁴⁹, A.M. Mendes Jacques Da Costa ¹⁰³,
 H.Y. Meng ¹⁵⁸, L. Meng ⁹³, S. Menke ¹¹², M. Mentink ³⁷, E. Meoni ^{44b,44a}, G. Mercado ¹¹⁸,
 S. Merianos ¹⁵⁵, C. Merlassino ^{70a,70c}, L. Merola ^{73a,73b}, C. Meroni ^{72a,72b}, J. Metcalfe ⁶,
 A.S. Mete ⁶, E. Meuser ¹⁰², C. Meyer ⁶⁹, J-P. Meyer ¹³⁸, R.P. Middleton ¹³⁷, L. Mijović ⁵³,
 G. Mikenberg ¹⁷², M. Mikestikova ¹³⁴, M. Mikuž ⁹⁵, H. Mildner ¹⁰², A. Milic ³⁷,
 D.W. Miller ⁴⁰, E.H. Miller ¹⁴⁶, L.S. Miller ³⁵, A. Milov ¹⁷², D.A. Milstead ^{48a,48b}, T. Min ^{114a},
 A.A. Minaenko ³⁸, I.A. Minashvili ^{152b}, L. Mince ⁶⁰, A.I. Mincer ¹²⁰, B. Mindur ^{87a},
 M. Mineev ³⁹, Y. Mino ⁸⁹, L.M. Mir ¹³, M. Miralles Lopez ⁶⁰, M. Mironova ^{18a},
 M.C. Missio ¹¹⁶, A. Mitra ¹⁷⁰, V.A. Mitsou ¹⁶⁶, Y. Mitsumori ¹¹³, O. Miu ¹⁵⁸,
 P.S. Miyagawa ⁹⁶, T. Mkrtychyan ^{64a}, M. Mlinarevic ⁹⁸, T. Mlinarevic ⁹⁸, M. Mlynarikova ³⁷,
 S. Mobius ²⁰, P. Mogg ¹¹¹, M.H. Mohamed Farook ¹¹⁵, A.F. Mohammed ^{14,114c}, S. Mohapatra ⁴²,
 G. Mokgatitwane ^{34g}, L. Moleri ¹⁷², B. Mondal ¹⁴⁴, S. Mondal ¹³⁵, K. Mönig ⁴⁹,
 E. Monnier ¹⁰⁴, L. Monsonis Romero ¹⁶⁶, J. Montejo Berlingen ¹³, A. Montella ^{48a,48b},

M. Montella [ID 122](#), F. Montereali [ID 78a,78b](#), F. Monticelli [ID 92](#), S. Monzani [ID 70a,70c](#), A. Morancho Tarda [ID 43](#),
N. Morange [ID 67](#), A.L. Moreira De Carvalho [ID 49](#), M. Moreno Llácer [ID 166](#), C. Moreno Martinez [ID 57](#),
J.M. Moreno Perez [ID 23b](#), P. Morettini [ID 58b](#), S. Morgenstern [ID 37](#), M. Morii [ID 62](#), M. Morinaga [ID 156](#),
M. Moritsu [ID 90](#), F. Morodei [ID 76a,76b](#), P. Moschovakos [ID 37](#), B. Moser [ID 129](#), M. Mosidze [ID 152b](#),
T. Moskalets [ID 45](#), P. Moskvitina [ID 116](#), J. Moss [ID 32,j](#), P. Moszkowicz [ID 87a](#), A. Moussa [ID 36d](#),
E.J.W. Moyse [ID 105](#), O. Mtintsilana [ID 34g](#), S. Muanza [ID 104](#), J. Mueller [ID 132](#), D. Muenstermann [ID 93](#),
R. Müller [ID 37](#), G.A. Mullier [ID 164](#), A.J. Mullin [ID 33](#), J.J. Mullin [ID 131](#), A.E. Mulski [ID 62](#), D.P. Mungo [ID 158](#),
D. Munoz Perez [ID 166](#), F.J. Munoz Sanchez [ID 103](#), M. Murin [ID 103](#), W.J. Murray [ID 170,137](#), M. Muškinja [ID 95](#),
C. Mwewa [ID 30](#), A.G. Myagkov [ID 38,a](#), A.J. Myers [ID 8](#), G. Myers [ID 108](#), M. Myska [ID 135](#),
B.P. Nachman [ID 18a](#), O. Nackenhorst [ID 50](#), K. Nagai [ID 129](#), K. Nagano [ID 85](#), J.L. Nagle [ID 30,ae](#), E. Nagy [ID 104](#),
A.M. Nairz [ID 37](#), Y. Nakahama [ID 85](#), K. Nakamura [ID 85](#), K. Nakkalil [ID 5](#), H. Nanjo [ID 127](#),
E.A. Narayanan [ID 115](#), I. Naryshkin [ID 38](#), L. Nasella [ID 72a,72b](#), M. Naseri [ID 35](#), S. Nasri [ID 119b](#), C. Nass [ID 25](#),
G. Navarro [ID 23a](#), J. Navarro-Gonzalez [ID 166](#), R. Nayak [ID 154](#), A. Nayaz [ID 19](#), P.Y. Nechaeva [ID 38](#),
S. Nechaeva [ID 24b,24a](#), F. Nechansky [ID 134](#), L. Nedic [ID 129](#), T.J. Neep [ID 21](#), A. Negri [ID 74a,74b](#),
M. Negrini [ID 24b](#), C. Nellist [ID 117](#), C. Nelson [ID 106](#), K. Nelson [ID 108](#), S. Nemecek [ID 134](#), M. Nessi [ID 37,g](#),
M.S. Neubauer [ID 165](#), F. Neuhaus [ID 102](#), J. Neundorf [ID 49](#), J. Newell [ID 94](#), P.R. Newman [ID 21](#), C.W. Ng [ID 132](#),
Y.W.Y. Ng [ID 49](#), B. Ngair [ID 119a](#), H.D.N. Nguyen [ID 110](#), R.B. Nickerson [ID 129](#), R. Nicolaidou [ID 138](#),
J. Nielsen [ID 139](#), M. Niemeyer [ID 56](#), J. Niermann [ID 56](#), N. Nikiforou [ID 37](#), V. Nikolaenko [ID 38,a](#),
I. Nikolic-Audit [ID 130](#), K. Nikolopoulos [ID 21](#), P. Nilsson [ID 30](#), I. Ninca [ID 49](#), G. Ninio [ID 154](#), A. Nisati [ID 76a](#),
N. Nishu [ID 2](#), R. Nisius [ID 112](#), N. Nitika [ID 70a,70c](#), J-E. Nitschke [ID 51](#), E.K. Nkadimeng [ID 34g](#), T. Nobe [ID 156](#),
T. Nommensen [ID 150](#), M.B. Norfolk [ID 142](#), B.J. Norman [ID 35](#), M. Noury [ID 36a](#), J. Novak [ID 95](#), T. Novak [ID 95](#),
L. Novotny [ID 135](#), R. Novotny [ID 115](#), L. Nozka [ID 125](#), K. Ntekas [ID 162](#), N.M.J. Nunes De Moura Junior [ID 84b](#),
J. Ocariz [ID 130](#), A. Ochi [ID 86](#), I. Ochoa [ID 133a](#), S. Oerdek [ID 49,t](#), J.T. Offermann [ID 40](#), A. Ogrodnik [ID 136](#),
A. Oh [ID 103](#), C.C. Ohm [ID 147](#), H. Oide [ID 85](#), R. Oishi [ID 156](#), M.L. Ojeda [ID 37](#), Y. Okumura [ID 156](#),
L.F. Oleiro Seabra [ID 133a](#), I. Oleksiyuk [ID 57](#), S.A. Olivares Pino [ID 140d](#), G. Oliveira Correa [ID 13](#),
D. Oliveira Damazio [ID 30](#), J.L. Oliver [ID 162](#), Ö.O. Öncel [ID 55](#), A.P. O'Neill [ID 20](#), A. Onofre [ID 133a,133e](#),
P.U.E. Onyisi [ID 11](#), M.J. Oreglia [ID 40](#), G.E. Orellana [ID 92](#), D. Orestano [ID 78a,78b](#), N. Orlando [ID 13](#),
R.S. Orr [ID 158](#), L.M. Osojnak [ID 131](#), R. Ospanov [ID 63a](#), Y. Osumi [ID 113](#), G. Otero y Garzon [ID 31](#), H. Otono [ID 90](#),
P.S. Ott [ID 64a](#), G.J. Ottino [ID 18a](#), M. Ouchrif [ID 36d](#), F. Ould-Saada [ID 128](#), T. Ovsianikova [ID 141](#),
M. Owen [ID 60](#), R.E. Owen [ID 137](#), V.E. Ozcan [ID 22a](#), F. Ozturk [ID 88](#), N. Ozturk [ID 8](#), S. Ozturk [ID 83](#),
H.A. Pacey [ID 129](#), A. Pacheco Pages [ID 13](#), C. Padilla Aranda [ID 13](#), G. Padovano [ID 76a,76b](#),
S. Pagan Griso [ID 18a](#), G. Palacino [ID 69](#), A. Palazzo [ID 71a,71b](#), J. Pampel [ID 25](#), J. Pan [ID 175](#), T. Pan [ID 65a](#),
D.K. Panchal [ID 11](#), C.E. Pandini [ID 117](#), J.G. Panduro Vazquez [ID 137](#), H.D. Pandya [ID 1](#), H. Pang [ID 15](#),
P. Pani [ID 49](#), G. Panizzo [ID 70a,70c](#), L. Panwar [ID 130](#), L. Paolozzi [ID 57](#), S. Parajuli [ID 165](#), A. Paramonov [ID 6](#),
C. Paraskevopoulos [ID 54](#), D. Paredes Hernandez [ID 65b](#), A. Pareti [ID 74a,74b](#), K.R. Park [ID 42](#), T.H. Park [ID 158](#),
M.A. Parker [ID 33](#), F. Parodi [ID 58b,58a](#), E.W. Parrish [ID 118](#), V.A. Parrish [ID 53](#), J.A. Parsons [ID 42](#),
U. Parzefall [ID 55](#), B. Pascual Dias [ID 110](#), L. Pascual Dominguez [ID 101](#), E. Pasqualucci [ID 76a](#),
S. Passaggio [ID 58b](#), F. Pastore [ID 97](#), P. Patel [ID 88](#), U.M. Patel [ID 52](#), J.R. Pater [ID 103](#), T. Pauly [ID 37](#),
F. Pauwels [ID 136](#), C.I. Pazos [ID 161](#), M. Pedersen [ID 128](#), R. Pedro [ID 133a](#), S.V. Peleganchuk [ID 38](#), O. Penc [ID 37](#),
E.A. Pender [ID 53](#), S. Peng [ID 15](#), G.D. Penn [ID 175](#), K.E. Penski [ID 111](#), M. Penzin [ID 38](#), B.S. Peralva [ID 84d](#),
A.P. Pereira Peixoto [ID 141](#), L. Pereira Sanchez [ID 146](#), D.V. Perepelitsa [ID 30,ae](#), G. Perera [ID 105](#),
E. Perez Codina [ID 159a](#), M. Perganti [ID 10](#), H. Pernegger [ID 37](#), S. Perrella [ID 76a,76b](#), O. Perrin [ID 41](#),
K. Peters [ID 49](#), R.F.Y. Peters [ID 103](#), B.A. Petersen [ID 37](#), T.C. Petersen [ID 43](#), E. Petit [ID 104](#), V. Petousis [ID 135](#),
C. Petridou [ID 155,d](#), T. Petru [ID 136](#), A. Petrukhin [ID 144](#), M. Pettee [ID 18a](#), A. Petukhov [ID 38](#), K. Petukhova [ID 37](#),
R. Pezoa [ID 140f](#), L. Pezzotti [ID 37](#), G. Pezzullo [ID 175](#), A.J. Pflieger [ID 37](#), T.M. Pham [ID 173](#), T. Pham [ID 107](#),
P.W. Phillips [ID 137](#), G. Piacquadio [ID 148](#), E. Pianori [ID 18a](#), F. Piazza [ID 126](#), R. Piegai [ID 31](#), D. Pietreanu [ID 28b](#),
A.D. Pilkington [ID 103](#), M. Pinamonti [ID 70a,70c](#), J.L. Pinfold [ID 2](#), B.C. Pinheiro Pereira [ID 133a](#),

J. Pinol Bel [ID13](#), A.E. Pinto Pinoargote [ID138,138](#), L. Pintucci [ID70a,70c](#), K.M. Piper [ID149](#), A. Pirttikoski [ID57](#),
 D.A. Pizzi [ID35](#), L. Pizzimento [ID65b](#), A. Pizzini [ID117](#), M.-A. Pleier [ID30](#), V. Pleskot [ID136](#), E. Plotnikova [ID39](#),
 G. Poddar [ID96](#), R. Poettgen [ID100](#), L. Poggioli [ID130](#), I. Pokharel [ID56](#), S. Polacek [ID136](#), G. Polesello [ID74a](#),
 A. Poley [ID145,159a](#), A. Polini [ID24b](#), C.S. Pollard [ID170](#), Z.B. Pollock [ID122](#), E. Pompa Pacchi [ID76a,76b](#),
 N.I. Pond [ID98](#), D. Ponomarenko [ID69](#), L. Pontecorvo [ID37](#), S. Popa [ID28a](#), G.A. Popeneciu [ID28d](#),
 A. Poreba [ID37](#), D.M. Portillo Quintero [ID159a](#), S. Pospisil [ID135](#), M.A. Postill [ID142](#), P. Postolache [ID28c](#),
 K. Potamianos [ID170](#), P.A. Potepa [ID87a](#), I.N. Potrap [ID39](#), C.J. Potter [ID33](#), H. Potti [ID150](#), J. Poveda [ID166](#),
 M.E. Pozo Astigarraga [ID37](#), A. Prades Ibanez [ID77a,77b](#), J. Pretel [ID168](#), D. Price [ID103](#), M. Primavera [ID71a](#),
 L. Primomo [ID70a,70c](#), M.A. Principe Martin [ID101](#), R. Privara [ID125](#), T. Procter [ID60](#), M.L. Proffitt [ID141](#),
 N. Proklova [ID131](#), K. Prokofiev [ID65c](#), G. Proto [ID112](#), J. Proudfoot [ID6](#), M. Przybycien [ID87a](#),
 W.W. Przygoda [ID87b](#), A. Psallidas [ID47](#), J.E. Puddefoot [ID142](#), D. Pudzha [ID55](#), D. Pyatiiybyantseva [ID38](#),
 J. Qian [ID108](#), D. Qichen [ID103](#), Y. Qin [ID13](#), T. Qiu [ID53](#), A. Quadt [ID56](#), M. Queitsch-Maitland [ID103](#),
 G. Quetant [ID57](#), R.P. Quinn [ID167](#), G. Rabanal Bolanos [ID62](#), D. Rafanoharana [ID55](#), F. Raffaelli [ID77a,77b](#),
 F. Ragusa [ID72a,72b](#), J.L. Rainbolt [ID40](#), J.A. Raine [ID57](#), S. Rajagopalan [ID30](#), E. Ramakoti [ID38](#),
 L. Rambelli [ID58b,58a](#), I.A. Ramirez-Berend [ID35](#), K. Ran [ID49,114c](#), D.S. Rankin [ID131](#), N.P. Rapheeha [ID34g](#),
 H. Rasheed [ID28b](#), V. Raskina [ID130](#), D.F. Rassloff [ID64a](#), A. Rastogi [ID18a](#), S. Rave [ID102](#), S. Ravera [ID58b,58a](#),
 B. Ravina [ID56](#), I. Ravinovich [ID172](#), M. Raymond [ID37](#), A.L. Read [ID128](#), N.P. Readioff [ID142](#),
 D.M. Rebuzzi [ID74a,74b](#), G. Redlinger [ID30](#), A.S. Reed [ID112](#), K. Reeves [ID27](#), J.A. Reidelsturz [ID174](#),
 D. Reikher [ID126](#), A. Rej [ID50](#), C. Rembser [ID37](#), M. Renda [ID28b](#), F. Renner [ID49](#), A.G. Rennie [ID162](#),
 A.L. Rescia [ID49](#), S. Resconi [ID72a](#), M. Ressegotti [ID58b,58a](#), S. Rettie [ID37](#), J.G. Reyes Rivera [ID109](#),
 E. Reynolds [ID18a](#), O.L. Rezanova [ID38](#), P. Reznicek [ID136](#), H. Riani [ID36d](#), N. Ribaric [ID52](#), E. Ricci [ID79a,79b](#),
 R. Richter [ID112](#), S. Richter [ID48a,48b](#), E. Richter-Was [ID87b](#), M. Ridel [ID130](#), S. Ridouani [ID36d](#), P. Rieck [ID120](#),
 P. Riedler [ID37](#), E.M. Riefel [ID48a,48b](#), J.O. Rieger [ID117](#), M. Rijssenbeek [ID148](#), M. Rimoldi [ID37](#),
 L. Rinaldi [ID24b,24a](#), P. Rincke [ID56,164](#), T.T. Rinn [ID30](#), M.P. Rinnagel [ID111](#), G. Ripellino [ID164](#), I. Riu [ID13](#),
 J.C. Rivera Vergara [ID168](#), F. Rizatdinova [ID124](#), E. Rizvi [ID96](#), B.R. Roberts [ID18a](#), S.S. Roberts [ID139](#),
 S.H. Robertson [ID106,w](#), D. Robinson [ID33](#), M. Robles Manzano [ID102](#), A. Robson [ID60](#), A. Rocchi [ID77a,77b](#),
 C. Roda [ID75a,75b](#), S. Rodriguez Bosca [ID37](#), Y. Rodriguez Garcia [ID23a](#), A. Rodriguez Rodriguez [ID55](#),
 A.M. Rodríguez Vera [ID118](#), S. Roe [ID37](#), J.T. Roemer [ID37](#), A.R. Roepe-Gier [ID139](#), O. Røhne [ID128](#),
 R.A. Rojas [ID105](#), C.P.A. Roland [ID130](#), J. Roloff [ID30](#), A. Romaniouk [ID38](#), E. Romano [ID74a,74b](#),
 M. Romano [ID24b](#), A.C. Romero Hernandez [ID165](#), N. Rompotis [ID94](#), L. Roos [ID130](#), S. Rosati [ID76a](#),
 B.J. Rosser [ID40](#), E. Rossi [ID129](#), E. Rossi [ID73a,73b](#), L.P. Rossi [ID62](#), L. Rossini [ID55](#), R. Rosten [ID122](#),
 M. Rotaru [ID28b](#), B. Rottler [ID55](#), C. Rougier [ID91](#), D. Rousseau [ID67](#), D. Rousso [ID49](#), A. Roy [ID165](#),
 S. Roy-Garand [ID158](#), A. Rozanov [ID104](#), Z.M.A. Rozario [ID60](#), Y. Rozen [ID153](#), A. Rubio Jimenez [ID166](#),
 A.J. Ruby [ID94](#), V.H. Ruelas Rivera [ID19](#), T.A. Ruggeri [ID1](#), A. Ruggiero [ID129](#), A. Ruiz-Martinez [ID166](#),
 A. Rummler [ID37](#), Z. Rurikova [ID55](#), N.A. Rusakovich [ID39](#), H.L. Russell [ID168](#), G. Russo [ID76a,76b](#),
 J.P. Rutherford [ID7](#), S. Rutherford Colmenares [ID33](#), M. Rybar [ID136](#), E.B. Rye [ID128](#), A. Ryzhov [ID45](#),
 J.A. Sabater Iglesias [ID57](#), H.F-W. Sadrozinski [ID139](#), F. Safai Tehrani [ID76a](#), B. Safarzadeh Samani [ID137](#),
 S. Saha [ID1](#), M. Sahinsoy [ID83](#), A. Saibel [ID166](#), M. Saimpert [ID138](#), M. Saito [ID156](#), T. Saito [ID156](#),
 A. Sala [ID72a,72b](#), D. Salamani [ID37](#), A. Salnikov [ID146](#), J. Salt [ID166](#), A. Salvador Salas [ID154](#),
 D. Salvatore [ID44b,44a](#), F. Salvatore [ID149](#), A. Salzburger [ID37](#), D. Sammel [ID55](#), E. Sampson [ID93](#),
 D. Sampsonidis [ID155,d](#), D. Sampsonidou [ID126](#), J. Sánchez [ID166](#), V. Sanchez Sebastian [ID166](#),
 H. Sandaker [ID128](#), C.O. Sander [ID49](#), J.A. Sandesara [ID105](#), M. Sandhoff [ID174](#), C. Sandoval [ID23b](#),
 L. Sanfilippo [ID64a](#), D.P.C. Sankey [ID137](#), T. Sano [ID89](#), A. Sansoni [ID54](#), L. Santi [ID37,76b](#), C. Santoni [ID41](#),
 H. Santos [ID133a,133b](#), A. Santra [ID172](#), E. Sanzani [ID24b,24a](#), K.A. Saoucha [ID163](#), J.G. Saraiva [ID133a,133d](#),
 J. Sardain [ID7](#), O. Sasaki [ID85](#), K. Sato [ID160](#), C. Sauer [ID64b](#), E. Sauvan [ID4](#), P. Savard [ID158,ac](#), R. Sawada [ID156](#),
 C. Sawyer [ID137](#), L. Sawyer [ID99](#), C. Sbarra [ID24b](#), A. Sbrizzi [ID24b,24a](#), T. Scanlon [ID98](#),
 J. Schaarschmidt [ID141](#), U. Schäfer [ID102](#), A.C. Schaffer [ID67,45](#), D. Schaile [ID111](#), R.D. Schamberger [ID148](#),

C. Scharf ¹⁹, M.M. Schefer ²⁰, V.A. Schegelsky ³⁸, D. Scheirich ¹³⁶, M. Schernau ¹⁶²,
 C. Scheulen ⁵⁶, C. Schiavi ^{58b,58a}, M. Schioppa ^{44b,44a}, B. Schlag ^{146,1}, S. Schlenker ³⁷,
 J. Schmeing ¹⁷⁴, M.A. Schmidt ¹⁷⁴, K. Schmieden ¹⁰², C. Schmitt ¹⁰², N. Schmitt ¹⁰²,
 S. Schmitt ⁴⁹, L. Schoeffel ¹³⁸, A. Schoening ^{64b}, P.G. Scholer ³⁵, E. Schopf ¹²⁹, M. Schott ²⁵,
 J. Schovancova ³⁷, S. Schramm ⁵⁷, T. Schroer ⁵⁷, H-C. Schultz-Coulon ^{64a}, M. Schumacher ⁵⁵,
 B.A. Schumm ¹³⁹, Ph. Schune ¹³⁸, A.J. Schuy ¹⁴¹, H.R. Schwartz ¹³⁹, A. Schwartzman ¹⁴⁶,
 T.A. Schwarz ¹⁰⁸, Ph. Schwemling ¹³⁸, R. Schwienhorst ¹⁰⁹, F.G. Sciacca ²⁰, A. Sciandra ³⁰,
 G. Sciolla ²⁷, F. Scuri ^{75a}, C.D. Sebastiani ⁹⁴, K. Sedlaczek ¹¹⁸, S.C. Seidel ¹¹⁵, A. Seiden ¹³⁹,
 B.D. Seidlitz ⁴², C. Seitz ⁴⁹, J.M. Seixas ^{84b}, G. Sekhniaidze ^{73a}, L. Selem ⁶¹,
 N. Semprini-Cesari ^{24b,24a}, D. Sengupta ⁵⁷, V. Senthilkumar ¹⁶⁶, L. Serin ⁶⁷, M. Sessa ^{77a,77b},
 H. Severini ¹²³, F. Sforza ^{58b,58a}, A. Sfyrta ⁵⁷, Q. Sha ¹⁴, E. Shabalina ⁵⁶, A.H. Shah ³³,
 R. Shaheen ¹⁴⁷, J.D. Shahinian ¹³¹, D. Shaked Renous ¹⁷², L.Y. Shan ¹⁴, M. Shapiro ^{18a},
 A. Sharma ³⁷, A.S. Sharma ¹⁶⁷, P. Sharma ⁸¹, P.B. Shatalov ³⁸, K. Shaw ¹⁴⁹, S.M. Shaw ¹⁰³,
 Q. Shen ^{63c}, D.J. Sheppard ¹⁴⁵, P. Sherwood ⁹⁸, L. Shi ⁹⁸, X. Shi ¹⁴, S. Shimizu ⁸⁵,
 C.O. Shimmin ¹⁷⁵, J.D. Shinner ⁹⁷, I.P.J. Shipsey ¹²⁹, S. Shirabe ⁹⁰, M. Shiyakova ^{39,u},
 M.J. Shochet ⁴⁰, D.R. Shope ¹²⁸, B. Shrestha ¹²³, S. Shrestha ^{122,af}, I. Shreyber ³⁸,
 M.J. Shroff ¹⁶⁸, P. Sicho ¹³⁴, A.M. Sickles ¹⁶⁵, E. Sideras Haddad ^{34g}, A.C. Sidley ¹¹⁷,
 A. Sidoti ^{24b}, F. Siegert ⁵¹, Dj. Sijacki ¹⁶, F. Sili ⁹², J.M. Silva ⁵³, I. Silva Ferreira ^{84b},
 M.V. Silva Oliveira ³⁰, S.B. Silverstein ^{48a}, S. Simion ⁶⁷, R. Simoniello ³⁷, E.L. Simpson ¹⁰³,
 H. Simpson ¹⁴⁹, L.R. Simpson ¹⁰⁸, S. Simsek ⁸³, S. Sindhu ⁵⁶, P. Sinervo ¹⁵⁸, S. Singh ³⁰,
 S. Sinha ⁴⁹, S. Sinha ¹⁰³, M. Sioli ^{24b,24a}, I. Siral ³⁷, E. Sitnikova ⁴⁹, J. Sjölin ^{48a,48b},
 A. Skaf ⁵⁶, E. Skorda ²¹, P. Skubic ¹²³, M. Slawinska ⁸⁸, V. Smakhtin ¹⁷², B.H. Smart ¹³⁷,
 S.Yu. Smirnov ³⁸, Y. Smirnov ³⁸, L.N. Smirnova ^{38,a}, O. Smirnova ¹⁰⁰, A.C. Smith ⁴²,
 D.R. Smith ¹⁶², E.A. Smith ⁴⁰, J.L. Smith ¹⁰³, R. Smith ¹⁴⁶, M. Smizanska ⁹³, K. Smolek ¹³⁵,
 A.A. Snesarev ³⁸, H.L. Snoek ¹¹⁷, S. Snyder ³⁰, R. Sobie ^{168,w}, A. Soffer ¹⁵⁴,
 C.A. Solans Sanchez ³⁷, E.Yu. Soldatov ³⁸, U. Soldevila ¹⁶⁶, A.A. Solodkov ³⁸, S. Solomon ²⁷,
 A. Soloshenko ³⁹, K. Solovieva ⁵⁵, O.V. Solovyanov ⁴¹, P. Sommer ⁵¹, A. Sonay ¹³,
 W.Y. Song ^{159b}, A. Sopczak ¹³⁵, A.L. Soppio ⁵³, F. Sopkova ^{29b}, J.D. Sorenson ¹¹⁵,
 I.R. Sotarriva Alvarez ¹⁵⁷, V. Sothilingam ^{64a}, O.J. Soto Sandoval ^{140c,140b}, S. Sottocornola ⁶⁹,
 R. Soualah ¹⁶³, Z. Soumami ^{36e}, D. South ⁴⁹, N. Soybelman ¹⁷², S. Spagnolo ^{71a,71b},
 M. Spalla ¹¹², D. Sperlich ⁵⁵, G. Spigo ³⁷, B. Spisso ^{73a,73b}, D.P. Spiteri ⁶⁰, M. Spousta ¹³⁶,
 E.J. Staats ³⁵, R. Stamen ^{64a}, A. Stampeki ²¹, E. Stanecka ⁸⁸, W. Stanek-Maslouska ⁴⁹,
 M.V. Stange ⁵¹, B. Stanislaus ^{18a}, M.M. Stanitzki ⁴⁹, B. Stapf ⁴⁹, E.A. Starchenko ³⁸,
 G.H. Stark ¹³⁹, J. Stark ⁹¹, P. Staroba ¹³⁴, P. Starovoitov ^{64a}, S. Stärz ¹⁰⁶, R. Staszewski ³⁸,
 G. Stavropoulos ⁴⁷, P. Steinberg ³⁰, B. Stelzer ^{145,159a}, H.J. Stelzer ¹³², O. Stelzer-Chilton ^{159a},
 H. Stenzel ⁵⁹, T.J. Stevenson ¹⁴⁹, G.A. Stewart ³⁷, J.R. Stewart ¹²⁴, M.C. Stockton ³⁷,
 G. Stoicea ^{28b}, M. Stolarski ^{133a}, S. Stonjek ¹¹², A. Straessner ⁵¹, J. Strandberg ¹⁴⁷,
 S. Strandberg ^{48a,48b}, M. Stratmann ¹⁷⁴, M. Strauss ¹²³, T. Strebler ¹⁰⁴, P. Strizenec ^{29b},
 R. Ströhmer ¹⁶⁹, D.M. Strom ¹²⁶, R. Stroynowski ⁴⁵, A. Strubig ^{48a,48b}, S.A. Stucci ³⁰,
 B. Stugu ¹⁷, J. Stupak ¹²³, N.A. Styles ⁴⁹, D. Su ¹⁴⁶, S. Su ^{63a}, W. Su ^{63d}, X. Su ^{63a},
 D. Suchy ^{29a}, K. Sugizaki ¹⁵⁶, V.V. Sulim ³⁸, M.J. Sullivan ⁹⁴, D.M.S. Sultan ¹²⁹,
 L. Sultanaliev ³⁸, S. Sultansoy ^{3b}, T. Sumida ⁸⁹, S. Sun ¹⁷³, O. Sunneborn Gudnadottir ¹⁶⁴,
 N. Sur ¹⁰⁴, M.R. Sutton ¹⁴⁹, H. Suzuki ¹⁶⁰, M. Svatos ¹³⁴, M. Swiatlowski ^{159a}, T. Swirski ¹⁶⁹,
 I. Sykora ^{29a}, M. Sykora ¹³⁶, T. Sykora ¹³⁶, D. Ta ¹⁰², K. Tackmann ^{49,t}, A. Taffard ¹⁶²,
 R. Tafirout ^{159a}, J.S. Tafoya Vargas ⁶⁷, Y. Takubo ⁸⁵, M. Talby ¹⁰⁴, A.A. Talyshev ³⁸,
 K.C. Tam ^{65b}, N.M. Tamir ¹⁵⁴, A. Tanaka ¹⁵⁶, J. Tanaka ¹⁵⁶, R. Tanaka ⁶⁷, M. Tanasini ¹⁴⁸,
 Z. Tao ¹⁶⁷, S. Tapia Araya ^{140f}, S. Tapprogge ¹⁰², A. Tarek Abouelfadl Mohamed ¹⁰⁹,

S. Tarem ¹⁵³, K. Tariq ¹⁴, G. Tarna ^{28b}, G.F. Tartarelli ^{72a}, M.J. Tartarin ⁹¹, P. Tas ¹³⁶,
 M. Tasevsky ¹³⁴, E. Tassi ^{44b,44a}, A.C. Tate ¹⁶⁵, G. Tateno ¹⁵⁶, Y. Tayalati ^{36e,v}, G.N. Taylor ¹⁰⁷,
 W. Taylor ^{159b}, R. Teixeira De Lima ¹⁴⁶, P. Teixeira-Dias ⁹⁷, J.J. Teoh ¹⁵⁸, K. Terashi ¹⁵⁶,
 J. Terron ¹⁰¹, S. Terzo ¹³, M. Testa ⁵⁴, R.J. Teuscher ^{158,w}, A. Thaler ⁸⁰, O. Theiner ⁵⁷,
 T. Thevenaux-Pelzer ¹⁰⁴, O. Thielmann ¹⁷⁴, D.W. Thomas ⁹⁷, J.P. Thomas ²¹, E.A. Thompson ^{18a},
 P.D. Thompson ²¹, E. Thomson ¹³¹, R.E. Thornberry ⁴⁵, C. Tian ^{63a}, Y. Tian ⁵⁷,
 V. Tikhomirov ^{38,a}, Yu.A. Tikhonov ³⁸, S. Timoshenko ³⁸, D. Timoshyn ¹³⁶, E.X.L. Ting ¹,
 P. Tipton ¹⁷⁵, A. Tishelman-Charny ³⁰, S.H. Tlou ^{34g}, K. Todome ¹⁵⁷, S. Todorova-Nova ¹³⁶,
 S. Todt ⁵¹, L. Toffolin ^{70a,70c}, M. Togawa ⁸⁵, J. Tojo ⁹⁰, S. Tokár ^{29a}, K. Tokushuku ⁸⁵,
 O. Toldaiev ⁶⁹, M. Tomoto ^{85,113}, L. Tompkins ^{146,1}, K.W. Topolnicki ^{87b}, E. Torrence ¹²⁶,
 H. Torres ⁹¹, E. Torró Pastor ¹⁶⁶, M. Toscani ³¹, C. Tosciri ⁴⁰, M. Tost ¹¹, D.R. Tovey ¹⁴²,
 I.S. Trandafir ^{28b}, T. Trefzger ¹⁶⁹, A. Tricoli ³⁰, I.M. Trigger ^{159a}, S. Trincaz-Duvoid ¹³⁰,
 D.A. Trischuk ²⁷, B. Trocmé ⁶¹, A. Tropina ³⁹, L. Truong ^{34c}, M. Trzebinski ⁸⁸, A. Trzupiek ⁸⁸,
 F. Tsai ¹⁴⁸, M. Tsai ¹⁰⁸, A. Tsiamis ¹⁵⁵, P.V. Tsiareshka ³⁸, S. Tsigaridas ^{159a}, A. Tsirigotis ^{155,q},
 V. Tsiskaridze ¹⁵⁸, E.G. Tskhadadze ^{152a}, M. Tsopoulou ¹⁵⁵, Y. Tsujikawa ⁸⁹, I.I. Tsukerman ³⁸,
 V. Tsulaia ^{18a}, S. Tsuno ⁸⁵, K. Tsuru ¹²¹, D. Tsybychev ¹⁴⁸, Y. Tu ^{65b}, A. Tudorache ^{28b},
 V. Tudorache ^{28b}, A.N. Tuna ⁶², S. Turchikhin ^{58b,58a}, I. Turk Cakir ^{3a}, R. Turra ^{72a},
 T. Turtuvshin ³⁹, P.M. Tuts ⁴², S. Tzamarias ^{155,d}, E. Tzovara ¹⁰², F. Ukegawa ¹⁶⁰,
 P.A. Ulloa Poblete ^{140c,140b}, E.N. Umaka ³⁰, G. Unal ³⁷, A. Undrus ³⁰, G. Unel ¹⁶², J. Urban ^{29b},
 P. Urrejola ^{140a}, G. Usai ⁸, R. Ushioda ¹⁵⁷, M. Usman ¹¹⁰, F. Ustuner ⁵³, Z. Uysal ⁸³,
 V. Vacek ¹³⁵, B. Vachon ¹⁰⁶, T. Vafeiadis ³⁷, A. Vaitkus ⁹⁸, C. Valderanis ¹¹¹,
 E. Valdes Santurio ^{48a,48b}, M. Valente ^{159a}, S. Valentinetti ^{24b,24a}, A. Valero ¹⁶⁶,
 E. Valiente Moreno ¹⁶⁶, A. Vallier ⁹¹, J.A. Valls Ferrer ¹⁶⁶, D.R. Van Arneman ¹¹⁷,
 T.R. Van Daalen ¹⁴¹, A. Van Der Graaf ⁵⁰, P. Van Gemmeren ⁶, M. Van Rijnbach ³⁷,
 S. Van Stroud ⁹⁸, I. Van Vulpen ¹¹⁷, P. Vana ¹³⁶, M. Vanadia ^{77a,77b}, U.M. Vande Voorde ¹⁴⁷,
 W. Vandelli ³⁷, E.R. Vandewall ¹²⁴, D. Vannicola ¹⁵⁴, L. Vannoli ⁵⁴, R. Vari ^{76a}, E.W. Varnes ⁷,
 C. Varni ^{18b}, T. Varol ¹⁵¹, D. Varouchas ⁶⁷, L. Varriale ¹⁶⁶, K.E. Varvell ¹⁵⁰, M.E. Vasile ^{28b},
 L. Vaslin ⁸⁵, G.A. Vasquez ¹⁶⁸, A. Vasyukov ³⁹, L.M. Vaughan ¹²⁴, R. Vavricka ¹⁰²,
 T. Vazquez Schroeder ³⁷, J. Veatch ³², V. Vecchio ¹⁰³, M.J. Veen ¹⁰⁵, I. Veliscek ³⁰,
 L.M. Veloce ¹⁵⁸, F. Veloso ^{133a,133c}, S. Veneziano ^{76a}, A. Ventura ^{71a,71b}, S. Ventura Gonzalez ¹³⁸,
 A. Verbytskyi ¹¹², M. Verducci ^{75a,75b}, C. Vergis ⁹⁶, M. Verissimo De Araujo ^{84b},
 W. Verkerke ¹¹⁷, J.C. Vermeulen ¹¹⁷, C. Vernieri ¹⁴⁶, M. Vessella ¹⁰⁵, M.C. Vetterli ^{145,ac},
 A. Vgenopoulos ¹⁰², N. Viaux Maira ^{140f}, T. Vickey ¹⁴², O.E. Vickey Boeriu ¹⁴²,
 G.H.A. Viehhauser ¹²⁹, L. Vigani ^{64b}, M. Vigil ¹¹², M. Villa ^{24b,24a}, M. Villaplana Perez ¹⁶⁶,
 E.M. Villhauer ⁵³, E. Vilucchi ⁵⁴, M.G. Vincter ³⁵, A. Visibile ¹¹⁷, C. Vittori ³⁷, I. Vivarelli ^{24b,24a},
 E. Voevodina ¹¹², F. Vogel ¹¹¹, J.C. Voigt ⁵¹, P. Vokac ¹³⁵, Yu. Volkotrub ^{87b}, E. Von Toerne ²⁵,
 B. Vormwald ³⁷, V. Vorobel ¹³⁶, K. Vorobev ³⁸, M. Vos ¹⁶⁶, K. Voss ¹⁴⁴, M. Vozak ¹¹⁷,
 L. Vozdecky ¹²³, N. Vranjes ¹⁶, M. Vranjes Milosavljevic ¹⁶, M. Vreeswijk ¹¹⁷, N.K. Vu ^{63d,63c},
 R. Vuillermet ³⁷, O. Vujinovic ¹⁰², I. Vukotic ⁴⁰, I.K. Vyas ³⁵, S. Wada ¹⁶⁰, C. Wagner ¹⁴⁶,
 J.M. Wagner ^{18a}, W. Wagner ¹⁷⁴, S. Wahdan ¹⁷⁴, H. Wahlberg ⁹², C.H. Waits ¹²³, J. Walder ¹³⁷,
 R. Walker ¹¹¹, W. Walkowiak ¹⁴⁴, A. Wall ¹³¹, E.J. Wallin ¹⁰⁰, T. Wamorkar ⁶, A.Z. Wang ¹³⁹,
 C. Wang ¹⁰², C. Wang ¹¹, H. Wang ^{18a}, J. Wang ^{65c}, P. Wang ⁹⁸, R. Wang ⁶², R. Wang ⁶,
 S.M. Wang ¹⁵¹, S. Wang ^{63b}, S. Wang ¹⁴, T. Wang ^{63a}, W.T. Wang ⁸¹, W. Wang ¹⁴,
 X. Wang ^{114a}, X. Wang ¹⁶⁵, X. Wang ^{63c}, Y. Wang ^{63d}, Y. Wang ^{114a}, Y. Wang ^{63a},
 Z. Wang ¹⁰⁸, Z. Wang ^{63d,52,63c}, Z. Wang ¹⁰⁸, A. Warburton ¹⁰⁶, R.J. Ward ²¹, N. Warrack ⁶⁰,
 S. Waterhouse ⁹⁷, A.T. Watson ²¹, H. Watson ⁵³, M.F. Watson ²¹, E. Watton ^{60,137}, G. Watts ¹⁴¹,
 B.M. Waugh ⁹⁸, J.M. Webb ⁵⁵, C. Weber ³⁰, H.A. Weber ¹⁹, M.S. Weber ²⁰, S.M. Weber ^{64a},

C. Wei ^{63a}, Y. Wei ⁵⁵, A.R. Weidberg ¹²⁹, E.J. Weik ¹²⁰, J. Weingarten ⁵⁰, C. Weiser ⁵⁵, C.J. Wells ⁴⁹, T. Wenaus ³⁰, B. Wendland ⁵⁰, T. Wengler ³⁷, N.S. Wenke ¹¹², N. Wermes ²⁵, M. Wessels ^{64a}, A.M. Wharton ⁹³, A.S. White ⁶², A. White ⁸, M.J. White ¹, D. Whiteson ¹⁶², L. Wickremasinghe ¹²⁷, W. Wiedenmann ¹⁷³, M. Wielers ¹³⁷, C. Wiglesworth ⁴³, D.J. Wilbern ¹²³, H.G. Wilkens ³⁷, J.J.H. Wilkinson ³³, D.M. Williams ⁴², H.H. Williams ¹³¹, S. Williams ³³, S. Willocq ¹⁰⁵, B.J. Wilson ¹⁰³, P.J. Windischhofer ⁴⁰, F.I. Winkel ³¹, F. Winklmeier ¹²⁶, B.T. Winter ⁵⁵, J.K. Winter ¹⁰³, M. Wittgen ¹⁴⁶, M. Wobisch ⁹⁹, T. Wojtkowski ⁶¹, Z. Wolffs ¹¹⁷, J. Wollrath ¹⁶², M.W. Wolter ⁸⁸, H. Wolters ^{133a,133c}, M.C. Wong ¹³⁹, E.L. Woodward ⁴², S.D. Worm ⁴⁹, B.K. Wosiek ⁸⁸, K.W. Woźniak ⁸⁸, S. Wozniwski ⁵⁶, K. Wraight ⁶⁰, C. Wu ²¹, M. Wu ^{114b}, M. Wu ¹¹⁶, S.L. Wu ¹⁷³, X. Wu ⁵⁷, Y. Wu ^{63a}, Z. Wu ⁴, J. Wuerzinger ^{112,aa}, T.R. Wyatt ¹⁰³, B.M. Wynne ⁵³, S. Xella ⁴³, L. Xia ^{114a}, M. Xia ¹⁵, M. Xie ^{63a}, S. Xin ^{14,114c}, A. Xiong ¹²⁶, J. Xiong ^{18a}, D. Xu ¹⁴, H. Xu ^{63a}, L. Xu ^{63a}, R. Xu ¹³¹, T. Xu ¹⁰⁸, Y. Xu ¹⁵, Z. Xu ⁵³, Z. Xu ^{114a}, B. Yabsley ¹⁵⁰, S. Yacoub ^{34a}, Y. Yamaguchi ⁸⁵, E. Yamashita ¹⁵⁶, H. Yamauchi ¹⁶⁰, T. Yamazaki ^{18a}, Y. Yamazaki ⁸⁶, S. Yan ⁶⁰, Z. Yan ¹⁰⁵, H.J. Yang ^{63c,63d}, H.T. Yang ^{63a}, S. Yang ^{63a}, T. Yang ^{65c}, X. Yang ³⁷, X. Yang ¹⁴, Y. Yang ⁴⁵, Y. Yang ^{63a}, Z. Yang ^{63a}, W.-M. Yao ^{18a}, H. Ye ^{114a}, H. Ye ⁵⁶, J. Ye ¹⁴, S. Ye ³⁰, X. Ye ^{63a}, Y. Yeh ⁹⁸, I. Yeletsikh ³⁹, B.K. Yeo ^{18b}, M.R. Yexley ⁹⁸, T.P. Yildirim ¹²⁹, P. Yin ⁴², K. Yorita ¹⁷¹, S. Younas ^{28b}, C.J.S. Young ³⁷, C. Young ¹⁴⁶, C. Yu ^{14,114c}, Y. Yu ^{63a}, J. Yuan ^{14,114c}, M. Yuan ¹⁰⁸, R. Yuan ^{63d,63c}, L. Yue ⁹⁸, M. Zaazoua ^{63a}, B. Zabinski ⁸⁸, E. Zaid ⁵³, Z.K. Zak ⁸⁸, T. Zakareishvili ¹⁶⁶, S. Zambito ⁵⁷, J.A. Zamora Saa ^{140d,140b}, J. Zang ¹⁵⁶, D. Zanzi ⁵⁵, O. Zaplatilek ¹³⁵, C. Zeitnitz ¹⁷⁴, H. Zeng ¹⁴, J.C. Zeng ¹⁶⁵, D.T. Zenger Jr ²⁷, O. Zenin ³⁸, T. Ženiš ^{29a}, S. Zenz ⁹⁶, S. Zerradi ^{36a}, D. Zerwas ⁶⁷, M. Zhai ^{14,114c}, D.F. Zhang ¹⁴², J. Zhang ^{63b}, J. Zhang ⁶, K. Zhang ^{14,114c}, L. Zhang ^{63a}, L. Zhang ^{114a}, P. Zhang ^{14,114c}, R. Zhang ¹⁷³, S. Zhang ¹⁰⁸, S. Zhang ⁹¹, T. Zhang ¹⁵⁶, X. Zhang ^{63c}, Y. Zhang ¹⁴¹, Y. Zhang ⁹⁸, Y. Zhang ^{114a}, Z. Zhang ^{18a}, Z. Zhang ^{63b}, Z. Zhang ⁶⁷, H. Zhao ¹⁴¹, T. Zhao ^{63b}, Y. Zhao ¹³⁹, Z. Zhao ^{63a}, Z. Zhao ^{63a}, A. Zhemchugov ³⁹, J. Zheng ^{114a}, K. Zheng ¹⁶⁵, X. Zheng ^{63a}, Z. Zheng ¹⁴⁶, D. Zhong ¹⁶⁵, B. Zhou ¹⁰⁸, H. Zhou ⁷, N. Zhou ^{63c}, Y. Zhou ¹⁵, Y. Zhou ^{114a}, Y. Zhou ⁷, C.G. Zhu ^{63b}, J. Zhu ¹⁰⁸, X. Zhu ^{63d}, Y. Zhu ^{63c}, Y. Zhu ^{63a}, X. Zhuang ¹⁴, K. Zhukov ⁶⁹, N.I. Zimine ³⁹, J. Zinsser ^{64b}, M. Ziolkowski ¹⁴⁴, L. Živković ¹⁶, A. Zoccoli ^{24b,24a}, K. Zoch ⁶², T.G. Zorbas ¹⁴², O. Zormpa ⁴⁷, W. Zou ⁴², L. Zwalinski ³⁷.

¹Department of Physics, University of Adelaide, Adelaide; Australia.

²Department of Physics, University of Alberta, Edmonton AB; Canada.

³(^a)Department of Physics, Ankara University, Ankara; (^b)Division of Physics, TOBB University of Economics and Technology, Ankara; Türkiye.

⁴LAPP, Université Savoie Mont Blanc, CNRS/IN2P3, Annecy; France.

⁵APC, Université Paris Cité, CNRS/IN2P3, Paris; France.

⁶High Energy Physics Division, Argonne National Laboratory, Argonne IL; United States of America.

⁷Department of Physics, University of Arizona, Tucson AZ; United States of America.

⁸Department of Physics, University of Texas at Arlington, Arlington TX; United States of America.

⁹Physics Department, National and Kapodistrian University of Athens, Athens; Greece.

¹⁰Physics Department, National Technical University of Athens, Zografou; Greece.

¹¹Department of Physics, University of Texas at Austin, Austin TX; United States of America.

¹²Institute of Physics, Azerbaijan Academy of Sciences, Baku; Azerbaijan.

¹³Institut de Física d'Altes Energies (IFAE), Barcelona Institute of Science and Technology, Barcelona; Spain.

¹⁴Institute of High Energy Physics, Chinese Academy of Sciences, Beijing; China.

- ¹⁵Physics Department, Tsinghua University, Beijing; China.
- ¹⁶Institute of Physics, University of Belgrade, Belgrade; Serbia.
- ¹⁷Department for Physics and Technology, University of Bergen, Bergen; Norway.
- ¹⁸(^a)Physics Division, Lawrence Berkeley National Laboratory, Berkeley CA; (^b)University of California, Berkeley CA; United States of America.
- ¹⁹Institut für Physik, Humboldt Universität zu Berlin, Berlin; Germany.
- ²⁰Albert Einstein Center for Fundamental Physics and Laboratory for High Energy Physics, University of Bern, Bern; Switzerland.
- ²¹School of Physics and Astronomy, University of Birmingham, Birmingham; United Kingdom.
- ²²(^a)Department of Physics, Bogazici University, Istanbul; (^b)Department of Physics Engineering, Gaziantep University, Gaziantep; (^c)Department of Physics, Istanbul University, Istanbul; Türkiye.
- ²³(^a)Facultad de Ciencias y Centro de Investigaciones, Universidad Antonio Nariño, Bogotá; (^b)Departamento de Física, Universidad Nacional de Colombia, Bogotá; Colombia.
- ²⁴(^a)Dipartimento di Fisica e Astronomia A. Righi, Università di Bologna, Bologna; (^b)INFN Sezione di Bologna; Italy.
- ²⁵Physikalisches Institut, Universität Bonn, Bonn; Germany.
- ²⁶Department of Physics, Boston University, Boston MA; United States of America.
- ²⁷Department of Physics, Brandeis University, Waltham MA; United States of America.
- ²⁸(^a)Transilvania University of Brasov, Brasov; (^b)Horia Hulubei National Institute of Physics and Nuclear Engineering, Bucharest; (^c)Department of Physics, Alexandru Ioan Cuza University of Iasi, Iasi; (^d)National Institute for Research and Development of Isotopic and Molecular Technologies, Physics Department, Cluj-Napoca; (^e)National University of Science and Technology Politehnica, Bucharest; (^f)West University in Timisoara, Timisoara; (^g)Faculty of Physics, University of Bucharest, Bucharest; Romania.
- ²⁹(^a)Faculty of Mathematics, Physics and Informatics, Comenius University, Bratislava; (^b)Department of Subnuclear Physics, Institute of Experimental Physics of the Slovak Academy of Sciences, Kosice; Slovak Republic.
- ³⁰Physics Department, Brookhaven National Laboratory, Upton NY; United States of America.
- ³¹Universidad de Buenos Aires, Facultad de Ciencias Exactas y Naturales, Departamento de Física, y CONICET, Instituto de Física de Buenos Aires (IFIBA), Buenos Aires; Argentina.
- ³²California State University, CA; United States of America.
- ³³Cavendish Laboratory, University of Cambridge, Cambridge; United Kingdom.
- ³⁴(^a)Department of Physics, University of Cape Town, Cape Town; (^b)iThemba Labs, Western Cape; (^c)Department of Mechanical Engineering Science, University of Johannesburg, Johannesburg; (^d)National Institute of Physics, University of the Philippines Diliman (Philippines); (^e)University of South Africa, Department of Physics, Pretoria; (^f)University of Zululand, KwaDlangezwa; (^g)School of Physics, University of the Witwatersrand, Johannesburg; South Africa.
- ³⁵Department of Physics, Carleton University, Ottawa ON; Canada.
- ³⁶(^a)Faculté des Sciences Ain Chock, Université Hassan II de Casablanca; (^b)Faculté des Sciences, Université Ibn-Tofail, Kénitra; (^c)Faculté des Sciences Semlalia, Université Cadi Ayyad, LPHEA-Marrakech; (^d)LPMR, Faculté des Sciences, Université Mohamed Premier, Oujda; (^e)Faculté des sciences, Université Mohammed V, Rabat; (^f)Institute of Applied Physics, Mohammed VI Polytechnic University, Ben Guerir; Morocco.
- ³⁷CERN, Geneva; Switzerland.
- ³⁸Affiliated with an institute covered by a cooperation agreement with CERN.
- ³⁹Affiliated with an international laboratory covered by a cooperation agreement with CERN.
- ⁴⁰Enrico Fermi Institute, University of Chicago, Chicago IL; United States of America.
- ⁴¹LPC, Université Clermont Auvergne, CNRS/IN2P3, Clermont-Ferrand; France.

- ⁴²Nevis Laboratory, Columbia University, Irvington NY; United States of America.
- ⁴³Niels Bohr Institute, University of Copenhagen, Copenhagen; Denmark.
- ⁴⁴(^a)Dipartimento di Fisica, Università della Calabria, Rende; (^b)INFN Gruppo Collegato di Cosenza, Laboratori Nazionali di Frascati; Italy.
- ⁴⁵Physics Department, Southern Methodist University, Dallas TX; United States of America.
- ⁴⁶Physics Department, University of Texas at Dallas, Richardson TX; United States of America.
- ⁴⁷National Centre for Scientific Research "Demokritos", Agia Paraskevi; Greece.
- ⁴⁸(^a)Department of Physics, Stockholm University; (^b)Oskar Klein Centre, Stockholm; Sweden.
- ⁴⁹Deutsches Elektronen-Synchrotron DESY, Hamburg and Zeuthen; Germany.
- ⁵⁰Fakultät Physik , Technische Universität Dortmund, Dortmund; Germany.
- ⁵¹Institut für Kern- und Teilchenphysik, Technische Universität Dresden, Dresden; Germany.
- ⁵²Department of Physics, Duke University, Durham NC; United States of America.
- ⁵³SUPA - School of Physics and Astronomy, University of Edinburgh, Edinburgh; United Kingdom.
- ⁵⁴INFN e Laboratori Nazionali di Frascati, Frascati; Italy.
- ⁵⁵Physikalisches Institut, Albert-Ludwigs-Universität Freiburg, Freiburg; Germany.
- ⁵⁶II. Physikalisches Institut, Georg-August-Universität Göttingen, Göttingen; Germany.
- ⁵⁷Département de Physique Nucléaire et Corpusculaire, Université de Genève, Genève; Switzerland.
- ⁵⁸(^a)Dipartimento di Fisica, Università di Genova, Genova; (^b)INFN Sezione di Genova; Italy.
- ⁵⁹II. Physikalisches Institut, Justus-Liebig-Universität Giessen, Giessen; Germany.
- ⁶⁰SUPA - School of Physics and Astronomy, University of Glasgow, Glasgow; United Kingdom.
- ⁶¹LPSC, Université Grenoble Alpes, CNRS/IN2P3, Grenoble INP, Grenoble; France.
- ⁶²Laboratory for Particle Physics and Cosmology, Harvard University, Cambridge MA; United States of America.
- ⁶³(^a)Department of Modern Physics and State Key Laboratory of Particle Detection and Electronics, University of Science and Technology of China, Hefei; (^b)Institute of Frontier and Interdisciplinary Science and Key Laboratory of Particle Physics and Particle Irradiation (MOE), Shandong University, Qingdao; (^c)School of Physics and Astronomy, Shanghai Jiao Tong University, Key Laboratory for Particle Astrophysics and Cosmology (MOE), SKLPPC, Shanghai; (^d)Tsung-Dao Lee Institute, Shanghai; (^e)School of Physics and Microelectronics, Zhengzhou University; China.
- ⁶⁴(^a)Kirchhoff-Institut für Physik, Ruprecht-Karls-Universität Heidelberg, Heidelberg; (^b)Physikalisches Institut, Ruprecht-Karls-Universität Heidelberg, Heidelberg; Germany.
- ⁶⁵(^a)Department of Physics, Chinese University of Hong Kong, Shatin, N.T., Hong Kong; (^b)Department of Physics, University of Hong Kong, Hong Kong; (^c)Department of Physics and Institute for Advanced Study, Hong Kong University of Science and Technology, Clear Water Bay, Kowloon, Hong Kong; China.
- ⁶⁶Department of Physics, National Tsing Hua University, Hsinchu; Taiwan.
- ⁶⁷IJCLab, Université Paris-Saclay, CNRS/IN2P3, 91405, Orsay; France.
- ⁶⁸Centro Nacional de Microelectrónica (IMB-CNM-CSIC), Barcelona; Spain.
- ⁶⁹Department of Physics, Indiana University, Bloomington IN; United States of America.
- ⁷⁰(^a)INFN Gruppo Collegato di Udine, Sezione di Trieste, Udine; (^b)ICTP, Trieste; (^c)Dipartimento Politecnico di Ingegneria e Architettura, Università di Udine, Udine; Italy.
- ⁷¹(^a)INFN Sezione di Lecce; (^b)Dipartimento di Matematica e Fisica, Università del Salento, Lecce; Italy.
- ⁷²(^a)INFN Sezione di Milano; (^b)Dipartimento di Fisica, Università di Milano, Milano; Italy.
- ⁷³(^a)INFN Sezione di Napoli; (^b)Dipartimento di Fisica, Università di Napoli, Napoli; Italy.
- ⁷⁴(^a)INFN Sezione di Pavia; (^b)Dipartimento di Fisica, Università di Pavia, Pavia; Italy.
- ⁷⁵(^a)INFN Sezione di Pisa; (^b)Dipartimento di Fisica E. Fermi, Università di Pisa, Pisa; Italy.
- ⁷⁶(^a)INFN Sezione di Roma; (^b)Dipartimento di Fisica, Sapienza Università di Roma, Roma; Italy.
- ⁷⁷(^a)INFN Sezione di Roma Tor Vergata; (^b)Dipartimento di Fisica, Università di Roma Tor Vergata,

Roma; Italy.

^{78(a)}INFN Sezione di Roma Tre; ^(b)Dipartimento di Matematica e Fisica, Università Roma Tre, Roma; Italy.

^{79(a)}INFN-TIFPA; ^(b)Università degli Studi di Trento, Trento; Italy.

⁸⁰Universität Innsbruck, Department of Astro and Particle Physics, Innsbruck; Austria.

⁸¹University of Iowa, Iowa City IA; United States of America.

⁸²Department of Physics and Astronomy, Iowa State University, Ames IA; United States of America.

⁸³Istinye University, Sariyer, Istanbul; Türkiye.

^{84(a)}Departamento de Engenharia Elétrica, Universidade Federal de Juiz de Fora (UFJF), Juiz de Fora; ^(b)Universidade Federal do Rio De Janeiro COPPE/EE/IF, Rio de Janeiro; ^(c)Instituto de Física, Universidade de São Paulo, São Paulo; ^(d)Rio de Janeiro State University, Rio de Janeiro; ^(e)Federal University of Bahia, Bahia; Brazil.

⁸⁵KEK, High Energy Accelerator Research Organization, Tsukuba; Japan.

⁸⁶Graduate School of Science, Kobe University, Kobe; Japan.

^{87(a)}AGH University of Krakow, Faculty of Physics and Applied Computer Science, Krakow; ^(b)Marian Smoluchowski Institute of Physics, Jagiellonian University, Krakow; Poland.

⁸⁸Institute of Nuclear Physics Polish Academy of Sciences, Krakow; Poland.

⁸⁹Faculty of Science, Kyoto University, Kyoto; Japan.

⁹⁰Research Center for Advanced Particle Physics and Department of Physics, Kyushu University, Fukuoka ; Japan.

⁹¹L2IT, Université de Toulouse, CNRS/IN2P3, UPS, Toulouse; France.

⁹²Instituto de Física La Plata, Universidad Nacional de La Plata and CONICET, La Plata; Argentina.

⁹³Physics Department, Lancaster University, Lancaster; United Kingdom.

⁹⁴Oliver Lodge Laboratory, University of Liverpool, Liverpool; United Kingdom.

⁹⁵Department of Experimental Particle Physics, Jožef Stefan Institute and Department of Physics, University of Ljubljana, Ljubljana; Slovenia.

⁹⁶School of Physics and Astronomy, Queen Mary University of London, London; United Kingdom.

⁹⁷Department of Physics, Royal Holloway University of London, Egham; United Kingdom.

⁹⁸Department of Physics and Astronomy, University College London, London; United Kingdom.

⁹⁹Louisiana Tech University, Ruston LA; United States of America.

¹⁰⁰Fysiska institutionen, Lunds universitet, Lund; Sweden.

¹⁰¹Departamento de Física Teórica C-15 and CIAFF, Universidad Autónoma de Madrid, Madrid; Spain.

¹⁰²Institut für Physik, Universität Mainz, Mainz; Germany.

¹⁰³School of Physics and Astronomy, University of Manchester, Manchester; United Kingdom.

¹⁰⁴CPPM, Aix-Marseille Université, CNRS/IN2P3, Marseille; France.

¹⁰⁵Department of Physics, University of Massachusetts, Amherst MA; United States of America.

¹⁰⁶Department of Physics, McGill University, Montreal QC; Canada.

¹⁰⁷School of Physics, University of Melbourne, Victoria; Australia.

¹⁰⁸Department of Physics, University of Michigan, Ann Arbor MI; United States of America.

¹⁰⁹Department of Physics and Astronomy, Michigan State University, East Lansing MI; United States of America.

¹¹⁰Group of Particle Physics, University of Montreal, Montreal QC; Canada.

¹¹¹Fakultät für Physik, Ludwig-Maximilians-Universität München, München; Germany.

¹¹²Max-Planck-Institut für Physik (Werner-Heisenberg-Institut), München; Germany.

¹¹³Graduate School of Science and Kobayashi-Maskawa Institute, Nagoya University, Nagoya; Japan.

^{114(a)}Department of Physics, Nanjing University, Nanjing; ^(b)School of Science, Shenzhen Campus of Sun Yat-sen University; ^(c)University of Chinese Academy of Science (UCAS), Beijing; China.

- ¹¹⁵Department of Physics and Astronomy, University of New Mexico, Albuquerque NM; United States of America.
- ¹¹⁶Institute for Mathematics, Astrophysics and Particle Physics, Radboud University/Nikhef, Nijmegen; Netherlands.
- ¹¹⁷Nikhef National Institute for Subatomic Physics and University of Amsterdam, Amsterdam; Netherlands.
- ¹¹⁸Department of Physics, Northern Illinois University, DeKalb IL; United States of America.
- ¹¹⁹^(a)New York University Abu Dhabi, Abu Dhabi;^(b)United Arab Emirates University, Al Ain; United Arab Emirates.
- ¹²⁰Department of Physics, New York University, New York NY; United States of America.
- ¹²¹Ochanomizu University, Otsuka, Bunkyo-ku, Tokyo; Japan.
- ¹²²Ohio State University, Columbus OH; United States of America.
- ¹²³Homer L. Dodge Department of Physics and Astronomy, University of Oklahoma, Norman OK; United States of America.
- ¹²⁴Department of Physics, Oklahoma State University, Stillwater OK; United States of America.
- ¹²⁵Palacký University, Joint Laboratory of Optics, Olomouc; Czech Republic.
- ¹²⁶Institute for Fundamental Science, University of Oregon, Eugene, OR; United States of America.
- ¹²⁷Graduate School of Science, Osaka University, Osaka; Japan.
- ¹²⁸Department of Physics, University of Oslo, Oslo; Norway.
- ¹²⁹Department of Physics, Oxford University, Oxford; United Kingdom.
- ¹³⁰LPNHE, Sorbonne Université, Université Paris Cité, CNRS/IN2P3, Paris; France.
- ¹³¹Department of Physics, University of Pennsylvania, Philadelphia PA; United States of America.
- ¹³²Department of Physics and Astronomy, University of Pittsburgh, Pittsburgh PA; United States of America.
- ¹³³^(a)Laboratório de Instrumentação e Física Experimental de Partículas - LIP, Lisboa;^(b)Departamento de Física, Faculdade de Ciências, Universidade de Lisboa, Lisboa;^(c)Departamento de Física, Universidade de Coimbra, Coimbra;^(d)Centro de Física Nuclear da Universidade de Lisboa, Lisboa;^(e)Departamento de Física, Universidade do Minho, Braga;^(f)Departamento de Física Teórica y del Cosmos, Universidad de Granada, Granada (Spain);^(g)Departamento de Física, Instituto Superior Técnico, Universidade de Lisboa, Lisboa; Portugal.
- ¹³⁴Institute of Physics of the Czech Academy of Sciences, Prague; Czech Republic.
- ¹³⁵Czech Technical University in Prague, Prague; Czech Republic.
- ¹³⁶Charles University, Faculty of Mathematics and Physics, Prague; Czech Republic.
- ¹³⁷Particle Physics Department, Rutherford Appleton Laboratory, Didcot; United Kingdom.
- ¹³⁸IRFU, CEA, Université Paris-Saclay, Gif-sur-Yvette; France.
- ¹³⁹Santa Cruz Institute for Particle Physics, University of California Santa Cruz, Santa Cruz CA; United States of America.
- ¹⁴⁰^(a)Departamento de Física, Pontificia Universidad Católica de Chile, Santiago;^(b)Millennium Institute for Subatomic physics at high energy frontier (SAPHIR), Santiago;^(c)Instituto de Investigación Multidisciplinario en Ciencia y Tecnología, y Departamento de Física, Universidad de La Serena;^(d)Universidad Andres Bello, Department of Physics, Santiago;^(e)Instituto de Alta Investigación, Universidad de Tarapacá, Arica;^(f)Departamento de Física, Universidad Técnica Federico Santa María, Valparaíso; Chile.
- ¹⁴¹Department of Physics, University of Washington, Seattle WA; United States of America.
- ¹⁴²Department of Physics and Astronomy, University of Sheffield, Sheffield; United Kingdom.
- ¹⁴³Department of Physics, Shinshu University, Nagano; Japan.
- ¹⁴⁴Department Physik, Universität Siegen, Siegen; Germany.

- ¹⁴⁵Department of Physics, Simon Fraser University, Burnaby BC; Canada.
- ¹⁴⁶SLAC National Accelerator Laboratory, Stanford CA; United States of America.
- ¹⁴⁷Department of Physics, Royal Institute of Technology, Stockholm; Sweden.
- ¹⁴⁸Departments of Physics and Astronomy, Stony Brook University, Stony Brook NY; United States of America.
- ¹⁴⁹Department of Physics and Astronomy, University of Sussex, Brighton; United Kingdom.
- ¹⁵⁰School of Physics, University of Sydney, Sydney; Australia.
- ¹⁵¹Institute of Physics, Academia Sinica, Taipei; Taiwan.
- ¹⁵²^(a)E. Andronikashvili Institute of Physics, Iv. Javakhishvili Tbilisi State University, Tbilisi;^(b)High Energy Physics Institute, Tbilisi State University, Tbilisi;^(c)University of Georgia, Tbilisi; Georgia.
- ¹⁵³Department of Physics, Technion, Israel Institute of Technology, Haifa; Israel.
- ¹⁵⁴Raymond and Beverly Sackler School of Physics and Astronomy, Tel Aviv University, Tel Aviv; Israel.
- ¹⁵⁵Department of Physics, Aristotle University of Thessaloniki, Thessaloniki; Greece.
- ¹⁵⁶International Center for Elementary Particle Physics and Department of Physics, University of Tokyo, Tokyo; Japan.
- ¹⁵⁷Department of Physics, Tokyo Institute of Technology, Tokyo; Japan.
- ¹⁵⁸Department of Physics, University of Toronto, Toronto ON; Canada.
- ¹⁵⁹^(a)TRIUMF, Vancouver BC;^(b)Department of Physics and Astronomy, York University, Toronto ON; Canada.
- ¹⁶⁰Division of Physics and Tomonaga Center for the History of the Universe, Faculty of Pure and Applied Sciences, University of Tsukuba, Tsukuba; Japan.
- ¹⁶¹Department of Physics and Astronomy, Tufts University, Medford MA; United States of America.
- ¹⁶²Department of Physics and Astronomy, University of California Irvine, Irvine CA; United States of America.
- ¹⁶³University of Sharjah, Sharjah; United Arab Emirates.
- ¹⁶⁴Department of Physics and Astronomy, University of Uppsala, Uppsala; Sweden.
- ¹⁶⁵Department of Physics, University of Illinois, Urbana IL; United States of America.
- ¹⁶⁶Instituto de Física Corpuscular (IFIC), Centro Mixto Universidad de Valencia - CSIC, Valencia; Spain.
- ¹⁶⁷Department of Physics, University of British Columbia, Vancouver BC; Canada.
- ¹⁶⁸Department of Physics and Astronomy, University of Victoria, Victoria BC; Canada.
- ¹⁶⁹Fakultät für Physik und Astronomie, Julius-Maximilians-Universität Würzburg, Würzburg; Germany.
- ¹⁷⁰Department of Physics, University of Warwick, Coventry; United Kingdom.
- ¹⁷¹Waseda University, Tokyo; Japan.
- ¹⁷²Department of Particle Physics and Astrophysics, Weizmann Institute of Science, Rehovot; Israel.
- ¹⁷³Department of Physics, University of Wisconsin, Madison WI; United States of America.
- ¹⁷⁴Fakultät für Mathematik und Naturwissenschaften, Fachgruppe Physik, Bergische Universität Wuppertal, Wuppertal; Germany.
- ¹⁷⁵Department of Physics, Yale University, New Haven CT; United States of America.
- ¹⁷⁶Yerevan Physics Institute, Yerevan; Armenia.
- ^a Also Affiliated with an institute covered by a cooperation agreement with CERN.
- ^b Also at An-Najah National University, Nablus; Palestine.
- ^c Also at Borough of Manhattan Community College, City University of New York, New York NY; United States of America.
- ^d Also at Center for Interdisciplinary Research and Innovation (CIRI-AUTH), Thessaloniki; Greece.
- ^e Also at CERN, Geneva; Switzerland.
- ^f Also at CMD-AC UNEC Research Center, Azerbaijan State University of Economics (UNEC); Azerbaijan.

- ^g Also at Département de Physique Nucléaire et Corpusculaire, Université de Genève, Genève; Switzerland.
- ^h Also at Departament de Física de la Universitat Autònoma de Barcelona, Barcelona; Spain.
- ⁱ Also at Department of Financial and Management Engineering, University of the Aegean, Chios; Greece.
- ^j Also at Department of Physics, California State University, Sacramento; United States of America.
- ^k Also at Department of Physics, King's College London, London; United Kingdom.
- ^l Also at Department of Physics, Stanford University, Stanford CA; United States of America.
- ^m Also at Department of Physics, Stellenbosch University; South Africa.
- ⁿ Also at Department of Physics, University of Fribourg, Fribourg; Switzerland.
- ^o Also at Department of Physics, University of Thessaly; Greece.
- ^p Also at Department of Physics, Westmont College, Santa Barbara; United States of America.
- ^q Also at Hellenic Open University, Patras; Greece.
- ^r Also at Imam Mohammad Ibn Saud Islamic University; Saudi Arabia.
- ^s Also at Institutio Catalana de Recerca i Estudis Avancats, ICREA, Barcelona; Spain.
- ^t Also at Institut für Experimentalphysik, Universität Hamburg, Hamburg; Germany.
- ^u Also at Institute for Nuclear Research and Nuclear Energy (INRNE) of the Bulgarian Academy of Sciences, Sofia; Bulgaria.
- ^v Also at Institute of Applied Physics, Mohammed VI Polytechnic University, Ben Guerir; Morocco.
- ^w Also at Institute of Particle Physics (IPP); Canada.
- ^x Also at Institute of Physics, Azerbaijan Academy of Sciences, Baku; Azerbaijan.
- ^y Also at Institute of Theoretical Physics, Ilia State University, Tbilisi; Georgia.
- ^z Also at National Institute of Physics, University of the Philippines Diliman (Philippines); Philippines.
- ^{aa} Also at Technical University of Munich, Munich; Germany.
- ^{ab} Also at The Collaborative Innovation Center of Quantum Matter (CICQM), Beijing; China.
- ^{ac} Also at TRIUMF, Vancouver BC; Canada.
- ^{ad} Also at Università di Napoli Parthenope, Napoli; Italy.
- ^{ae} Also at University of Colorado Boulder, Department of Physics, Colorado; United States of America.
- ^{af} Also at Washington College, Chestertown, MD; United States of America.
- ^{ag} Also at Yeditepe University, Physics Department, Istanbul; Türkiye.
- * Deceased